STRONGLY CORRELATED SYSTEMS IN ULTRACOLD QUANTUM GASES

Von der Fakultät für Mathematik und Physik
der Universität Hannover
zur Erlangung des Grades
Doktor der Naturwissenschaften
Dr. rer. nat.
genehmigte Dissertation
von

Dipl.-Phys. Henning Fehrmann
geboren am 7. Oktober 1975 in Havelberg

Abstrakt

In dieser Dissertation wird das Verhalten sehr kalter stark korrelierter Quantengase, sowohl in optischen Gittern, als auch in rotierenden Fallen, untersucht.

Im ersten Teil betrachten wir Fermionen auf einen bosonenischem Motthintergrund in einem zweidimensionalen optischen Gitter mit quadratischen Einheitszellen. Aufgrund der Wechselwirkung zwischen Fermionen und Bosonen bilden sich "Composite Fermions", Fermionen gepaart mit bosnischen Löchern oder mit Bosonen. Für eine kleine Tunnelrate leiten wir einen effektiven Hamiltonian her, der das Verhalten der "Composite Fermions" beschreibt. Mit Hilfe einer einfachen Mean-Field-Rechnung finden wir einen Mottisolator-Superflüssigkeit Phasenübergang, den wir nummerisch bestätigen

Das nächste Kapitel beschäftigt sich mit Quantengasen in optischen "trimerized" Kagomégittern. Für Bosonen finden wir einem Mottisolator mit einer rationalen Anzahl von Atomen $(1/3, 2/3, 1, \cdots)$ in einer Zelle. Im Falle einer Fermion-Fermion-Mischung können wir einen effektiven Hamiltonian für einen Heisenbergantiferromagneten herleiten. Außerdem betrachten ein Gas bestehend aus polarisierten Fermion. Auch dieses System kann mit einem effektiven Hamiltonian dargestellt werden. Durch eine exakte Diagonalisierung gelangen wir zu einer, in frustrierten Systemen, unerwarteten Schlußfolgerung: Es gibt keine Energielücke zwischen Grundzustand und dem ersten angeregten Zustand aber trotzdem finden wir eine langreichweitige Spin-Spin-Korrelation.

Im letzten Kapitel untersuchen wir die Möglichkeit, Wignerkristallisation in schnell rotierenden polarisiertem Dipolgasen zu beobachten. Wir vergleichen die Energie eines Wignerkristalls mit der Energie eines Laughlinzustandes und stellen fest, dass unter einer kritischen Füllrate der Wignerkristall energetisch günstiger ist. Weiterhin beschäftigen wir uns mit der Stabilität einer solchen Kristalls und finden unter Berücksichtigung von Phonon-Phonon Wechselwirkungen heraus, dass der Wignerkristall schmilzt, wenn die Füllrate einen kritischen Wert überschreitet. Wir können nun das Lindemannkriterium für den schnell rotierenden dipolaren Wignerkristall formulieren. Die kritische Füllrate für den energetischen Phasenübergang ist etwas größer als für den Schmelzpunkt.

Schlagwörter: stark korrelierte Systeme, optische Gitter, Wigner Kristall

Abstract

In this thesis we examine the properties of ultracold strongly correlated quantum gases in optical lattices and rotating traps.

In the first chapter we consider fermions on top of a bosonic Mott background in an optical 2D lattice with a square unitary cell. Due to the interaction between fermions and bosons "composite fermions", i.e. fermions paired with bosons, or bosonic holes, are formed. For a small tunneling rate we can derive an effective Hamiltonian, describing the dynamics of the "composite fermions". A simple mean-field calculation yields a Mott-insulator-superfluid phase boundary, which we confirm then numerically.

The next chapter deals with quantum gases in optical trimerized kagomé lattices. Loading bosons into the lattice we find a new kind of Mott insulator with a fractional number of atoms per trimer $(1/3, 2/3, 1, \cdots)$. For a fermion-fermion mixture we obtain an effective Hamiltonian, describing a Heisenberg antiferromagnet. Moreover, we explore a gas of single component (polarized) interacting fermions, and obtain also here an effective Hamiltonian. Diagonalizing the system exactly we discover a new quantum state: a "quantum spin-liquid crystal".

In the last chapter we consider Wigner crystallization in rapidly rotating dipolar fermion gases. For low filling factors ($\nu < 1/7$) the Wigner crystal is energetically more favorable than another quantum state: the Laughlin liquid. We analyze also the stability of the Wigner crystal by incorporating phonon-phonon interactions, and realize that below a critical filling factor the Wigner crystal is stable. We formulate the Lindemann criterion for the Wigner crystal in a rapidly rotating dipolar gas.

Keywords: strongly correlated systems, optical lattices, Wigner crystal

CONTENTS

Chapter 1

Introduction

1.1 Atomic and molecular BEC

1.1.1 Historical review

Many of the branches of cold atom physics, which have been developed in the last few years, owe their existence to the observation of atomic Bose-Einstein condensate (BEC).

BEC was predicted by Bose and Einstein [30, 73] in 1924 as a quantum phase characterized, below a critical temperature, by a macroscopic occupation of the single particle ground state. Einstein has shown that this phase occurs in a non-interacting gas. A remarkable feature of BEC in weakly interacting gases is that the coherence length can be of the order of the system size, or even longer. Already in 1938 London conjectured that BEC could be the explanation for another phenomenon, namely the superfluidity of liquid helium [147], which has been confirmed by Penrose and Onsager [183]. Although these two phenomena are tightly related, they share also differences. For instance, strictly speaking, BEC does not exist in 1D, whereas there are 1D superfluid systems.

In order to realize atomic BEC, extremely low temperatures (in the nK regime), "high" atom densities, and long storage times are required. Intensive studies and progress in cooling techniques led, in 1995, to the seminal observation of atomic BEC of Rubidium (Rb^{87}) by the group of Cornell and Wieman [10], and of Sodium by the group of Ketterle [63].

1.1.2 Cooling methods

Laser cooling

Already before the first BEC experiments a lot of efforts have been done to develop reliable cooling techniques, such as laser cooling [47], where atoms

moving towards a red detuned laser beam will shift into the resonance with the laser. The absorbed photons transfer a momentum opposite to the moving direction, while the emission goes in an arbitrary direction and has on average no effect. An atom moving away from the red detuned laser is shifted out of resonance and will unlikely absorb a photon. Laser pointing from all directions have the effect of a viscous damping force. Laser cooling of alkali atoms has led to yet another discovery of polarization gradient cooling and the Sysiphus effect [57], that allow to reach μK temperatures, although it was not sufficient to obtain a BEC.

Evaporative cooling

The final breakthrough came with the development of the evaporative cooling, where the Rabi-frequency transition between magnetically trapped and free states removes the hottest atoms (i.e. those with the highest energy) from the velocity distribution. Elastic collisions between the remaining particles restore the thermal equilibrium at a lower temperature. Using this method in early experiments spin-polarized hydrogen atoms have been cooled down into the mK regime [113, 158]. Already 1994 Sodium was successfully cooled down to tens of μK [64]. In order to achieve a condensate its life-time should be longer than the rethermalization time. In some cases, it is not possible to fulfill this condition. For instance, polarized fermions do not rethermalize at all, because Pauli's principle forbids the exchange of energy via s-wave scattering.

Sympathetic cooling

A third method to cool atoms, which are, due to their intrinsic properties, not appropriate for evaporative cooling, is sympathetic cooling [109, 170]. The atoms exchange energy with another species via s-wave scattering. The atoms of the second species, acting as a reservoir, are cooled down with a lossy evaporative cooling. Using this method fermionic Li^6-atoms have been already cooled down to $0.05 T_F$ [108], where T_F is the Fermi temperature.

1.1.3   So far achieved atomic condensates

Motivated by the successful condensation of Rb^{87} and Sodium atoms, several groups created successfully BEC's with other species, such as Li^7 [32], atomic Hydrogen [54], metastable Helium [197], Rb^{85} [51], Potassium [168], Ytterbium [210], quite recently Cesium [230], and Chromium [208].

1.1.4   Molecular condensates

Further important achievements are the creation of ultracold molecules and molecular condensates using Cesium [125], with Potassium [102], Rb^{85} [67], and Li^6 [242]. By sweeping the magnetic field over a Feshbach resonance, the cooled fermions are brought in to a relative stable molecular state, where the size of the molecules are of the order of the scattering length.

1.1.5   Coherence phenomena and phase fluctuations

Due to the long coherence length, the question arose whether phenomena appearing in electro-magnetic waves are also observable in BEC. Consequently, efforts towards the development of an atom laser [162] have been done and succeeded by the coherent out-coupling of atoms from a BEC reservoir. Another phenomenon in 2D, known to appear also in liquid helium, is the occurrence of vortices [2, 28, 45, 160], a quantized circulation of the condensate. The dynamics of vortices itself is an interesting topic (see e.g. [152, 202]).

In order to make reliable predictions for the lifetime of the condensate, it is also important to understand the finite temperature effects [185] and phase fluctuations [112].

1.1.6   Contact interaction between atoms

Atoms approaching each other start to reciprocally perturb their electronical states, which is for low energy essentially the s-wave scattering. The strength of this interaction depends on the energy difference between the levels of the two atoms. Feshbach resonance [212] allows the shifting of molecular energy-levels and provides a useful tool for tailoring the amplitude, and sign of the interaction. Since the interaction regime is, compared to typical system size and coherence length, weak and very short-ranged, one can often treat this problem in the mean-field approximation. The dynamics is well described by the Gross-Pitaevski-Equation, which binds again cold matter physics to nonlinear electrodynamics and other branches of nonlinear physics [69]. A striking experiment was the creation of dark solitons [39] for repulsive and bright solitons [130, 207] for attractive interatomic interaction.

In recent experiments the optically manipulation of the scattering length a has been examined [211]. The so-called optical Feshbach resonance has been therotically studied in reference [77].

1.1.7   Dipole-dipole interaction

The exploration of systems with long range interaction is also a very fascinating enterprise. An experimentally feasible system could be a dipolar gas. Chromium with its relatively strong magnetic dipole [208], is the first example of experimentally achieved dipolar gas. Also the effects of the dipole-dipole interaction have been observed clearly, the dipole interaction is several orders of magnitude higher when electrical dipole forces, present in heteronuclear molecules, are involved. Therefore, efforts towards the creation of dipolar molecular gases have been made (e.g. see [23, 123, 216, 217]). Another important feature of the dipolar gases are the effects caused by the anisotropy of the dipole-dipole interaction.

1.2   Strongly correlated systems

Although interacting atoms are a perfect playground for studying weakly interacting gases, it is possible also to study in these settings the, so-called, strongly correlated systems.

1.2.1   Low dimensional systems

Examples of strongly correlated systems are low dimensional gases, such as a 1D Bose gas in the Tonks regime, which has been experimentally observed by the groups of Bloch and Kenoshita [132, 181]. Progress in the realization of a Luttiger liquid, whose key signature is the spin-charge separation [134], has been reached by the cooling of fermionic atoms into the quantum degenerated regime [192].

1.2.2   Quantum computing

Quantum information has given new impulses towards the understanding of quantum phase transitions [117, 137, 163, 172, 176, 178, 221, 222, 226, 238], and helps to get a better insight into the known (and develop new) numerical methods of treating strongly correlated many-body systems [49, 56, 223]. In general, the physics of strongly correlated systems provides various ways of quantum information processing (cf. [119, 155]). It has been also suggested to realize special purpose quantum computers, so-called, quantum simulators [48] of strongly correlated systems. For the original idea of quantum simulators see [79].

1.2.3 Rapidly rotating dipolar gases

A rapidly rotating gas can be properly described by a model of charged particles moving in a magnetic field. Cold atom physics uses here the results of many years of research in electronic systems. But, the $1/r^3$ behavior for dipole-dipole interactions, compared to the $1/r$ potential of electrons, is a new aspect. In the first Landau level, for high filling factors, the ground state of electrons are described by Laughlin wavefunctions [138, 188]. Such solutions are suggested to appear also in dipolar gases [15], hence cold atom physics links to the field of the fractional quantum Hall effect. Contrary, at very low filling factors, Wigner crystallization is expected to appear. Localizations of atoms in strongly correlated systems with long range interactions have been first suggested by Wigner [237].

1.2.4 BEC-BCS transition

Another many-body effect is connected to recently observed BEC-BCS transition [46, 102, 131]. For a positive scattering length in a gas of fermionic atoms in two different internal states the formation of molecules has been observed. At sufficiently low temperatures the bimodal momentum distribution indicates a condensate of these molecules. On the other hand, sweeping the scattering length two negative values weakly bound BCS pairs have been created. BCS denotes the Bardeen-Schrieffer-Cooper transition to a superfluid state in a Fermi gas or liquid. (see also [17, 18, 103, 240, 241, 243]). Beside the possibility of creating a molecular BEC, the experiment deals indirectly with open questions of high T_c superconductivity.

1.3 Optical lattices

The research on condensates stimulated the development of tools for manipulations and engineering of quantum states.

A very widely used, maybe the most important tool, employs the interaction of atoms and light. Depending on the square of the laser field amplitude $|E_0(\mathbf{x}, t)|^2$, the energy of the atoms is either lifted up for red- or shifted down for blue-detuned light, where the detuning denotes the difference of the shifted light beam from the resonance frequency of the atom. This is the so-called dynamical (AC) Stark effect. The laser intensity pattern acts as a conservative potential $V(\mathbf{x})$. The dynamics of the atoms is effectively described by $H = \mathbf{p}^2/2m + V(\mathbf{x})$. This simple technique proved to be a very useful tool in many aspects. For instance, alternatively to a magnetic field, it can be used to build an external trapping potential.

A laser field can be used to manipulate *in situ* and "*in vivo*" the potential for the condensate by varying the desired configurations of $V(\mathbf{x}, t)$. In this way it is possible to produce dark solitons [39], stirring condensates to create crystallized vortices [153, 161] and populate excited modes such as quadropol modes [175].

The opportunity to build arbitrary potentials with light fields inspired Jaksch [120] to employ the superfluid-Mott-insulator transition, which can be used for quantum computing. One of the elements of this proposal was the perfect preparation of the initial state of the quantum register (atoms in the lattice). To this aim Jaksch *et. al* proposed to perform an optical lattice using off-resonant light fields. Using optical lattices the observation of the phase transition between Mott insulator and superfluid phase, predicted by [120] has been experimentally achieved [100, 101] with ^{87}Rb atoms. By changing the laser intensity and/or detuning, one can control the tunneling to neighboring sites, as well as the strength of the on-site repulsive interactions, and therefore one is able to switch between the superfluid phase (dominated by the tunneling), and the Mott insulator phase with a fixed number of atoms per site [100, 101]. The free tunability of parameters "*in vivo*" is a remarkable advantage compared to systems considered in condensed matter physics [122].

1.3.1   Application of optical lattices

Without exaggerating, it can be said that the development of optical lattices created a new and rich field within the area of cold atomic physics, which is now linked not only to condensed mater physics [100, 101], but also examines topics related to quantum information theory [119] and even high energy physics [121, 180, 194].

1.3.2   Lattices in different dimensions

Atoms in optical lattices can be examined in quasi-1D, quasi-2D, or 3D systems. For example, in the Tonks Giradeau limit in 1D lattices, where bosons with a strong repulsive interaction, the so-called hardcore bosons, behave in many aspects like fermion [174]. A very deep potential in two dimensions and a weak confining in the third dimension leads to an array of 1D configurations [169].

1.3.3 The models

The physics of ultracold atomic gases in optical lattices is in general described by various versions of the Hubbard model, which is probably the most important and structurally simplest model of condensed matter physics, capable nevertheless to describe an enormous variety of physical phenomena, effects and quantum phases [14, 75], hence atomic ultracold gases serve as a "Hubbard model tool-kit" [122]. Moreover, a fermion-fermion model eventually allows for quantum simulations of high T_c superconductivity [115]. A boson-fermion model describes the creation of composite fermions via fermion-boson, or fermion-bosonic hole pairing, c.f. [7, 78, 135, 142]. In a certain limit Hubbard models reduce to spin models and this possibility has been also intensively investigated recently for both atomic gases [68, 70, 89, 90], and ion chains [165, 187]. Spin models enjoy particular interest because of their simplicity, and thus possible applications for quantum information processing (c.f. [68, 71]).

1.3.4 Different lattice types

Of course, using lasers one is not confined to square lattices. It is relatively easy to implement setups that can create triangular lattices [186]. In the regime of current experimental accessibility lies the possibility of creating trimerized kagomé lattices [198], or even more complicated and exotic super-lattices, not necessarily having a periodic structure, which is also an interesting topic to study [105, 106, 186, 190]. Naturally, with higher complexity, the number of tunable parameter increases. In trimerized kagomé lattice, for instance, one can control the trimerization degree from a perfect kagomé lattice to a perfect triangular lattice. The topic of particular interest in this context is the behavior of single species, either bosons or fermions, or mixtures in trimerized kagomé lattices. Loading fermions in a kagomé lattice opens the possibility of studying frustrated atomic systems [59], that have been long investigated and are in the center of interests of modern condensed matter physics [144, 166].

1.3.5 Analytical and numerical methods

By creating ultracold quantum gases in optical lattices, atom optics is inheriting a body of still open questions. The difficulties lie in the fact that apart from renormalization group approaches, that have limited applications, numerical methods offer the only possibility to examine such systems. In this respect, Quantum Monte Carlo simulations of the Heisenberg antiferromag-

net on frustrated lattices, such as triangular and kagomé lattices, are known to suffer from a "negative sign" problem, so that in 2D and 3D exact diagonalization seems to be the only reliable method to simulate these systems. In 1D one has more methods such as Density Matrix Renormalization Group methods [191, 235], the Vidal algorithm [224, 225] or the projected entangled pair state method of Verstraete and Cirac [220] which, in principle, works also in 2D, but this requires further studies. Moreover, exact diagonalizations are only possible up to a small number of particles [24]. Analytically one has to rely either on bosonization methods [93, 96, 159] or, in certain specific 1D systems, the Bethe ansatz [22, 75]. With optical lattices the opportunity to study experimentally frustrated antiferromagnets is opened.

1.3.6   Bose glass and Anderson localization

One assumes that by introducing a random pattern either for the potential, or for the hopping elements, and by taking only one bosonic species one can already create Anderson localization [11], Bose glass [61] or, in boson-fermion mixtures, a spin glass [5, 196], beside superfluid and Mott insulator phases. Over many years, the Anderson localization itself attracted a lot of attentions [88] and there is the hope of getting a deeper understanding of this phenomenon by using optical lattices. Pseudo-randomness can be generated by a standing waves with incommensurate frequencies [66]. To create real randomness one can use a speckle pattern [151, 201], or one can also "quench" auxiliary atoms at random lattice sites as random scatters [91].

1.4   Outline

Beside the introduction and the outline, in chapter 1 tools and methods are described. In particular, we explain briefly the derivation of the Hubbard model from the field equation. Moreover, the mean-field approximation is illustrated.

Chapter 2 is devoted to boson-fermion mixtures in square optical lattices. The bosons form a Mott state. Depending on the sign and the strength of the interaction between fermions and bosons, the presence of a fermions in a particular lattice cell will expel or attract bosons. The fermion and the bosonic holes (or attracted bosons) form a composite fermion. Using a perturbative expansion, an effective model describing the dynamics of the composite fermions is derived. We consider the a phase transition between Mott insulator and superfluid phase, using a mean field theory. A numerical method based on the so-called time dependent Gutzwiller ansatz is illustrated, and

is used to confirm the analytical results for the phase boundary.

Chapter 3 deals with quantum gases in trimerized kagomé lattices. First, experimental setup is discussed. The Hubbard model is derived using Wannier functions, respectively Gauss functions, obtained in a variational ansatz. We examine three cases: A fermion-fermion mixture can be effectively described with a Heisenberg antiferromagnet model. Applying a mean-field theory to a Hubbard model describing a Bose gas, leads to Mott insulator phases with non-integer filling factor per elementary lattice cell. For a single component fermionic gas we obtain after an exact diagonalization an quantum gas with properties of a Néel antiferromagnet and a spin-liquid, hence, we term this gas a *"spin-liquid crystal"*.

In Chapter 4 the possibility of Wigner crystallization in a rapidly rotating dipolar gas is considered. A rapidly rotating gas can be effectively described, apart from the interaction terms, by a model of charged particles in a magnetic field. Together with long range dipole-dipole interaction, phenomena similar to those appearing in an electron gas under the influence of a strong magnetic field, can be expected. For example for a completely filled lowest Landau level the solution is predicted to be a Laughlin state [15]. In electronical systems it is known that for low filling factors, charge density waves, such as a Wigner crystal, are energetically favorable. First, we compare the ground state energy of the crystalline phase with the energy of a Laughlin wavefunction at various filling factors and expect a phase transition at a critical filling factor. We also study the stability by incorporating perturbatively contributions, coming from phonon-phonon interaction. An imaginary phonon dispersion relation is the signature of a melting Wigner crystal.

1.5 The Hubbard model

Standing electromagnetic waves create a periodic lattice potential for the atoms. Such a lattice can be 1D, 2D or 3D. In 3D, three standing laser waves, pointing in orthogonal directions are sufficient. In 2D the atoms have to be strongly confined in the z-direction. The confinement has to be strong enough to create an energy gap between two vibrational levels that is bigger than any other relevant energy in the system. In 1D one needs this confinement in two directions. The atoms interact via the potential $V_{\text{s}}(\mathbf{x}-\mathbf{y})$, where $\mathbf{x}$ and $\mathbf{y}$ are the positions of the atoms. The lattice potential is $V_{\text{l}}(\mathbf{r})$, which is periodic. The Hamiltonian reads:

$$H = H_0 + H_{\text{int}} \quad , \tag{1.1}$$

with:

$$H_0 = \int \mathrm{dx}^3 \Psi^\dagger(\mathbf{x}) \left(-\frac{\hbar^2}{2m}\Delta + V_\mathrm{l}(\mathbf{x}) \right) \Psi(\mathbf{x})$$

$$H_\mathrm{int} = \frac{1}{2} \int \mathrm{dx}^3 \int \mathrm{dy}^3 \Psi^\dagger(\mathbf{x})\Psi^\dagger(\mathbf{y})V_\mathrm{s}(\mathbf{x}-\mathbf{y})\Psi(\mathbf{y})\Psi(\mathbf{x}) \quad .$$

In the case, when the potential is:

$$V_\mathrm{s}(\mathbf{x}-\mathbf{y}) = \frac{4\pi a_\mathrm{s}\hbar^2}{2m}\delta(\mathbf{x}-\mathbf{y}) \quad ,$$

the interaction Hamiltonian reads:

$$H_\mathrm{int} = \frac{4\pi a_\mathrm{s}\hbar^2}{2m} \int \mathrm{dx}^3 \Psi^\dagger(\mathbf{x})\Psi^\dagger(\mathbf{x})\Psi(\mathbf{x})\Psi(\mathbf{x}) \quad , \qquad (1.2)$$

where a_s is the s-wave scattering length and H_int the self-interaction part of the equation (1.1).

1.5.1   Localized wavefunctions

In the case of a huge potential amplitude the wells can be treated independently. In a harmonic approximation the ground state of a single particle wave is shaped like a Gauss function [182]. In general we can make the following variational ansatz:

$$\psi(\mathbf{r}) = \frac{1}{\sqrt{\sigma_x\sigma_y\sigma_z\pi^{\frac{3}{2}}}} \mathrm{e}^{\left(-\frac{x^2}{2\sigma_x^2}\right)} \mathrm{e}^{\left(-\frac{y^2}{2\sigma_y^2}\right)} \mathrm{e}^{\left(-\frac{z^2}{2\sigma_z^2}\right)} \quad ,$$

where σ_i are free parameters to minimize the energy. The set of Gauss functions centered at different lattice sites is of course not a set of orthogonal functions, but as long as the overlaps are small that does not pose a problem. By decreasing the potential depth, however, the coupling between the wells becomes more pronounced. In a periodic potential the scheme of Bloch is then the quasi-correct treatment. There the Hamiltonian is diagonalized in momentum space, and the Bloch functions are completely delocalized. In order to combine the two opposite regimes Wannier [229] suggested a scheme to obtain localized atomic functions using Bloch waves. For now, we restrict ourselves to the first band. The Wannier function is constructed as [14]:

$$W_i(\mathbf{r}) \;=\; \frac{1}{\sqrt{N}} \sum_{\mathbf{k}} \mathrm{e}^{\mathrm{i}\phi_\mathbf{k}} \mathrm{e}^{\mathrm{i}\mathbf{r}_i\mathbf{k}} \psi_k(\mathbf{r}) \quad , \qquad (1.3)$$

where $\psi_k(\mathbf{r})$ are the Bloch functions with the quasi-momentum $\mathbf{k}$. The phase factor $\exp(\mathrm{i}\mathbf{r}_i\mathbf{k})$ shifts the center of the Wannier function to the lattice position $\mathbf{r}_i$, the ith lattice site. The Wannier functions centered at different lattice sites are orthogonal. The phase coming with every Bloch functions $\exp(\mathrm{i}\phi_\mathbf{k})$ is arbitrary, which leads, for N Bloch functions, to $N-1$ free parameters. Here we do not count the overall phase. These parameters can be used to put certain restrictions to the Wannier function. For instance, the Coloumb energy of two particles, described by Wannier functions, can be extremized. Minimizing the width of the density function $\langle W_i|\mathbf{r}^2|W_i\rangle - \langle W_i|\mathbf{r}|W_i\rangle^2$ is another method to uniquely determine the phases. In 1D Kohn [133] was able to show that a unique set of phases leads to maximally localized Wannier functions which are characterized by an exponential decay of the envelope functions in the tails. So far the spatial exponential decay of envelope functions in 3D, taking into account only the first band, has not yet been proven [157]. From now on, we consider only maximally localized Wannier functions. Increasing the lattice potential, the shape of Wannier functions is approaching Gauss functions.

1.5.2   Hubbard Hamiltonian

Having a relatively deep lattice potential and a small interaction, the Wannier functions form a reliable basis. The field operator is expressed in the Wannier basis and reads:

$$\Psi^\dagger(\mathbf{r}) = \sum_i W_i(\mathbf{r})c_i^\dagger \quad , \tag{1.4}$$

where W_i is the Wannier function localized around the lattice site i. Plugging equation (1.4) into the Hamiltonian (1.1), and using the mean-field approximation in equation (1.2) the Hamiltonian can be brought into the from:

$$H = -\sum_{\langle ij\rangle} t_{ij}(c_i^\dagger c_j + h.c) + \frac{1}{2}\sum_i U_i\hat{n}_i(\hat{n}_i - 1) + \frac{1}{2}\sum_{\langle ij\rangle} U_{ij}\hat{n}_i\hat{n}_j \quad , \tag{1.5}$$

where the coefficients are:

$$t_{ij} = \int \mathrm{dx}^3 W_i(\mathbf{x})\left(\frac{\hbar^2}{2m}\Delta + V(\mathbf{x})\right)W_j(\mathbf{x}) \quad , \tag{1.6}$$

$$U_i = \frac{4\pi a_\mathrm{s}\hbar^2}{m}\int \mathrm{dx}^3 |W_i(\mathbf{x})|^4 \quad , \tag{1.7}$$

$$U_{ij} = \frac{4\pi a_\mathrm{s}\hbar^2}{m}\int \mathrm{dx}^3 |W_i(\mathbf{x})|^2|W_j(\mathbf{x})|^2 \quad .$$

t_{ij} are the tunneling rates, also called hopping elements, between site i and site j; U_i (U_{ij}) are the self-interaction amplitudes. The c_i and $c_i^\dagger$ are annihilation and creation operators at lattice site i, which can obey, depending on the considered model, fermionic or bosonic commutation relations. In the following we denote fermionic annihilation operators with f_i and bosonic annihilation operators with b_i. Of curse in the case of single component fermions we set $U_i = U_{ij} = 0$. If the wavefunctions are sufficiently strong localized, for instance, when the lattice potential is deep, the density-density overlap of Wannier function at different, not nearest neighbored, lattice sites is negligible. The same holds for the tunneling. Therefore, we consider tunneling and density-density overlap only between neighbored lattice sites. This is in the Hubbard model (1.5) depicted with a sum over $\langle ij \rangle$, labeling the neighboring sites i and j. The model describes i) hopping between sites with a hopping probability t_{ij}, ii) self-interaction energy between particles with amplitude U_i iii) interaction between particles in neighboring sites with the amplitude U_{ij}. Depending on the commutation relation of the operators the model describes bosonic or fermionic atoms. In the homogeneous case U_i, t_{ij} and U_{ij} do not depend on the lattice site.

1.5.3   Delocalized states

Without nonlinear interactions U_i and U_{ij} the system is exact diagonalizable. The eigenfunctions are Bloch functions, which are completely delocalized and phase correlated. Unfortunately, such states are not present in the spatial description of the Hubbard model. Therefore, it is difficult to classify phase correlation in this frame directly. In principle, one could describe the system with the Hubbard model in momentum space. The field operators are a linear combination of operators, creating and annihilating Bloch waves. The tunneling is calculated similar as in equation (1.6). The Wannier functions at lattice position i and j are replaced by Bloch function with quasi-momentum $\mathbf{k}$ and $\mathbf{k}'$. Unfortunately, the self-interaction terms for larger differences of $\mathbf{k}$ and $\mathbf{k}'$ are non-vanishing. Hence, one has to sum in the tunneling term and in the self-interaction term over all pairs $\mathbf{k}$ and $\mathbf{k}'$, which is, compared to the spatial Hubbard Hamiltonian, a demanding task.

Fortunately, the number of particles does not commute with the phase operator $[\hat{n}, \Phi] = i\mathbb{1}$, where $\hat{n}$ is the number operator, and $\hat{\Phi}$ is the phase operator [43]. Therefore, when in a given system the particle number per lattice site is fixed (Mott insulator) a common phase can not be determined. On the other hand, when the phase is fixed (superfluid phase), the particle number at each lattice site fluctuates. Possible candidates for an order parameter are the deviation of the particle number $\Delta n^2 = \langle \hat{n}^2 \rangle - \langle \hat{n} \rangle^2$, and the

superfluid order parameter $\psi = \langle c_i \rangle$, where c_i is the annihilation operator at the site i and $\hat{n} = c^\dagger c$ is the number operator. In subsection 1.5.4 it is shown, that the superfluid order parameter minimizes also a variational parameter in the mean-field theory.

1.5.4 Mean-field theory

The Hubbard Hamiltonian is acting in a Hilbert space of an enormous size. M bosons distributed in a lattice with N cells leads to $N^M/M!$ orthogonal states. Brute force diagonalization is only possible for small systems with a small number of atoms, it suffers then from finite size effects. A way to treat systems with bigger size are analytical methods, such as the Bethe ansatz, which however is limited to certain specific 1D systems [22, 75]. A very powerful method to treat a huge range of systems is the Quantum Monte Carlo algorithm (see e.g. [233]). In some frustrated spin systems, the Quantum Monte Carlo algorithm suffers from the so-called " negative sign" problem. Moreover, this method is numerical demanding, since the computation time grows rapidly with the demanded accuracy. Another way is the truncation of the Hilbert space. In the past years successful methods have been developed, such as the Density Matrix Renormalization Group methods [191, 235], or the Vidal algorithm [224, 225]. Although attempts to treat systems with higher dimensions have been made [219, 220], the main applications are 1D systems with a sufficiently short ranged correlation length. Yet another method is the strong coupling method [86], which can be applied to higher dimensions. With relatively little effort one gets results, which have almost the accuracy obtained in a Quantum Monte Carlo simulation. For many problems, the easiest method to get a good insight into the problem are the mean-field considerations. In the mean-field description [195] one analyzes a local cell exactly, and treats the site to site tunnel couplings perturbatively. The Hamiltonian H_{MF} is a sum of single-site Hamiltonians, and reads:

$$H_{\mathrm{MF}} = \sum_i \left(-t2d \left(\psi c_i^\dagger + \psi^* c_i - \psi\psi^* \right) + U\hat{n}_i \left(\hat{n}_i - 1 \right) - \mu\hat{n}_i \right) \quad , \quad (1.8)$$

where ψ is a variational parameter, and d the dimension of the system. The form of ψ can be obtained by calculating the energy of the ground state of H_{MF}, and subtracting the energy of this wavefunctions in the Hubbard model. Since H_{MF} is a sum of single site Hamiltonians, the ground state is a product state of single site solutions. The energy difference per site is:

$$\Delta E = \frac{E_0}{N} - \frac{E_{\mathrm{MF}}}{2}$$
$$= 2dt \left(\psi\langle c^\dagger \rangle + \psi^*\langle c \rangle - \psi\psi^* - \langle c^\dagger \rangle\langle c \rangle \right) \quad .$$

Apparently, the difference is minimal at $\psi = \langle c \rangle$. In many cases the interest lies in the energy, which is perturbatively shifted by the neighbored cells. The perturbation part in equation (1.8) is $\mathcal{W} = -t2d\left(\psi c^\dagger + \psi^* c\right)$. Up to second order perturbation theory the ground state energy reads:

$$E = E_0 - t\psi^2 + \sum_{j \neq 0} \frac{|\langle \Psi_0 | \mathcal{W} | \Psi_j \rangle|^2}{E_0 - E_j} \quad .$$

This simple tool gives, in many cases, a good hint for phase transitions in a system. The method can be improved with little numerical effort by modifying the superfluidity order parameter self-consistently [38].

In Bose systems for small hopping elements the ground state is a Mott insulator, which is classified in the mean-field treatment with a vanishing superfluid order parameter $\psi = 0$. Considering a square lattice in 2D or 3D respectively, one has an integer filling per lattice site, and an exponential decay of the phase coherence length. Creating a particle hole excitation requires a finite energy, therefore, the Mott insulator phase is incompressible [80]. In the superfluid phase $|\psi|^2 > 0$ is finite. In 2D the phase correlation decays algebraically with an increasing distance, and exhibits true long range order in 3D. The latter statements are modified by the presence of external trap potentials.

CHAPTER 2

COMPOSITE FERMIONS IN OPTICAL LATTICES

2.1 Introduction

The rethermalization time of an atom gas that initially is not in thermal equilibrium depends on the scattering rate of the atoms, and determines the applicability of evaporative cooling. However, for ultracold fermions evaporative cooling is unreliable since they do not interact via s-wave scattering. In this case, a suitable method is sympathetic cooling using a bosonic reservoir. This possibility has led to several recent experiments on trapped ultracold boson-fermion mixtures [108, 109, 167, 200]. So far, temperatures $T \sim 0.05$ T_F have been obtained, where T_F is the Fermi temperature at which the Fermi gas starts to exhibit quantum degeneracy (typically of the order of 1 - 10 μK).

Although the main goal of these experiments is to achieve the BCS transition in atomic Fermi gases, several groups have recently shown a growing interest in the physics of ultracold boson-fermion mixtures themselves, including the analysis of the ground state properties, stability, excitations, and the effective fermion-fermion interaction mediated by the bosons [6, 42, 146, 189, 227]. Additionally, new experimental developments have drawn attention to the behavior of these mixtures in 1D geometries [44, 62] and optical lattices [8, 35, 159, 204]. Recently, the first experimental results of bose-fermion mixtures in optical lattices have been reported [107, 177].

In this chapter a boson-fermion lattice gas is investigated, i.e. a mixture of ultracold bosonic and fermionic atoms in an optical lattice. We discuss the limit of strong atom-atom interactions (strong coupling regime) $t \ll U, V$ at low temperatures, where t is the tunneling rate, U denotes the self-interaction strength of bosons, and V is the interaction strength between bosons and fermions (see equation (1.5)). In the first part of this chapter

the existence of novel quantum phases is predicted. In these phases fermions
are paired either with bosonic holes, if the interaction between fermions and
bosons is repulsive [1], or with bosons, if the interaction is attractive. In
the strong coupling limit the hopping can be treated perturbatively. For
sufficiently low temperatures (in real experiments in the order of $10nK$)
we derive an effective Hamiltonian expressed solely with the new composite
fermions. The composite fermions may form a normal Fermi liquid, a density
wave, a superfluid, or an insulator with fermionic domains, depending on the
parameters characterizing the system.

In the second part of this chapter we determine the phase diagram of the
system for arbitrary values of the chemical potential, boson-fermion coupling
and tunneling (hopping) amplitudes, using a relatively simple mean-field
theory [195]. In this sense our results can be considered as a generalization
of the seminal analysis of the Bose-Hubbard model by Fisher *et al.* [80]. We
obtain the analytic form of the phase boundaries separating the composite
fermion phases, and the phase consisting of a bosonic superfluid coexisting
with a Fermi liquid.

The third part considers a numerical method to verify the analytic results
of the mean-field theory. First, we obtain the ground state by minimizing
the energy using a downhill method; then, the phase diagram is derived by
quasi-statically changing the system parameter using the time dependent
Gutzwiller ansatz. The results are shown to agree with the analytical deriva-
tions.

2.2   Description of the model

The system of fermions and bosons loaded in a lattice is described by the
Bose-Fermi-Hubbard model, which is an extension of equation (1.5):

$$H_{\mathrm{BFH}} = -\sum_{\langle ij \rangle} (t_B b_i^\dagger b_j + t_F f_i^\dagger f_j + \mathrm{h.c.})$$
$$+ \sum_i \left[\frac{1}{2} n_i(n_i - 1) - \mu n_i \right] + \alpha \sum_i n_i m_i \quad , \qquad (2.1)$$

The boson-boson interaction amplitude U has been set here to be the energy
unit (see equation (1.7)); $b_i^\dagger$, b_j, $f_i^\dagger$, f_j are the bosonic and fermionic cre-
ation and annihilation operators, respectively, $n_i = b_i^\dagger b_i$, $m_i = f_i^\dagger f_i$, μ is the
bosonic chemical potential, and α is the interaction energy between bosons

---

[1]The formation of composite fermions in gaseous boson-fermion mixtures was consid-
ered recently for the case of attractive boson-fermion interaction by [129].

and fermions. The fermionic chemical potential is absent in H_{BFH}, since the fermion number is fixed. We assume that the temperature is sufficiently low, or the lattice wells are deep enough, so that $k_{\mathrm{B}}T \ll \Delta E$, where ΔE is the energy gap between the first and the second band. If the number of fermions is smaller than the number of lattice sites $\rho_F \leq 1$, the atoms occupy the lowest band [8] (c.f. [14]).

The Bose-Fermi-Hubbard model describes:

- nearest neighbor boson (fermion) hopping, with an associated negative energy, $-t_B$ $(-t_F)$; in the following we assume $t_F = t_B = t$.

- on-site repulsive boson-boson interactions with an associated energy $U = 1$.

- on-site boson-fermion interactions with an associated energy $\alpha = V/U$, which is positive (repulsive) in our consideration.

In the limit of small hopping $t \ll 1$ and, $\alpha \simeq 1$ the hopping part can be treated perturbatively.

2.3   Composite fermions

2.3.1   Composite fermions without tunneling

In order to get a first insight into the physics of the system we analyze the case of vanishing hopping ($t = 0$). By setting also $\alpha = 0$, we obtain the simplest case. Now fermions and bosons are decoupled, which means the fermions can occupy any available many-body state on top of a bosonic Mott insulator background.

The energy per lattice cell, which is caused by bosons, is $E_B = 1/2n(n - 1) - n\mu_B$. For $\mu = 0$ the energy is minimized, if $n = 0$ or $n = 1$. At integer $\mu = K$ the ground state is degenerated with boson numbers $n = K$, and $n = K + 1$. Consequently, for any chemical potential $K \leq \mu \leq K + 1$ the energy is minimized for $n = K + 1$. In other words, the number of bosons in the ground state is $n = [\mu] + 1$, where $[\mu]$ is the integer part of μ. If α is positive and sufficiently large the fermions push the bosons out of the sites that they are occupying, or, if α is negative, they attract bosons. On a site occupied by a fermion, the energy reads $E_{bf} = 1/2n(n-1) - n(\mu - \alpha)$. Using the same argumentation as above the energy is minimized if the number of bosons is $n = [\mu - \alpha] + 1$. The presence of a fermion at a lattice site alters the number of bosons by $s = [\mu] - [\mu - \alpha]$. Depending on α, s can be positive, when s bosons are repelled or negative, when $(-s)$ bosons are

attracted. Summarizing, for $\mu - [\mu] + s > \alpha > \mu - [\mu] + s - 1$, a fermion creates s holes or, in the case of $s < 0$, attracts $(-s)$ bosons. The bosons form a Mott insulator with $\tilde{n}$ particles per site. If a fermion is placed at a particular lattice site, it will expel s bosons. Hence, for the ground state we obtain the following conservation law:

$$n(m) = \tilde{n} - sm \quad . \tag{2.2}$$

In the unperturbed ground state we will meet a fermion always paired with s bosonic holes, or, in the case of $s < 0$ with $(-s)$ additional bosons. Therefore, we define the operator:

$$\tilde{f}_i = \sqrt{\frac{(\tilde{n} - s)!}{\tilde{n}!}} (b_i^\dagger)^s f_i$$

$$\text{or} \left(\sqrt{\frac{\tilde{n}!}{(\tilde{n} - s)!}} (b_i)^{-s} f_i \right) \quad . \tag{2.3}$$

The proof, that $\tilde{f}_i$ obeys the fermionic commutation relations is written in the appendix (A.1). It is clear that s must not exceed the maximal possible numbers of holes limited by $\tilde{n}$. On the other hand, s may attain arbitrary negative integer values, i.e., we may have composite fermions containing one fermion and many bosons in the case of very strong attractive interactions, $\alpha < 0$, and $|\alpha| \gg 1$. From the point of view of experience, the cases of small s are more interesting, since as we shall see below, the composite fermions are more mobile for small s.

2.3.2   Phase diagram for zero tunneling

As it was described in the subsection 2.3.1 the form of the composite fermions depends on the chemical potential for bosons μ and on interaction amplitude between bosons and fermions α. A phase diagram for different forms of composite fermions in the α-μ plane is depicted in figure 2.1. Crossing the border lines between the phases means a fermion is attracting or repulsing an altered number of bosons, or the number of bosons in the Mott background changes. Hence, while the number of fermions is fixed, the number of bosons varies. Of course, this is only possible in a grand canonical system, e.g. we determine the number of bosons with the chemical potential. In experiments the system is in a shallow harmonic trap. The r-dependent on-site potential is equivalent to the spatially dependent chemical potential. With this setup, one can examine more than one region at the same time.

2.3.3   Composite fermions at a finite tunneling rate

Tracing out all sites apart of site i, the wavefunction is a linear combination of all possible Fock states at the position i: $|\psi\rangle_i = \sum_{b=0}^{\infty} \sum_{f=0}^{1} c_{b,f} |b, f\rangle_i$, where the coefficients $c_{b,f}$ are normalized $\sum_{b=0}^{\infty} \sum_{f=0}^{1} |c_{b,f}|^2 = 1$; b (f)is the number of bosons (fermions) in a particular Fock state. For zero tunneling the system can be entirely described using the composite fermions, which corresponds for the case of $s = 1$ and $\tilde{n} = 1$, to the state $|\psi\rangle_i = \alpha |01\rangle_i + \beta |10\rangle_i$. The mean number of composite fermions at lattice site i is α^2. On the other hand, for finite tunneling one has to check carefully that $\alpha^2 + \beta^2 \approx 1$, which means, the most relevant Fock states are $|01\rangle$ and $|10\rangle$.
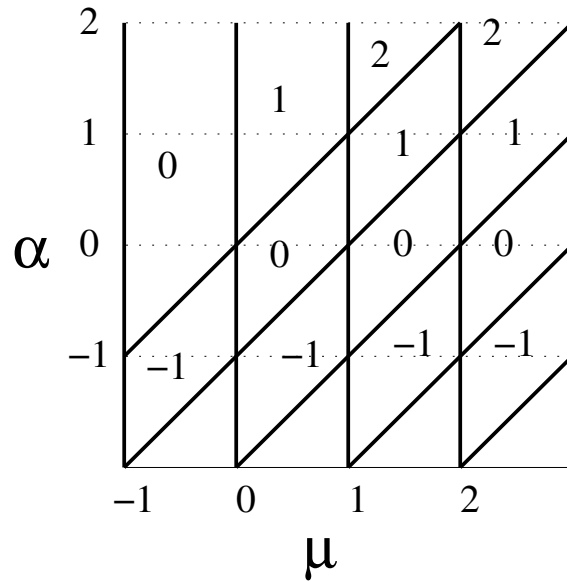

Figure 2.1.   *The number of bosons per site in the Mott back-ground depends on the chemical potential μ. For example the number of bosons per site is 1 for $0 \leq \mu \leq 1$. The number in the phase diagram show the number of bosonic holes in the presence of a fermion. If the number is negative, the fermion attracts bosons.*

2.4   Degenerate perturbation theory

If the kinetic part $H_1 = -t \sum_{\langle ij \rangle} \left[b_i^\dagger b_j + f_i^\dagger f_j + h.c. \right]$ is sufficiently small it acts as a perturbation of the diagonal part of the Hamiltonian:

$$H_0 = \sum_i \frac{1}{2} n_i (n_i - 1) - \mu n_i + \alpha m_i n_i \quad .$$

In the case of vanishing t, and a filling between 0 and 1 fermions per lattice site, the ground state consisting of composite fermions, is highly degenerated, e.g. a lattice with N sites and $0 < M < N$ fermions has

$$\# = \left(\begin{array}{c} N \\ M \end{array} \right)$$

orthogonal ground states. We introduce a projector $\mathcal{P}$, which is projecting any state into the subspace of ground states. The operator $\mathcal{Q}$ is orthogonal to $\mathcal{P}$ ($\mathcal{Q} + \mathcal{P} = 1$). Hence $\mathcal{P}\psi = \psi_0$ and $\mathcal{Q}\psi = \psi_1$, where ψ_0 is an element of the subspace of degenerated ground states with the corresponding energy E_0 and ψ_1 is an exited states. We now apply $\mathcal{Q}$ on the Hubbard model (2.1):

$$\mathcal{Q} \left(H_0 + H_1 \right) \left(\psi_0 + \psi_1 \right) = \left(E_0 + E_1 \right) \psi_1$$
$$\Rightarrow \quad \mathcal{Q} H_0 \psi_1 + \mathcal{Q} H_1 \psi_0 = \mathcal{Q} \left(E_0 + E_1 \right) \psi_1 \quad ,$$

here $\mathcal{Q} H_1 \mathcal{Q} \psi = \mathcal{Q} H_1 \psi_1$ is omitted. Therefore, we can express:

$$\psi_1 = \mathcal{Q} \frac{1}{E_0 + E_1 - H_0} \mathcal{Q} H_1 \psi_0 \quad .$$

On the other hand, applying $\mathcal{P}$ to equation (2.1) yields:

$$\mathcal{P} H_0 \psi_0 + \mathcal{P} H_1 \psi_1 = \left(E_0 + E_1 \right) \psi_0$$
$$\Rightarrow \left(\mathcal{P} H_0 \mathcal{P} + \mathcal{P} H_1 \mathcal{Q} \frac{1}{E_0 + E_1 - H_0} \mathcal{Q} H_1 \right) \mathcal{P} \psi_0 = \left(E_0 + E_1 \right) \psi_0 \quad . \quad (2.4)$$

This is an effective Hamiltonian acting in the space of the ground states of H_0. We expand equation (2.4) up to second order in t:

$$\left\{ \mathcal{P} H_0 \mathcal{P} + \mathcal{P} H_1 \mathcal{Q} \frac{1}{E_0 - H_0} \mathcal{Q} H_1 \mathcal{P} \right\} \psi_0 = E \psi_0 \quad . \quad (2.5)$$

The left hand site of this equation acting on any state yields elements of the degenerated ground state. H_1 describes the process of tunneling. For the
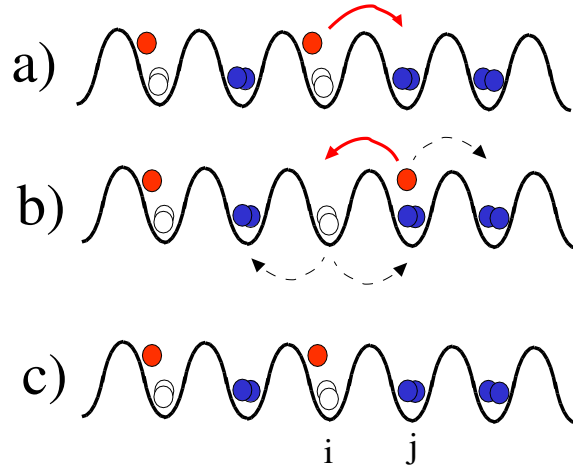
Figure 2.2. *a) With the hopping of a fermion from site i to site j one application of H_1 transforms the ground state to an excited state (big red line). b) Only one part of the second H_1 brings the state back into the subspace of degenerated ground states as shown in c) (big red line, while the small dashed lines would lead to other excited states). In the same way the holes hopping to another place have to come back.*

non-trivial case, where $s \neq 0$ only few contributions of the twofold application of H_1 are important. A process where a boson (fermion) tunnels from site i to site j is only contributing when in the second hopping process brings it back from j to i. This virtual tunneling is illustrated in figure 2.2. In general, the perturbation part of equation (2.5) takes the form:

$$\mathcal{P}H_1\mathcal{Q}\frac{1}{E_0 - H_0}\mathcal{Q}H_1\mathcal{P}\psi_0 = \left(\sum_{\langle ij \rangle} b_i^\dagger b_j \frac{1}{E_0 - H_0} b_i b_j^\dagger + \sum_{\langle ij \rangle} f_i^\dagger f_j \frac{1}{E_0 - H_0} f_i f_j^\dagger \right) \psi_0.$$
(2.6)

Up to the second order perturbation theory hopping of composite fermions is allowed only for $|s| = 1$. For $s = 1$ the hopping for composite fermions

comprises the hopping of a boson and of a fermions and is:

$$
\mathcal{P}H_1\mathcal{Q}\frac{1}{E_0-H_0}\mathcal{Q}H_1\mathcal{P}\psi_0 = \left(\sum_{\langle ij \rangle} b_i^\dagger b_j \frac{1}{E_0-H_0} f_i f_j^\dagger \right.
$$

$$
\left. + \sum_{\langle ij \rangle} f_i^\dagger f_j \frac{1}{E_0-H_0} b_i b_j^\dagger + h.c. \right) \psi_0 \quad . \qquad (2.7)
$$

The situation is similar for $s = -1$, where, for the bosons, only the indices i and j have to be exchanged. In order to analyze equation (2.6) we need the values of the denominators, which are:

$$
E_0 - E(n_i + 1, n_j - 1, m_i = 0, m_j = 0) = -(1 - m_i)(1 - m_j)
$$
$$
E_0 - E(n_i + 1, n_j - 1, m_i = 1, m_j = 0) = m_i(1 - m_j)(-\alpha - 1 + s)
$$
$$
E_0 - E(n_i + 1, n_j - 1, m_i = 0, m_j = 1) = (1 - m_i)m_j(\alpha - 1 - s)
$$
$$
E_0 - E(n_i + 1, n_j - 1, m_i = 1, m_j = 1) = -m_i m_j
$$
$$
E_0 - E(n_i, n_j, m_i = 0, m_j = 1) = -(1 - m_i)m_j \alpha s \quad ,
$$

where $E(n_i, n_j, m_i, m_j)$ is the energy and n_i, n_j, m_i and m_j are the corresponding number of bosons and fermions occupying the places i and j. Terms, constant or linear in m_i, are energetically independent of the configuration. If we only consider bilinear terms $m_i m_j$, the perturbative part reads:

$$
\mathcal{P}H_1\mathcal{Q}\frac{1}{E_0-H_0}\mathcal{Q}H_1\mathcal{P}\psi_0 = \sum_{\langle ij \rangle} \delta_{m_i,1}\delta_{m_j,1} \left(\frac{\tilde{n}(\tilde{n}-s+1)}{1+\alpha-s} + \frac{(\tilde{n}-s)(\tilde{n}+1)}{1-\alpha+s} \right.
$$

$$
\left. -\tilde{n}(\tilde{n}+1) - (\tilde{n}-s)(\tilde{n}+1-2) + \frac{1}{\alpha^2} \right)
$$

$$
= K_{eff} \sum_{\langle ij \rangle} \tilde{m}_i \tilde{m}_j \quad ,
$$

with the density operator $\tilde{m}_i = \tilde{f}_i^\dagger \tilde{f}_i$ and:

$$
K_{eff} = 2t^2 \left\{ \frac{\tilde{n}(\tilde{n}+1-s)}{1+\alpha-s} + \frac{(\tilde{n}-s)(\tilde{n}+1)}{1-\alpha+s} \right.
$$

$$
\left. +\frac{1}{\alpha s} - \tilde{n}(\tilde{n}+1) - (\tilde{n}-s)(\tilde{n}+1-s) \right\} \quad .
$$

For $s = 0$ the fermions and bosons are practically independent, hence, a perturbative treatment is not required. If $|s| = 1$ the perturbative expansion

up to second order in t allows hopping of composite fermions. For $s = 1$ the corresponding terms of equation (2.7) can be analyzed:

$$\sum_{\langle ij \rangle} f_i^\dagger f_j \frac{1}{E_0 - H_0} b_i b_j^\dagger + b_i^\dagger b_j \frac{1}{E_0 - H_0} f_i f_j^\dagger = -t^2 \sum_{\langle ij \rangle} (1 - m_i) m_j 2 \frac{\tilde{n}}{\alpha} \quad ,$$

while for $s = -1$ the result is:

$$\sum_{\langle ij \rangle} f_i^\dagger f_j \frac{1}{E_0 - H_0} b_i^\dagger b_j + b_i^\dagger b_j \frac{1}{E_0 - H_0} f_i^\dagger f_j = t^2 \sum_{\langle ij \rangle} (1 - m_i) m_j 2 \frac{\tilde{n} + 1}{\alpha} \quad .$$

In terms of composite fermions the effective Hamiltonian reads:

$$H_{eff} = -J_{eff} \sum_{\langle ij \rangle} \left(\tilde{f}_i^\dagger \tilde{f}_j + h.c. \right) + K_{eff} \sum_{\langle ij \rangle} \tilde{m}_i \tilde{m}_j \quad , \qquad (2.8)$$

with $J_{eff} = t^2 2\tilde{n}/\alpha$ for $s = 1$ and $J_{eff} = t^2 2(\tilde{n} + 1)/\alpha$ for $s = -1$. This model was studied using a Gutzwiller ansatz in reference [196]. In order to consider hopping for composite fermions with $|s| > 1$, higher order terms in t are required. In experiments the temperature has to be lower than the typical energy scales of the system. Studying the effective Hamiltonian for $|s| = 1$ the required temperature is $kT \ll Ut^2$ (t is normalized by U). Considering the effects of higher order terms is more demanding, since the required temperature drops with higher orders in t.

2.5 "Simple man's" mean-field theory

With the quite simple technique of changing the hopping element for bosons by ramping the lattice depth, Greiner *et al.* have shown the transition from a Mott insulator to a superfluid phase and vice-versa in a 3D optical lattice. The same technique should be applicable for examining the phase transition in our system. When working with composite fermions it is necessary to know, at least, approximately the boundary of the phases. In this section we analyze this problem using a simple version of mean-field theory. These results, however can be confirmed using more sophisticated methods as quantum Quantum Monte Carlo simulation, strong coupling expansion, or in 1D with Vidal's algorithm or Density Matrix Renormalization Group methods [235], respectively in 2D with the method developed by F. Verstraete and J.I. Cirac [219]. For simplifications we consider the system in the case of vanishing temperature $T \rightarrow 0$, but still $k_B T \gg t_F$, in such a way that we can safely assume $t_F = 0$. In order to analyze the relevant intermediate

case $t_B \simeq U, V$, we employ a mean-field formalism [80, 195, 218], where we analyze only homogeneous phases. It is shown in appendix (A.2), that the homogeneous phase, at least, is energetically a local minimum in the Hilbert space. If the V is sufficiently small, the ground state is homogeneous. The analysis of finite temperature effects and inhomogeneities caused by the trap potential [19] is interesting in itself, and has been recently the subject of investigations in [52]. It is particularly interesting, that a random on-site chemical potential in a fermion-boson mixtures can lead to various phases in disordered systems [196].

We use the variational parameter, also known as the superfluid order parameter, $\psi = \langle b_i \rangle = \langle b_i^\dagger \rangle$, which is independent of the lattice site. Closed to a Mott insulator state $(\psi - b_i)(\psi - b_i^\dagger) = \mathcal{O}^2$ holds and, neglecting higher order in the fluctuations, we can substitute the kinetic term $b_j^\dagger b_i = \psi(b_j^\dagger + b_i) - \psi^2$. In this way, we model the Hamiltonian H_{BFH} (2.1) by a sum of single-site Hamiltonians:

$$H_{MF} = \sum_i H_{0i} - \mathcal{W}_i \quad , \tag{2.9}$$

with

$$H_{0i} = \frac{1}{2} n_i (n_i - 1) + \alpha n_i m_i - \mu_F m_i - \mu_B n_i + 2 d t_B \psi^2$$

$$\mathcal{W}_i = 2 d t_B \psi \left(b_i + b_i^\dagger \right) \quad ,$$

where d is the spatial dimension.

As previously discussed (see equation (2.2)), the ground state of H_{0i} consists of $n(m) = \tilde{n} - sm$ bosons per site, where m is the number of fermions at a particular lattice site. s depends on the particular region in the phase space plotted in figure 2.1. If one has a fermionic density of $0 \leq \rho_F \leq 1$ fermions per lattice the ground state can be chosen to be homogeneous:

$$|\psi\rangle = (1 - \rho_F)|\tilde{n}, m = 0\rangle + \rho_F |\tilde{n} - s, m = 1\rangle \quad .$$

In the ground state, for a given fermionic filling factor ρ_F, the probability that a fermion occupies a particular lattice site is ρ_F, respectively $(1 - \rho_F)$ for the absence of a fermion. Therefore, the ground state can be written as:

$$\begin{aligned} |\phi_0\rangle\langle\phi_0| &= (1 - \rho_F)|n = \tilde{n}, m = 0\rangle\langle n = \tilde{n}, m = 0| \\ &+ \rho_F |n = \tilde{n} - s, m = 1\rangle\langle n = \tilde{n} - s, m = 1|. \end{aligned}$$

The zeroth-order energy is of the form $E_0 + 2 d t_B \psi^2$, where $E_0 = E_0(\tilde{n}, 0)(1 - \rho_F) + E_0(\tilde{n} - s, 1)\rho_F$, with

$$E_0(n, m) = \frac{V}{2} n(n - 1) + Unm - \mu_B n - \mu_F m \quad . \tag{2.10}$$

Due to the form of $\mathcal{W}_i$ in equation (2.9), the lowest order correction introduced by the tunneling occurs at the second order perturbation theory:

$$E_2 = \psi^2 \sum_n \left\{ \frac{|\langle \tilde{n}, 0 | \mathcal{W} | n, 0 \rangle|^2}{E_0(\tilde{n}, 0) - E_0(n, 0)} (1 - \rho_F) \right.$$
$$\left. + \frac{|\langle \tilde{n} - s, 1 | \mathcal{W} | n, 1 \rangle|^2}{E_0(\tilde{n} - s, 1) - E_0(n, 1)} \rho_F \right\} \quad ,$$

where $\mathcal{W} = \sum_i \mathcal{W}_i$. Following the Landau argument for second order phase transitions, one can easily write $E = E_0 + 2dt_B r \psi^2 + \mathcal{O}(\psi^4)$. The form of r is derived in the appendix and reads:

$$r = 1 - t_B 2d \left[(1 - \rho_F) \left(\frac{\left(\sqrt{\tilde{n}} - \sqrt{\tilde{n}+1} \right)(\tilde{n} - \mu_B) + \sqrt{\tilde{n}+1}}{(\tilde{n} - \tilde{\mu}_B - 1)(\tilde{n} - \mu_B)} \right) \right.$$
$$\left. + \rho_F \left(\frac{\left(\sqrt{\tilde{n}-s} - \sqrt{\tilde{n}-s+1} \right)(\tilde{n} - s + \alpha - \mu_B) + \sqrt{\tilde{n}-s+1}}{(\tilde{n} - s + \alpha - \tilde{\mu}_B - 1)(\tilde{n} - s + \alpha - \mu_B)} \right) \right] \quad .$$

If $r > 0$ the system minimizes the energy at $\psi = 0$ (normal phase), whereas, if $r < 0$, a nonzero ψ (superfluid) is energetically favorable. Therefore, the curve $r = 0$ is a 2D manifold and describes the boundaries between a superfluid phase and a Mott insulator. We consider two limits. First, without fermions ($\rho_F = 0$), the Mott loops are independent of α, as it was discussed in reference [80]. If $\rho_F = 1$ the fermions form a background and change effectively the chemical potential for the bosons. The chemical potential increases linearly with α. Interesting are the intermediate states $0 < \rho_F < 1$.

In figure 2.3 we have depicted the phase boundaries ($r = 0$) for different values of α and different regions in the μ_B-t_B phase space at different filling factors.

2.6 Numerical results

An exact treatment of the problem can be performed by incorporating the complete Hilbert space. In a system with M lattice sites, F fermions and B bosons the number of orthogonal states is:

$$\# = \binom{M}{F} \frac{M^B}{B!} \quad .$$

The Hilbert space of a relative small square lattice with 10×10 sites and half filling of bosons, respectively fermions has $\approx 0.3 \times 10^{65}$ states. So far,
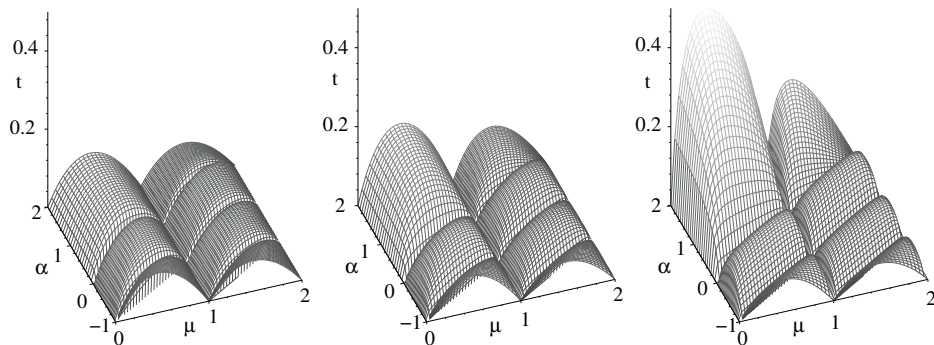
Figure 2.3.   *The phase boundary obtained in mean-field approximations are depicted by the surface plots for different fermion fillings: a) for $\rho_F = 0.1$, b) $\rho_F = 0.5$ and c) $\rho_F = 0.9$.*

we are not able to diagonalize such systems exactly. For large systems, every numerical method truncates the Hilbert space. It turned out that in 1D Vidal's algorithm [224, 225] and routines using density renormalization groups [235] are reliable. Both routines only consider the relevant low dimensional subspace of an exponential large Hilbert space. In 2D or higher dimension only in limited cases such routines are applicable [219]. In these dimensions, despite an exponential decay of the eigenvalues of the density matrix, the number of relevant non-truncated states is increasing too fast with the system size [53]. To examine systems in 2D and 3D the Quantum Monte Carlo simulation is an appropriate routine [233]. Satisfying results can be obtained using the mean-field approximation. In higher dimensions the mean-field approximation becomes exact [92], but it is already reliable in 2D or 3D.

One way of treating the system in a mean-field approximation is to use the Gutzwiller ansatz, which is a product state of independent local site solutions. The local solution is a linear combination of Fock states, hence, the general Gutzwiller ansatz reads:

$$|\phi\rangle = \prod_i \sum_{n_i=0}^{N_{max}} \sum_{m_i=0}^{1} f_{n,m}^{(i)}|n_i, m_i\rangle \quad ,$$

where n denotes the number of bosons and m the number of fermions. The Gutzwiller coefficients $f_{n,m}$ satisfy the normalization condition $\sum_{nm} |f_{n,m}|^2 = 1$. The index i runs over all lattice sites. We neglect fermionic anticommutation rules between operators at different sites [2]. As it is shown in figure 2.4,

---

[2]For a detailed discussion see appendix (A.4).

for a low average occupation density for bosons and relative small hopping, the value of the Gutzwiller coefficients for increasing n_i drops fast. For $n = 1$ we choose $N_{max} = 5$.
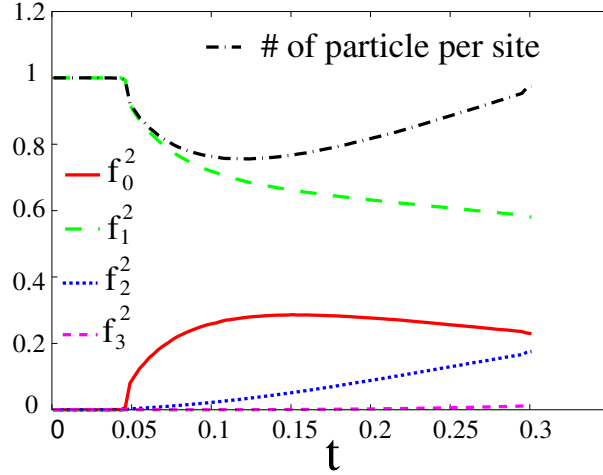
Figure 2.4. *The modulus square of Gutzwiller coefficients versus the tunneling rate for $\mu = 0.1$ and minimized energy. f_4^2 is already negligible. Also plotted is the number of particles.*

In the following, we consider only homogeneous phases, although the calculation can be straightforwardly extended to inhomogeneous phases. Using periodic boundary conditions, the ground state can be found by minimizing the energy on a single cell.

Starting from the chosen ground state, we evolve in the phase space by quasi-statically varying the parameters α and t in a time evolution. In order to perform this time evolution we extremize:

$$\frac{\partial}{\partial f_{n,m}^*} \langle i\hbar\partial_t - H \rangle = 0 \quad,$$

hence, for the Gutzwiller coefficients we get:

$$i\dot{f}_{n,m}^{(i)} = \left(\frac{1}{2}n(n-1)\right) f_{n,m}^{(i)} + t_b \left[\Phi_i^{b*}\sqrt{n+1}f_{n+1,m}^{(i)} + \Phi_i^b\sqrt{n}f_{n-1,m}^{(i)}\right]$$
$$+ t_f \left[\Phi_i^{f*}\delta_{m,0}f_{n,1}^{(i)} + \Phi_i^f\delta_{m,1}f_{n,0}^{(i)}\right] + \alpha\delta_{m,1}nf_{n,1}^{(i)} \quad,$$
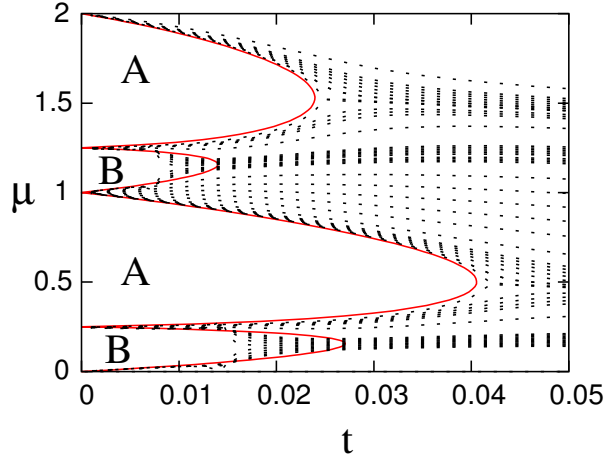
Figure 2.5.   *Phase diagram as a function of the hopping t, and the bosonic chemical potential μ, for $\alpha = 0.25$ and $\rho_F = 0.25$. Thin red solid lines: analytical results for $t_F = 0$; Dashed solid lines: numerical results for $t_F = t_B = t$. Phases A are formed by a Mott insulator phase for the bosons and a Fermi liquid for the fermions. Phases B are characterized by the formation of fermionic composites with one fermion and one bosonic hole.*

where

$$\Phi_i^b = \sum_{\langle ij \rangle} \langle \Psi_{MF} | b_j | \Psi_{MF} \rangle \quad ,$$

$$\Phi_i^f = \sum_{\langle ij \rangle} f_{n,0}^{(j)*} f_{n,1}^{(j)} \quad .$$

These equations determine the dynamics of the $f_{n,m}$ coefficients in the phase space, and constitute the basis of what has been called dynamical Gutzwiller ansatz.

In order to draw a phase diagram we want to evaluate the chemical potential at different points in the μ-t_B plane. We obtain the chemical potential by launching two trajectories $\psi_0(t=0)$, $\psi_1(t=0)$ with, respectively, a number of bosons N_B and $N_B + \delta N$, where $\delta N \ll N_B$. We evolve the parallel trajectories while changing the parameter t_B, or α. The chemical potential can be then approximated as:

$$\mu_B(t) \approx \frac{\langle \psi_1(t) | H(t) | \psi_1(t) \rangle - \langle \psi_0(t) | H(t) | \psi_0(t) \rangle}{\Delta N} \quad .$$

During the time evolution the number for bosons and fermions is conserved, which can be seen by computing the commutation relation of the bosonic number operator with the kinetic part of the Hamiltonian:

$$-t_B \sum_i \sum_{\langle kl \rangle} \left[b_i^\dagger b_i, b_k^\dagger b_l \right] = -t_B \sum_i \sum_{\langle kl \rangle} b_i^\dagger \left[b_i, b_k^\dagger \right] b_l + b_k^\dagger \left[b_i^\dagger, b_l \right] b_i$$

$$= -t_B \mathrm{i} \sum_{\langle kl \rangle} b_k^\dagger b_l - b_k^\dagger b_l = 0 \quad .$$

Also all other parts of the Hamiltonian (2.1) commute with the fermionic and bosonic number operator.

Technically, we compute in the first step the ground state by minimizing the energy using a standard downhill method. The ground state is calculated for a relative big $t_B = t_F$, to assure that we certainly enter a superfluid phase. We vary the chemical potential for bosons and fermions in order to get the desired number of particles.

For finite values of α the true energetically minimum is reached, when the fermionic and/or the bosonic particle number is zero. This can be easily illustrated for $t_B = t_F = 0$. The Hesse matrix for the energy reads:

$$\begin{pmatrix} \frac{\mathrm{d}^2 E}{\mathrm{d}n \mathrm{d}n} & \frac{\mathrm{d}^2 E}{\mathrm{d}n \mathrm{d}m} \\ \frac{\mathrm{d}^2 E}{\mathrm{d}m \mathrm{d}n} & \frac{\mathrm{d}^2 E}{\mathrm{d}m \mathrm{d}m} \end{pmatrix} = \begin{pmatrix} 1 & \alpha \\ \alpha & 0 \end{pmatrix} \quad ,$$

which is independent of the boson number n and the fermion number m. The eigenvalues of the Hesse matrix are $\lambda_\pm = 0.5 \pm \sqrt{0.25 + \alpha^2}$, hence $\lambda_- < 0$ and $\lambda_+ > 0$. At every set of $n \neq 0$ and $m \neq 0$ which has no gradient in the energy function is in fact a saddle point. Numerically, the routine will not stop at such saddle point, but run into a configuration, where either $n = 0$, or $m = 0$. In order to obtain finite numbers for bosons and fermions, we have to evaluate the ground state at $\alpha = 0$.

Once we find the ground state with the desired number of bosons and fermions, we increase quasi-statically α. In the next step we decrease t. By launching various trajectories, we can explore those regions with an incommensurate total number of bosons plus fermions. Consequently, the trajectories do not enter into the regions of the phase diagram, in which commensurate phases are expected. Therefore, the expected lob gaps are opened. As shown in figure 2.5, our numerical and analytical results are in a good agreement. We must stress out that the effects of the fermionic tunneling are not taken into account in the analytic calculations, but they can be easily included in our numerics. As expected, the lobes of the phases with composite fermions shrink due to the larger mobility of the fermions.

Finally, we would like to comment about the validity of the mean-field approach presented in this chapter. In general, the mean-field approach is exact at dimension $d = \infty$, and is expected to be reliable for $n \gg 1$, since the relative effects of fluctuations is then small. For the considered cases $n \sim 1$, in a general situation (not at the tips of the lobes) the upper critical dimension is $d_c = 2$ [80], and therefore, the mean-field approach is reliable. However, at the tips the transition belongs to an universality class with $d_c = 3$ [80], and thus our mean-field approach provides only a qualitative picture.

2.7   Results

In the first part of this chapter we have demonstrated the appearance of composite fermions, a fermion couplet with s bosonic holes in the case of repulsive interaction between fermions and bosons, or with $-s$ bosons in the case of an attractive interaction. Using degenerated perturbation theory we have derived an effective Hamiltonian for the composite fermions in the case of equal hopping of fermions and bosons. Only due to hopping to neighbor sites we found a nearest-neighbor interaction between composite fermions. This is of particular interest, since a direct zero-range fermion-fermion interaction cannot occur between spin-polarized fermions due to Pauli's principle.

2.7.1   Analysis of the effective Hamiltonian

The effective Hamiltonian (2.8) is analyzed in this section. It is worth to mention that in particular the case $1 > |s| > 0$ is easy to achieve, since the hopping amplitude is proportional to t^2. Nevertheless, the form of the Hamiltonian is in general valid for the complete phase space in the $\mu - \alpha$ plane. This Hamiltonian describes two processes. The left side contains nearest neighbor hopping of composite fermions with the corresponding negative energy $-J_{eff}$, while the second part shifts the energy due to composite fermion-fermion interactions. The associated amplitude K_{eff} may be repulsive (> 0) or attractive (< 0).

This effective model is equivalent to that of spinless interacting fermions (c.f. [206]). The interaction, which purely results from the interaction of the fermions via the bosonic background can not be easily achieved having a single component gas of ultracold fermions. Contact interaction via s-wave scattering is forbidden by the Pauli principle. Other alternatives are long range dipole-dipole interactions [23, 208, 216, 217] or interactions, caused by p-wave scattering. The latter are, unfortunately, very small.

From this point of view the problem of finding the ground state of the

original Bose-Fermi-Hubbard model is reduced to the analysis of the ground state of the spinless interactive Fermi model in equation (2.8).

The physics of the effective model is determined by the ratio

$$\Delta = K_{eff}/2J_{eff} \quad ,$$

and by the sign of K_{eff}. In figure 2.6a it is shown, that the interaction can be attractive (label A), or repulsive (label R). We distinguish the following cases: In the case of a repulsive effective interaction, $K_{eff} > 0$, and filling fraction close to zero, $\rho_F \ll 1$, or one, $1 - \rho_F \ll 1$, the ground state of H_{eff} corresponds to a Fermi liquid (a metal), and is well described in the Bloch representation. In the considered cases, the relevant momenta are small compared to the inverse lattice constant (the size of the Brillouin zone). One can thus take the continuous limit, in which the first term in H_{eff} corresponds to a quadratic dispersion with a positive (negative) effective mass for particles (holes), while the second term describes p-wave interactions. The lattice is irrelevant in this limit, and the system is equivalent to a Fermi gas of spinless fermions (for $\rho_F \ll 1$), or holes (for $1 - \rho_F \ll 1$). Remarkably, this gas is weakly interacting for every value of K_{eff}, even when $K_{eff} \to \infty$. The latter case corresponds to the exclusion of the sites that surround an occupied site from the space available for other fermions. As a result, the scattering length remains finite, being of the order of the lattice spacing. Therefore, $1 - \rho_F$ (ρ_F) acts as the gas parameter for the gas of holes (particles). This picture can be rigorously justified using renormalization group approach [206].

The weakly-interacting picture becomes inadequate near half-filling, $\rho_F \to 1/2$, and for large Δ, where the effects of the interactions between fermions become important, and one expects the appearance of localized phases. A physical insight on the properties of this regime can be obtained by using the Gutzwiller ansatz [142], in which the ground state is a product of on-site states with 0 or 1 composites, $\prod_i(\cos\theta_i/2|1\rangle_i + \sin\theta_i/2e^{\phi_i}|0\rangle_i)$, and which is in fact well-suited for describing the states with reduced mobility and, therefore, with small correlations between different sites. Such an approach allows the determination of the boundaries of various quantum phases relatively well in 3D, 2D, and even 1D, but does not provide the correct description of correlations and excitations; these failures become particularly important in 1D, where, strictly speaking, the Gutzwiller ansatz approach is inappropriate.

For $K_{eff} > 0$ the Gutzwiller ansatz approach maps H_{eff} onto the classical antiferromagnetic spin model with spins of length 1, $\vec{S}_i = (\sin\theta_i\cos\phi_i, \sin\theta_i\sin\phi_i, \cos\theta_i)$ [14]. The corresponding ground state is a spin-flop (canted) antiferromagnet [14] with a constant density, provided $\Delta < \Delta_{crit} = (1 + m_z^2)/(1 - m_z^2)$, where the "magnetization per spin" is $m_z = 2\rho_F - 1$. When

$\Delta > \Delta_{crit}$, the Gutzwiller ansatz ground state of the classical spin model exhibits modulations of m_z with a periodicity of two lattice constants. We expect that the employed Gutzwiller ansatz formalism predicts the phase boundary Δ_{crit} accurately for ρ_F close to 1/2. Coming back to the composite fermion picture, we predict thus that the ground state for $\Delta < \Delta_{crit}$ is a Fermi liquid, while for $\Delta > \Delta_{crit}$ it is a density wave. For the special case of half filling, $\rho_F = 1/2$, the ground state is the so-called checkerboard state, with every second site occupied by one composite fermion. One should stress that the value of Δ_{crit} in the Gutzwiller ansatz is incorrect for filling factors ρ_F close to 0 or 1. In particular, the Gutzwiller ansatz approach predicts that Δ_{crit} tends gradually to infinity and the density wave phase gradually shrinks as $\rho_F \to 0$ or 1, i.e. $1 - m_z^2 \to 0$.

The situation is different when the effective interaction is attractive, $K_{eff} < 0$, which in the spin description corresponds to ferromagnetic spin couplings. In the Gutzwiller ansatz approach the ground state for $0 > \Delta \geq -1$ is ferromagnetic and homogeneous. In this description, fixing the fermion number means fixing the z component of the magnetization $M_z = N(2\rho_F - 1)$. When $|\Delta| \ll 1$, and ρ_F is close to zero (one), i.e. low (high) lattice filling, a very good approach to the ground state is given by a BCS ansatz [65], in which the composite fermions (holes) of opposite momentum build p-wave Cooper pairs, $\prod_{\vec{k}}(v_{\vec{k}}|00\rangle_{\vec{k},-\vec{k}} + u_{\vec{k}}|1,1\rangle_{\vec{k},-\vec{k}})$, where $v_{\vec{k}}$ and $u_{\vec{k}}$ are the coefficients of the Bogoliubov transformation. The ground state becomes more complex for arbitrary ρ_F, and for Δ approaching -1 from above. The system becomes strongly correlated, and the composite fermions in the superfluid phase may build not only pairs, but also triplets, quadruplets etc. The situation becomes simpler when $\Delta < -1$. In the spin picture the spins form then ferromagnetic domains with spins ordered along the z-axis. In the fermionic language this corresponds to the formation of domains of composite fermions ("domain" insulator). This mean-field result is in fact exact.

2.8   Experimental accessibility

Figure 2.5(b) shows predicted quantum phases for different kind of composite fermions in the region $0 \leq \mu \leq 1$. The observation of the predicted phases, constitutes a challenging, but definitely accessible, goal for experiments. Systems of different dimensionalities are nowadays achievable by controlling the potential strength in different directions [40, 98, 99, 110]. Recently, also the bose-fermion mixtures in 3D optical lattice have been already established [107, 177]. The conditions for the exclusive occupancy of the lowest band, and for $t \ll \alpha, 1$, are fulfilled for sufficiently strong lattice potentials, as
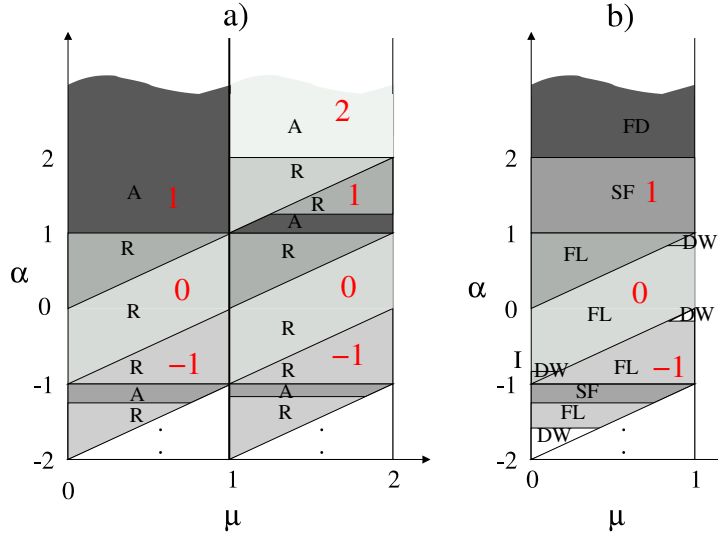
Figure 2.6. *(a) Phase space as a function of μ and α. The index R (A) denotes a repulsive (attractive) interaction for the composite fermions. (b) Full phase diagram for the region $0 < \mu < 1$, for $\rho_F = 0.4$ and $t = 0.02$. Different phases are present, including fermionic domains (FD), superfluid (SF), Fermi liquid (FL) and density-wave phase (DW). The red numbers label the number of bosonic holes, that are paired with the fermion.*

those typically employed in current experiments [100, 101] (10-20 recoil energies). Additionally, our $T = 0$ analysis is valid for T much lower than the smallest energy scale in our problem, namely the tunneling rate. This regime is definitely accessible for sufficiently large interactions. In typical experiments, the presence of an inhomogeneous trapping potential leads to the appearance of regions of different phases [19, 120], and it is crucial for the observation of Mott insulator phases [100, 101]. The inhomogeneity controls thus the bosonic chemical potential, which can also be tailored by changing the number of bosons in the lattice, regulating the strength of the lattice potential, and/or modifying the interatomic interactions by means of Feshbach resonances [212]. We would like also to note that composite fermions couplet with one boson or one bosonic hole are easier to study, since the effective hopping energies are, depending on t not too small, and can compete with the effective interactions K_{eff}. The predicted phases can be detected by using three already widely employed techniques. First, the removal of

the confining potentials, and the subsequent presence or absence of interferences in the time of flight image, would distinguish between phase-coherent and incoherent phases. Second, measuring the noise correlation of the boson (fermion) density after a free expansion reveals the density distribution of the atoms in the optical lattice before the release [9, 84]. Third, by ramping-up abruptly the lattice potential, it is possible to freeze the spatial density correlations, which could be later on probed by means of Bragg scattering. The latter two should allow to distinguish between homogeneous and modulated phases. An independent Bragg analysis for fermions and bosons should reveal the formation of composite fermions.

Chapter 3

Quantum Gases in Trimerized Kagomé Lattices

3.1 Introduction

The kagomé lattice derives from the triangular lattice. It is obtained from the latter by deleting every third site as demonstrated in figure 3.1. The distinguishing feature of the kagomé lattice is the absence of common edges between the elementary triangles, but it is a corner sharing lattice. This feature lies at the bottom of many remarkable features of physical systems on this lattice. It can be created by stacking three layers of parallel lines on top of each other, where the second layer is rotated by $2\pi/3$ and the third layer by $4\pi/3$. Every intersection corresponds to place which can in principle be occupied by a particle. Shifting one layer perpendicularly to the orientation of the parallel lines, the triangular lattice is obtained (figure 3.1b). The intermediate state between the triangular lattice and the kagomé lattice is called a trimerized kagomé lattice (figure 3.2). In order to examine all intermediate structures one needs a flexible tool which is tunable between these limits. Apparently, optical lattices created by laser beams provide such freedom and, additionally, optical lattices offer the possibility to change the lattice parameter *in situ* and "*in vivo*". We describe a scheme of a realization using super-lattice techniques [105, 106, 186, 190]. Non-rectangular lattices have already been realized (e.g. [127]) and, in an elaborate experiment, rotating triangular lattices have been demonstrated by the group of E. Cornell [50]. Hence, we believe it is nowadays feasible to create trimerized kagomé lattices.

From the theoretical point of view, for a sufficiently deep lattice potential, the dynamics of atoms in optical lattices is properly described by a Hubbard model. We examine this model and calculate its parameters using Wannier functions and Gaussian approximation. In the trimerized kagomé lattice we
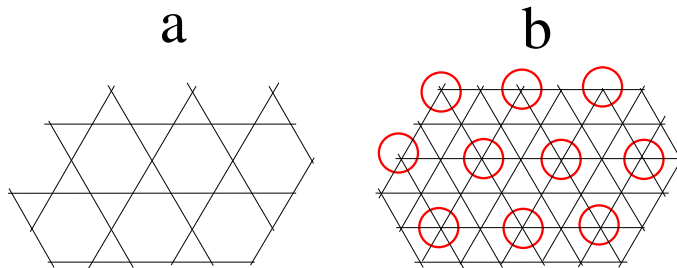
Figure 3.1.   *a) ideal kagomé lattice b) ideal triangular lattice.
The red circles denote the corners, which have to be removed in
order to obtain a kagomé lattice.*

will find two different kinds of tunneling, and nearest neighbor interactions,
which lead to new phases.

The first part of this chapter deals with the realization of the optical
kagomé lattice using standing laser waves. In our proposal the light has to
be red detuned. We discuss the effect of inaccuracy in the laser setup.

Moreover, we analyze three different kinds of quantum gases in this lattice:

- a single component Bose gas

- a single component (spin-polarized) interacting fermionic gas

- a two component ("spin" 1/2) fermion-fermion mixture.

For the Bose gas, the superfluid-Mott transition, that has been demonstrated
experimentally [100, 101] for rectangular lattices in 3D, is expected to occur
in the kagomé lattice too. We demonstrate in a mean-field calculation [36,
37, 198] the existence of Mott states with a fractional number of bosons
per trimer. Recently, by using Monte Carlo methods similar considerations
have been made on a triangular lattice [234], where a supersolid-superfluid
transition has been observed. More recently, a perfect kagomé lattice filled
with hardcore bosons has been examined [118] with the same method. In
any case, the solid and supersolid phases appear for a filling of $\rho = 1/3$ and
$\rho = 2/3$. We also observe this feature in the mean-field consideration in a
trimerized kagomé lattice.

Moreover, we focus our attention on a trimerized kagomé lattice loaded
with a spinless Fermi gas with nearest neighbor interactions. At 2/3 filling
we derive an effective spin Hamiltonian which has no continuous symmetries.
Using the method of exact diagonalization of the Hamiltonian we show that

the system exhibits an unexpected behavior at low temperatures. This allow us to propose a new class of possible behavior of frustrated antiferromagnets which we call "*spin-liquid crystals*". They are characterized by long range Néel type of order at low temperatures, a gapless excitation spectrum, and an anomalously large density of low energy excitations.

As it is very well known, fermion-fermion mixture with half filling of each species can be described effectively, in the strong coupling limit, by an antiferromagnet Heisenberg model [14].

3.2   Creation of optical kagomé lattices

In the following, we consider the atoms as confined magnetically or optically in the z-direction to $z = 0$. The atoms are effectively restricted in a 2D optical lattice, for instance in the x-y plane. In order to create a kagomé lattice in this plane one can use red detuned lasers, so that the potential minima coincide with the laser intensity maxima. A perfect triangular lattice can be created by three standing waves in the x-y plane: one laser field $\cos^2(\mathbf{k}_{11}\mathbf{r} + \phi)$ and two waves $\cos^2(\mathbf{k}_{12,13}\mathbf{r} - \phi)$ with the wave vectors:

$$\mathbf{k}_{11} = k_0 \begin{pmatrix} 0 \\ 1 \\ 0 \end{pmatrix} \quad \mathbf{k}_{12} = \frac{k_0}{2} \begin{pmatrix} \sqrt{3} \\ 1 \\ 0 \end{pmatrix} \quad \mathbf{k}_{13} = \frac{k_0}{2} \begin{pmatrix} -\sqrt{3} \\ 1 \\ 0 \end{pmatrix} \quad , \qquad (3.1)$$

where $\phi = 0$. The resulting triangles have a side length of $\lambda\sqrt{3}$, where λ is the wavelength of the laser. By varying ϕ the standing waves is shifted and, for $\phi = \pi/6$, an ideal kagomé pattern is realized. Unfortunately, this procedure has two problems. First, three lasers on a plane cannot have mutually orthogonal polarizations and consequently undesired interferences between different standing waves occur. This problem has, however, a fairly simple solution: undesired interferences can be avoided by randomizing the relative orientation of the polarization between different standing waves, or by introducing small frequency mismatches, which, however, have to be larger than any other relevant frequencies. The second problem is caused by the diffraction limit. Having three standing laser waves, it is only possible to create either an ideal kagomé or an ideal triangular lattice. This setup does not allow the creation of a trimerized kagomé lattice.

Let us denote by ξ the ratio of the separation between the maxima of laser intensity (i.e. minima of the resulting optical potential in the case of red detuned laser beam) and the half-width at half maximum. To have a good resolution of the potential minima ξ must be significantly larger than

2. In the case discussed above, however, ξ is only about 4 at $\phi = \pi/6$ which correspondents to an ideal kagomé lattice.

We propose to use the super-lattice technique [105, 106, 186, 190] which is described in the following paragraphs as a method to generate ideal and trimerized optical kagomé lattices. The proposed experimental preparation is schematically shown in figure 3.2. There are three planes of standing wave laser beams. In the particular case of figure 3.2, we have three standing waves (a triple) in each plane. The laser fields within each plane are phase-locked. A kagomé lattice will be formed by the intensity pattern that results from the sum of the laser intensities of the triples in the x-y plane.

In order to resolve the three potential minima in the unit cell of the kagomé lattice we need at least two standing waves in each of the three vertical planes shown in figure 3.2. The wave-fields in the same plane must have identical polarizations. With this setup consisting of 2 waves per vertical plane, we obtain the following intensity pattern in the x-y plane:

$$ I(\mathbf{r}) = I_0 \sum_{i=1}^{3} \left(\cos\left(\mathbf{k}_{1i}\mathbf{r} + \sigma_i \frac{\phi}{2} \right) + 2\cos\left(\mathbf{k}_{2i}\mathbf{r} + \sigma_i \frac{\phi}{2} \right) \right)^2 \quad , \qquad (3.2) $$

where $\sigma_2 = 1$ and $\sigma_1 = \sigma_3 = -1$ and $\mathbf{r} = (x, y)$. The index i enumerates the vertical planes. The momenta $\mathbf{k}_{1i}$ are described in equations 3.1 and $\mathbf{k}_{2i}$ read:

$$ \mathbf{k}_{21} = \frac{k_0}{3} \begin{pmatrix} 0 \\ 1 \\ -\sqrt{8} \end{pmatrix} \quad \mathbf{k}_{22} = \frac{k_0}{6} \begin{pmatrix} \sqrt{3} \\ 1 \\ -\sqrt{32} \end{pmatrix} \quad \mathbf{k}_{23} = \frac{k_0}{6} \begin{pmatrix} -\sqrt{3} \\ 1 \\ -\sqrt{32} \end{pmatrix} \quad . $$

The pattern formed by the minima of the intensity $I(\mathbf{r})$ changes between a triangular lattice at $\phi = 0$, and trimerized kagomé lattices by varying the phase difference width for $0 < \phi < \pi$, until at $\phi = \pi$ the uniform kagomé lattice is reached. In this limit one obtains the value $\xi \approx 7.6$ at $\phi = \pi$. This is sufficient to create a well resolved ideal kagomé lattice and we will show that it is large enough for our proposals.

With the additional third beam shown in figure 3.2 the value of ξ increases to ≈ 14 and remains large in wide range of angles ϕ. The resulting intensity pattern reads:

$$ I(\mathbf{r}) = I_0 \sum_{i=1}^{3} \Big[\cos(\mathbf{k}_i\mathbf{r} + 3\sigma_i\phi/2) $$
$$ + 2\cos(\mathbf{k}_i\mathbf{r}/3 + \sigma_i\phi/2) + 4\cos(\mathbf{k}_i\mathbf{r}/9 + \sigma_i\phi/6) \Big]^2. \qquad (3.3) $$
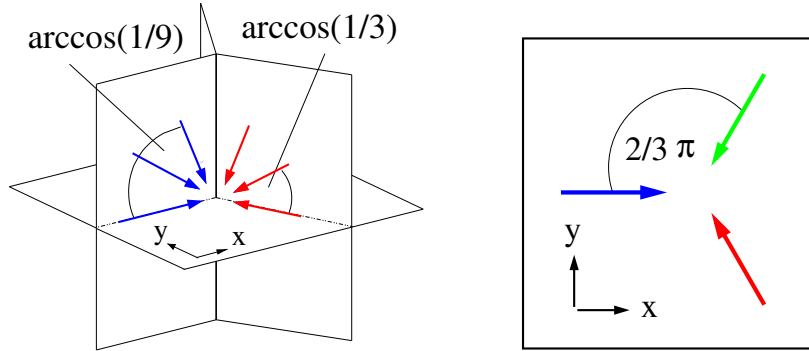
Figure 3.2. *Left: 3D arrangement of the standing laser. Phase-locked standing waves have equal color.*
Right: Top view to the setup. In order to avoid interferences due to equal polarizations, beams with different colors have to have either a phase mismatch, or mutually randomized phases.

A shift of the confining plane in z-direction of the order 0.1λ, where λ is the wave length of the laser, is not critical. Actually at certain shifts in z-direction one can have a similar behavior as for $z = 0$. One should avoid shifts from $z = 0.13 - 0.23, 0.45 - 0.65$ and $0.83 - 0.93\lambda$. If one chooses a z shift randomly the probability to find a regime where one can move from a triangular to kagomé lattice is 70%. A slight tilting of the potential plane produced by the z-axes laser creates stripes of kagomé lattices and triangular lattices in the x-y plane. Since triangular lattices have in general a deeper potential the atoms will go there. An external trap forces the atoms to be in a particular region of the lattice, so that experiments in trimerized kagomé lattices are possible, even if the setup is not ideal.

A different approach to create a superlattice uses multiphoton Raman processes to generate lattice potentials of periodicity $\lambda/(2N)$, where N is an integer [193, 231]. A trimerized kagomé lattice can be generated using periodicities $N = 1$ and $N = 3$. The advantage of this method is obvious: contrary to the setup in figure 3.2 we only need to align standing waves in the x-y plane.
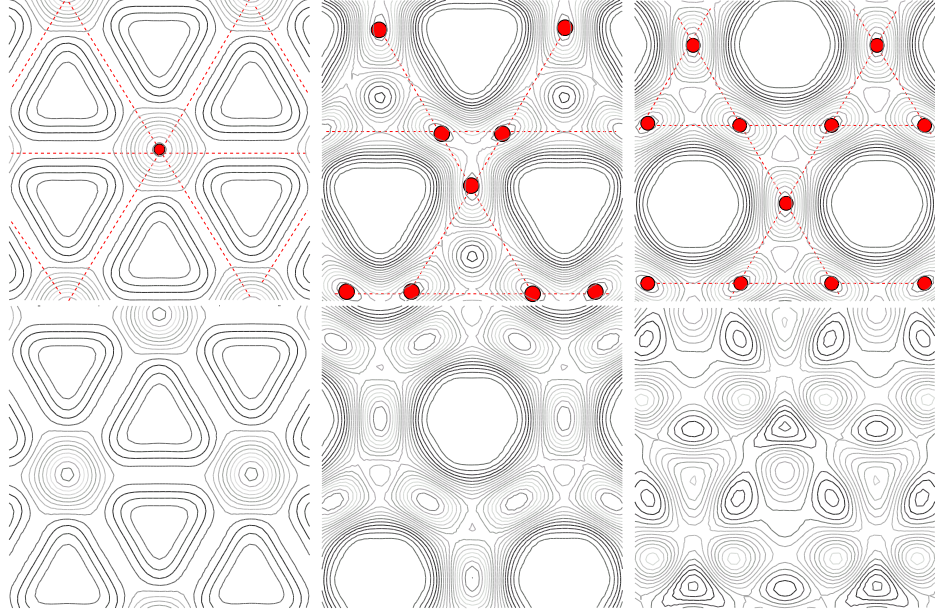
Figure 3.3. *Potential created by six standing waves. From left to right in the first row: $\phi = 0$, $z = 0$; $\phi = 0.7\pi$, $z = 0$, and $\phi = \pi$, $z = 0$. In the second row: $\phi = 1.3\pi$, $z = 0.7$; $\phi = 0.3\pi$, $z = 0.7$, and $\phi = 0$, $z = 0.2$.*

3.3 Hubbard Hamiltonian

In a sufficiently deep lattice the system in general can be described by a Hubbard model:

$$H_{\text{Hubbard}} = -\sum_{\langle ij \rangle} t_{ij}(c_i^\dagger c_j + c_i c_j^\dagger) + \frac{1}{2} \sum_i U n_i(n_i - 1) + \frac{1}{2} \sum_{\langle ij \rangle} U_{ij} n_i n_j. \quad (3.4)$$

Here $c_i^\dagger$ creates an atom in a Wannier state $|\mathcal{W}_i\rangle$ localized at the lattice site i. Depending on the atomic species the operators $c_i^\dagger$ and c_i represent either fermionic or bosonic creation and annihilation operators. The parameters t_{ij} in this Hamiltonian are the nearest neighbor hopping elements of the one-particle Hamiltonian in the Wannier representation:

$$t_{ij} = \langle \mathcal{W}_i | H_0 | \mathcal{W}_j \rangle, \quad (3.5)$$

where H_0 is the one-particle Hamiltonian:

$$H_0 = -\frac{\hbar^2}{2m}\Delta + v(\mathbf{r}) \,, \quad (3.6)$$

with the one-particle potential $v(\mathbf{r}) \propto I(\mathbf{r})$, written in equation (3.2) or equation (3.3). For the Bose gas interacting via short range Van der Waals forces, the scattering at low energies occurs via the s-wave channel, and is adequately described by the zero-range potential, so that we get for the interaction amplitudes the expressions:

$$U \;=\; g_{2\mathrm{D}} \int \mathrm{d}^2 x |\mathcal{W}_i(\mathbf{r})|^4, \qquad (3.7)$$

whereas

$$U_{ij} \;=\; g_{2\mathrm{D}} \int \mathrm{d}^2 x |\mathcal{W}_i(\mathbf{r})|^2 |\mathcal{W}_j(\mathbf{r})|^2, \qquad (3.8)$$

where the coupling is $g_{2\mathrm{D}} = 4\pi\hbar^2 a_s/mW$ with m the atomic mass, and W the effective transverse width of the 2D lattice in the z direction. In the case of polarized fermions U vanishes, since s-wave scattering is not possible due to the Pauli principle. Nearest neighbor interactions, on the other hand, are possible, and in the case when they are due to dipolar forces (cf.[97]), or similar long range forces, the couplings become:

$$U_{ij} \;\sim\; \int \mathrm{d}^2 x \mathrm{d}^2 x' |\mathcal{W}_i(\mathbf{r})|^2 V(\mathbf{r} - \mathbf{r}') |\mathcal{W}_j(\mathbf{r}')|^2, \qquad (3.9)$$

where $V(\mathbf{r})$ is the interparticle potential. Obviously, the same expression holds also for bosons interacting via the potential $V(\mathbf{r})$. The Hubbard Hamiltonian (3.4) does not necessarily describe the physics of bare particles; as it was discussed in chapter 2, it may equally well describe the physics of composite objects, such as, for instance, composite fermions that arise in the analysis of fermion-boson mixtures in the lattice in the strong interaction limit [142]. The nearest neighbor interactions and tunnelings are induced by the original hopping of bare fermions and bosons, and the corresponding values of t_{ij} and U_{ij} have to be calculated using Wannier functions [133]. Due to the form of the lattice in the case of trimerization we deal now with different types of hopping and nearest neighbor interaction elements. Contrary to the square lattice, this additional freedom promises to exhibit rich physics.

3.4 The coefficients of the Hubbard model

3.4.1 Wannier functions

For periodic boundary conditions the linear part of the Hamiltonian (3.6) can be diagonalized in the quasi-momentum space using the scheme of Bloch [13].

In the kagomé lattice a single cell contains three equivalent potential minima, and hence, three Wannier functions per unit cell are required, which can be obtained by transforming the Bloch states of the first three bands into the Wannier basis. Let us first consider one particle that is placed in an isolated trimer. The Hamiltonian for this system reads $H = -t\{c_1^\dagger c_2 + c_2^\dagger c_3 + c_3^\dagger c_1 + h.c.\}$ and its eigenfunctions of this model are obtained by diagonalizing H:

$$-t \begin{pmatrix} 0 & 1 & 1 \\ 1 & 0 & 1 \\ 1 & 1 & 0 \end{pmatrix} \vec{a} \;=\; \epsilon \vec{a} \quad .$$

The eigenfunctions of H are $\vec{a}_0 = (1,1,1)^T/\sqrt{3}$, $\vec{a}_1 = (-2,1,1)^T/2$ and $\vec{a}_2 = (0,-1,1)^T/\sqrt{2}$ with the respective eigenvalues $\{-2t,t,t\}$. The transformation matrix $(\vec{a}_0, \vec{a}_1, \vec{a}_2)^{-1}$ leads to the states for where just one site of the triangle is occupied. A similar scheme can also be applied for the Bloch functions $\psi_k^\mu(\mathbf{r}) = e^{-i\mathbf{k}\mathbf{r}} u_\mathbf{k}^\mu(\mathbf{r})$, where $\mathbf{k}$ is the quasi-momentum, and $u_\mathbf{k}^\mu(\mathbf{r})$ are the periodic functions of band $\mu \in \{1,2,3\}$. For a particular quasi-momentum
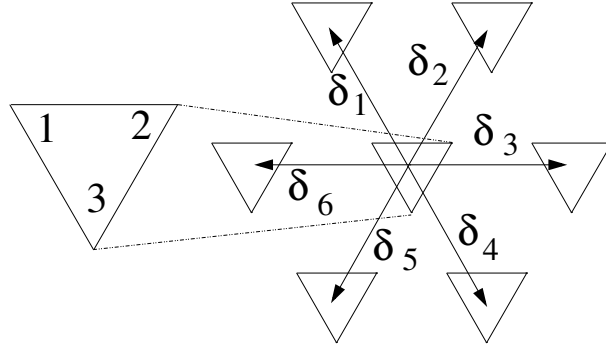
Figure 3.4.   *The vectors $\boldsymbol{\delta}_i$, $i = 1\ldots6$, pointing from the corners of a given trimer to the neighboring trimers. Numbering of the sites of the trimers is shown in the triangle on the left.*

$\mathbf{k}$, the values of $u_\mathbf{k}^i(\mathbf{r})$ at the potential minima are $a_{\mu\nu}(\mathbf{k})$, where $\nu \in \{1,2,3\}$ denotes the minimum within the trimer (see figure 3.4). Inverting the matrix $a_{\mu\nu}$ for a particular $\mathbf{k}$ one obtains complex coefficients c_{op}, which are then used to construct a periodic function having its density maximum in only one of the three potential minima: $w_\mathbf{k}^o = \sum_\mu c_{o\mu} u_\mathbf{k}^\mu$, where $o \in \{1,2,3\}$ denotes the corners of the trimer. Similarly as the $u_\mathbf{k}^\mu$, the $w_\mathbf{k}^o$ are functions with the same periodicity as the triangular lattice formed by the unit cells of the kagomé lattice. The summation of these functions over $\mathbf{k}$ with a proper

phase leads to the Wannier functions [133]: $W_{\mathbf{R}}^o = \frac{1}{N_l} \sum_{\mathbf{k}} e^{i\mathbf{k}\mathbf{R}} w_{\mathbf{k}}^o$, where $\mathbf{R}$ denotes the position of the particular trimer on which the maximum of the Wannier functions is located.

In this construction, the point group symmetry of the lattice is broken due to the choice of the particular set of basis vectors for the reciprocal lattice. A direct consequence of this fact is that the Wannier functions within a trimer cannot be transformed into each other by a rotation of $\pm 2/3\pi$ around the center of the trimer. Hence, one obtains different hopping probabilities between the sites of the triangle, $t_{ij} = \langle W_{\mathbf{R}}^i | H_0 | W_{\mathbf{R}}^j \rangle = \frac{1}{N_l^2} \sum_{\mathbf{k}} \sum_{\mu} c_{i,\mu} c_{j,\mu} \epsilon_{\mathbf{k}}^{\mu}$ where $\epsilon_{\mathbf{k}}^{\mu}$ is the energy for the quasi-momentum $\mathbf{k}$ in band μ. However, the Wannier functions can be symmetrized by summing up the periodic functions, which are now multiplied with a $\mathbf{k}$-dependent phase factor $e^{-i\mathbf{k}\mathbf{r}_i}$, where $\mathbf{r}_i$ is the position of one of the three potential minima within a cell. The hopping elements change then to $t_{ij} = (1/N_l^2) \sum_{\mathbf{k}} \cos \mathbf{k} (\mathbf{r}_i - \mathbf{r}_j) \sum_o c_{i,o} c_{j,o} \epsilon_{\mathbf{k}}^o$, which now are independent of the position. The cost of the symmetrization is that the Wannier functions are no longer orthogonal. The overlap, however, remains relatively small.

3.4.2 Gaussian ansatz

Apart from the case of the non-trimerized kagomé lattice, it is difficult to obtain the Wannier functions reliably. The coefficients for the Hubbard-Hamiltonian can be alternatively obtained using a Gaussian ansatz [182], which, in the case of a perfect kagomé lattice and for deep lattice potentials $> 5E_{\text{rec}}$, leads to results which are practically indistinguishable from those of the Wannier functions. The Gauss functions for the potential minimum at $x = 0$, $y = y_0$ takes the form:

$$f(x,y) = \sqrt{\frac{2}{\sigma_x \sigma_y \pi}} e^{\frac{-x^2}{\sigma_x^2}} e^{\frac{-(y-y_0)^2}{\sigma_y^2}} \quad .$$

The center y_0, the widths σ_x and σ_y are variational parameters which are determined by minimizing the energy functional:

$$E = \int_{\infty}^{\infty} dx \int_{\infty}^{\infty} dy \left[\nabla(f(x,y))^2 + f(x,y)^2 V(x,y) \right] \quad .$$

The Gauss functions for the other two minima in the trimer are obtained by rotating the Gauss function by $\pm \frac{2}{3}\pi$ around the center of the trimer. The figures 3.5a,b show a comparison of the hopping probability and contact interaction obtained using Wannier functions and the Gauss approximation

for a perfect kagomé lattice. Figure 3.6 shows the parameters for various degrees of trimerization. This latter plot was obtained using the Gauss functions. Significant differences in the hopping elements can be already obtained with relative small shifts of ϕ. Insofar, it is not essential to have a very high defraction limit. Using only six standing laser beams one can already access a large regime for $t/t' > 1$.

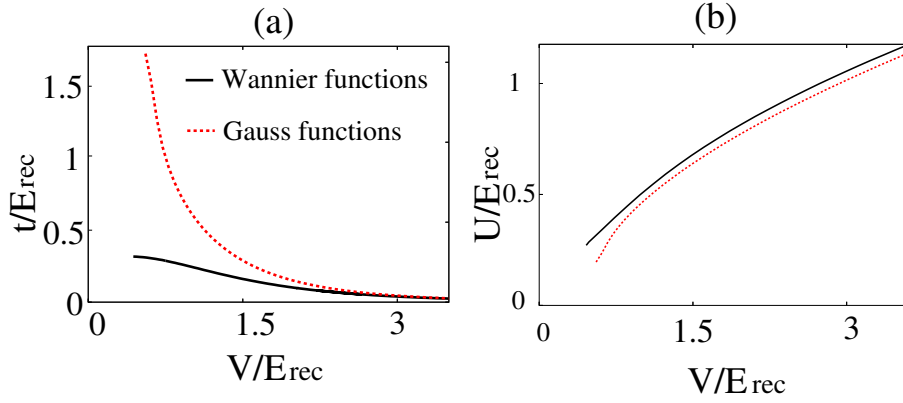Figure 3.5.   *Parameters for a perfect kagomé lattice obtained with a Gauss function (dotted) and with Wannier functions (solid). Plot (a): hopping elements, plot (b): self-interaction terms in units of* $3/4g_{2\mathrm{d}}$*.*
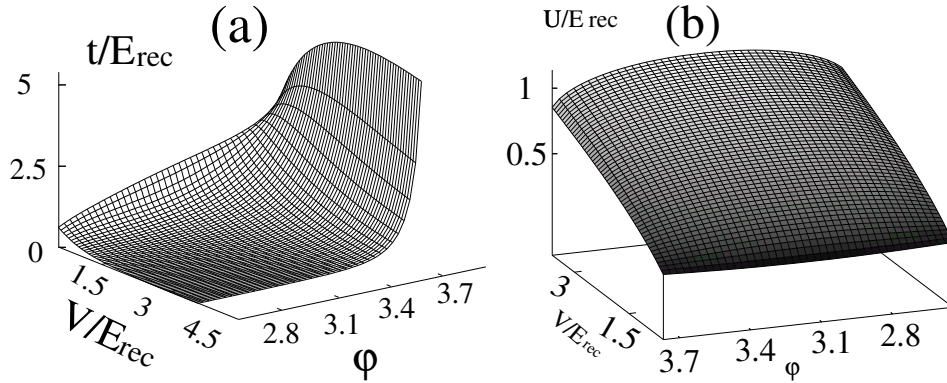

Figure 3.6.   *Parameters for trimerized lattices obtained with a Gauss function: (a) hopping elements, (b) self-interaction terms in units of* $3/4g_{2\mathrm{d}}$*.*

3.5 Spinless single component fermions

In this section we focus our attention on a trimerized kagomé lattice loaded with spinless fermionic atoms with nearest neighbor interaction. For this case we derive an effective spin Hamiltonian which shows a very interesting behavior that has not been observed previously in spin models.

In general frustrated antiferromagnets are attracting attention in modern condensed matter physics [144, 166]. According to C. Lhuillier and her collaborators quantum Heisenberg antiferromagnets at very low temperatures can exhibit 4 distinct kinds of quantum phases:

- Semi-classically ordered Néel phases, characterized by long-range ordered spin-spin correlation function, breaking of the $SU(2)$ symmetry, and a gapless spectrum of $\Delta S_z = 1$ magnon excitations. The standard example of such order is provided by the Heisenberg antiferromagnet on a square lattice in 2D. The theoretical description of such systems using the spin wave theory (cf. [14]) is quite accurate.

- Valence Bond Crystals (or Solids), characterized by long-range order in dimer coverings, with prominent examples being the AKLT model in 1D [4], or the Heisenberg model on a checker-board lattice [144, 166] (corresponding to a 2D projection of the pyrochlore lattice). Valence Bound Crystals exhibit no $SU(2)$ symmetry breaking, but the pattern of dimers or larger singlet plaquettes breaks the translational symmetry of the lattice. Spin-spin correlations are short ranged and the excitation spectrum is gaped.

- Resonating Valence Bond spin liquids (Type I), exhibiting a unique ground state, no symmetry breaking, gaped fractionized *"spinon"* excitations, and vanishing correlations in any local order parameter. An example of such a spin liquid is realized in the so-called ring exchange model in the triangular lattice [144, 166].

- Resonating Valence Bond spin liquids (Type II), exhibiting no symmetry breaking, no long-range correlations in any local order parameter, a gapless excitation spectrum, and an extraordinary density of states in each total S sector. The spin 1/2 Heisenberg antiferromagnet on the kagomé lattice exhibits this behavior [139, 141, 144, 154, 164, 166, 209, 228].

The effective spin model that will be discussed here exhibits a behavior that differs from the described classes. We call it a *"spin-liquid crystal"*.

The motivations to study this model is at least threefold:

- In a magnetic field such that the trimerized kagomé antiferromagnet is driven into the magnetization plateau at 1/3 of the saturation magnetization, the physics of the kagomé antiferromagnet is described precisely by our model [154, 164, 209]. Studying our model will thus shed light on the theory of the kagomé antiferromagnet and, hopefully, also on experiments.

- Theoretical studies (using exact diagonalization of the Hamiltonian) indicate that the model has fascinating properties of, what we have termed as "*quantum spin liquid-crystal*". We expect the behavior observed in this system indeed to be generic for other "multi"-merized systems. First of all it is clear that optical methods allow for creating many similar spin models with couplings depending on bond directions. In the simplest case this can be accomplished for a square lattice where one could achieve a "square lattice of small squares", for the triangular lattice to obtain a "triangular lattice of small triangles" etc. One can expect that when such procedures are realized for frustrated systems, this will lead to similar effects as for the kagomé lattice.

- One of the most fascinating possibilities provided by the optical lattices is the possibility of "online" modifications of the lattice geometry. We may go from triangular to kagomé lattice in real time in a controlled way. Trimerization (or generally "multi"-merization) is a new experimental option, and it is highly desirable to explore its consequences. Our model (apart from the model of the Bose gas in the trimerized kagomé lattice) is one of the simplest ones to explore these consequences.

One of the reasons for the widespread interest in the physics of 2D antiferromagnets is the challenging prediction that 2D antiferromagnetism is closely related to high temperature superconductivity [14, 140, 232, 236].

The analytical, or numerical treatment of antiferromagnets can be quite challenging. For systems with long-range Néel order semi-classical approximations and spin wave approach can be applied successfully. In 1D exact results are rare (c.f. [156]), and in practice one has to rely either on bosonization methods [93, 96, 159], or on numerical methods, such as the Density Matrix Renormalization Group method. 2D systems can be treated, apart from renormalization group approaches, with numerical methods, such as Quantum Monte Carlo simulations. Unfortunately Quantum Monte Carlo methods are known to suffer from the "negative sign" problem. This problem occurs in Heisenberg antiferromagnet on the triangular lattice. Therefore, attempts to solve this problem by Quantum Monte Carlo have been futile and

the main results have been obtained by using an exact diagonalization. Surprisingly, the results, contrary to earlier conjectures, the triangular lattice exhibits long range order [20, 21].

Moreover, kagomé spin 1/2 antiferromagnets are expected to form a type II Resonance Valence Bond spin liquid. So far there are no experimental realizations among solid state systems. Only spin 1 kagomé antiferromagnets can be realized in solid state experiments, but that system has a gap to all excitations, i.e. it does not belong to the type II spin liquids [114]. The physics of the spin 1/2 kagomé antiferromagnet is, however, not fully understood, and there are papers that suggest Valence Bound Crystal type of order with large unit cells [171].

3.5.1   The effective Hamiltonian

The spinless Fermi gas in the trimerized kagomé lattice is appropriately described by the Fermi-Hubbard Hamiltonian:

$$H_{FH} = -\sum_{\langle ij \rangle} t_{ij}(f_i^\dagger f_j + h.c.) + \sum_{\langle ij \rangle} U_{ij} n_i n_j - \sum_i \mu n_i \,, \qquad (3.10)$$

where t_{ij} and U_{ij} take the values t and U for intra-trimer bonds and t' and U' inter-trimer bonds. μ is the chemical potential, and $n_i = f_i^\dagger f_i$ are the occupation numbers with f_i, $f_i^\dagger$ being the fermion annihilation and creation operators. In the following we denote the sites of each trimer by 1, 2, 3 in the clockwise sense as shown in figure 3.4.

In this section, it is our aim to derive from the Hamiltonian (3.10) an effective spin Hamiltonian that captures in the strongly trimerized limit, $t', U' \ll t < U$, the low-energy physics.
The intra-trimer part of the Hamiltonian H_{FH} is diagonalized by introducing instead of the local fermion modes f_1, f_2 and f_3 the symmetric mode $f = (f_1 + f_2 + f_3)/\sqrt{3}$ and the left and right chiral modes $f_\pm = (f_1 + z_\pm f_2 + z_\pm^2 f_3)/\sqrt{3}$ with $z_\pm = \exp \pm i2\pi/3$:

$$H_{FH}^{intra} = -3tn + t\bar{n} + \frac{U}{2}(\bar{n}^2 - \bar{n}) - \mu\bar{n} \,, \qquad (3.11)$$

where $n = f^\dagger f$ and $\bar{n} = n + f_+^\dagger f_+ + f_-^\dagger f_-$ is the total number of fermions in the trimer. The operators f, f_+ and f_- fulfill the fermionic anticommutation relation. In the strongly trimerized limit the number of fermions is identical in each trimer. It is controlled by the chemical potential: for $U + t < \mu < 2U + t$ there are two particles in each trimer, one of them occupies the symmetric state, $|1\rangle = f^\dagger|0\rangle$, while the second one occupies one of the

chiral states $|1\pm\rangle = f_{\pm}^{\dagger}|1\rangle$. In the inter-trimer part of the Hamiltonian H_{HF}, equation (3.10), we consider only the nearest neighbor interaction and omit the hopping term,
$-\sum_{\langle\alpha i,\beta j\rangle} t'(f_{\alpha,i}^{\dagger}f_{\beta,j} + h.c.)$ $(\alpha,\beta = 1, 2, 3)$. Any real (first order) hopping process leads to a change of the occupation of a neighboring pair of trimers: one of them is occupied by three fermions while only one fermion remains in the other. Equation (3.11) shows that such a process increases the energy of the pair by an amount of the order of $\mathcal{O}(U)$. On the other hand, second order (virtual) hopping processes, which reproduces the original chiral state are consequently small of the order of t'^2/U and will be neglected. Then, the inter-trimer part of H_{HF} reduces to:

$$H_{HF}^{inter} = \frac{U'}{2}\sum_i (n_{1,i}n_{3,i+\delta_1} + n_{2,i}n_{3,i+\delta_2} + n_{2,i}n_{1,i+\delta_3}$$

$$n_{3,i}n_{1,i+\delta_4} + n_{3,i}n_{2,i+\delta_5} + n_{1,i}n_{2,i+\delta_6}) \quad . \tag{3.12}$$

Here, δ_ν, $\nu = 1, \cdots, 6$, denote the six vectors pointing from the central triangle to the six neighboring triangles, see figure 3.4.

The occupation numbers $n_{\alpha,i}$, $\alpha = 1, 2, 3$ can be expressed in terms of the fermion operators f, $f_\pm$ (we suppress the site index):

$$n_1 = \frac{1}{3}\left[\bar{n} + (f_+^{\dagger} + f_-^{\dagger})f + f^{\dagger}(f_+ + f_-) + \hat{\tau}^x\right],$$

$$n_2 = \frac{1}{3}\left[\bar{n} + (z_+f_+^{\dagger} + z_-f_-^{\dagger})f + f^{\dagger}(z_-f_+ + z_+f_-)\right.$$
$$\left. + \cos(2\pi/3)\hat{\tau}^x + \sin(2\pi/3)\hat{\tau}^y\right],$$

$$n_3 = \frac{1}{3}\left[\bar{n} + (z_+^2f_+^{\dagger} + z_-^2f_-^{\dagger})f + f^{\dagger}(z_-^2f_+ + z_+^2f_-)\right.$$
$$\left. + \cos(2\pi/3)\hat{\tau}^x - \sin(2\pi/3)\hat{\tau}^y\right] \quad . \tag{3.13}$$

Here, the (pseudo-)spin operators:

$$\hat{\tau}^x := \frac{1}{2}(f_+^{\dagger}f_- + f_-^{\dagger}f_+)$$

$$\hat{\tau}^y := -\frac{i}{2}(f_+^{\dagger}f_- - f_-^{\dagger}f_+) \quad ,$$

connect the right- and left-handed chiral fermion states. Inserting the expressions in (3.13) into H_{HF}^{inter}, equation (3.12), yields bilinear terms in $\hat{\tau}^x$, $\hat{\tau}^y$, linear terms in $\hat{\tau}^x$ and $\hat{\tau}^y$, bilinear terms in $f^{\dagger}$, f and linear terms in $f^{\dagger}$ and f. The Hamiltonian (3.12) commutes with the number operators for the fermions in any trimer, hence, we can set $\bar{n} = 2$ in the resulting expression

for H_{HF}^{inter}. However, terms containing the annihilation operator f promote the fermion in the symmetric state of a given trimer into the non-occupied chiral state of the same trimer which increases the energy by an amount of $\mathcal{O}(t)$. Moreover, the linear terms in $\hat{\tau}_i^x$, $\hat{\tau}_i^y$ sum to zero in the sum over the sites i. We arrive at the following effective inter-trimer Hamiltonian (we omit an irrelevant constant):

$$H_{eff} = \frac{J}{2} \sum_{i=1}^{N} \sum_{\nu=1}^{6} \hat{\tau}_i(\phi_{i,\delta_\nu}) \hat{\tau}_{i+\delta_\nu}(\tilde{\phi}_{i,\delta_\nu}) \,. \tag{3.14}$$

Here, i are the sites of a triangular lattice of N sites on which the trimers are located, $J = 4U'/9$, and the vectors δ_ν, $\nu = 1, \cdots 6$, are the same as in figure 3.4. In equation (3.14), $\hat{\tau}_i(\phi) = \cos(\phi)\hat{\tau}_i^x + \sin(\phi)\tau_i^y$ and $\phi_{i,\delta_1} = \phi_{i,\delta_6} = 0$, $\phi_{i,\delta_2} = \phi_{i,\delta_3} = 2\pi/3$, $\phi_{i,\delta_4} = \phi_{i,\delta_5} = -2\pi/3$, $\tilde{\phi}_{i,\delta_1} = \tilde{\phi}_{i,\delta_2} = -2\pi/3$, $\tilde{\phi}_{i,\delta_3} = \tilde{\phi}_{i,\delta_4} = 0$ and $\tilde{\phi}_{i,\delta_5} = \tilde{\phi}_{i,\delta_6} = 2\pi/3$.

3.5.2 Effective spin model: relation to the kagomé antiferromagnet

A similar model has been derived by Subrahmanyam [209] and has later been employed by Mila and Mambrini [154, 164] to explain the origin of the high density of low-lying singlets of the Heisenberg antiferromagnet on the kagomé lattice. Mila considers the spin 1/2 Heisenberg model on the trimerized kagomé lattice with a strong intra-trimer coupling J and a weak inter-trimer coupling J'. In the lowest order perturbation expansion with respect to J' he arrives at the effective Hamiltonian:

$$H_{eff}^{trim-kag} = \frac{J'}{18} \sum_{\langle ij \rangle} H_{ij}(S_\bigtriangledown) H_{ij}(\tau) \,, \tag{3.15}$$

where $H_{ij}(S_\bigtriangledown) = \mathbf{S}_{\bigtriangledown i} \mathbf{S}_{\bigtriangledown j}$ and where $H_{ij}(\tau)$ is that member of our model H_{eff} that is associated with the bond ij. The operator $\mathbf{S}_{\bigtriangledown i}$ acts on the total spin of the trimer at site i, the trimers form a triangular lattice. In the derivation $H_{eff}^{trim-kag}$ the Hilbert space of the three $S = 1/2$ spins of the individual trimers has been restricted to the subspace of total spin 1/2 states. The four states of this subspace can be specified by the z-component of their total spin and by two (spin)-chiralities. The Heisenberg type Hamiltonian $H_{ij}(S_\bigtriangledown)$ acts on the two spin states of the trimers at sites i and j , $H_{ij}(\tau)$ acts on their chiralities. Obviously, $H_{eff}^{trim-kag}$ turns into our model Hamiltonian H_{eff}, if the trimer spins $S_{\bigtriangledown i}$ are fully polarized, e.g. $S_\bigtriangledown^z = 1/2$ for all i. This state can be reached by applying a sufficiently strong magnetic field to the original

trimerized kagomé antiferromagnet such that the total magnetization reaches 1/3 of the saturation magnetization, *i. e.* a magnetic field that establishes the 1/3 magnetization plateau.

3.5.3   Effective spin model: classical aspects

As it is obvious from the derivation of the Hamiltonian (3.14), only its $\tau = 1/2$ quantum version can serve as a realistic effective model for the atomic Fermi gas in the trimerized kagomé lattice. Nevertheless, in order to get into the problem, it is useful to first consider this model in the classical limit and to also calculate its excitation spectrum in the semi-classical approximation, i. e. in the linear spin wave approximation [76]. We first describe the symmetries of the model equation (3.14). In the classical limit we replace the operators real numbers: $\hat{\tau}_i^x \to \cos\Theta_i$ and $\hat{\tau}_i^y \to \sin\Theta_i$.

Symmetries

We have found that this model, is not only translationally invariant, but is also invariant under the point group of order 6, $Z_6 = Z_3 \cdot Z_2$, where the generator of Z_3 (order 3) is the combined rotation of the lattice by the angle $4\pi/3$ and of the spins by the angle $2\pi/3$ around the z axis, while the generator of Z_2 (order 2) is the spin inversion in the x-y plane, $\hat{\tau}_i^x \to -\hat{\tau}_i^x$, $\hat{\tau}_i^y \to -\hat{\tau}_i^y$. The model possesses *no* continuous spin rotational symmetry and the lines bisecting the angle between two adjacent lattice directions of the triangular lattice are *not* mirror lines.

Classical ground states

In figures 3.7a, b, c we show the three ordered classical states with small unit cells on the triangular lattice that are compatible with this point group symmetry: a ferromagnetic state and two 120° Néel states labeled A and B which differ by the distributions of the chiralities χ over the cells of the lattice as indicated by "+" and "-" signs. For an elementary cell of the triangular lattice whose corners are labeled i,j,k in the counterclockwise, χ is defined as:

$$\chi_{ijk} = (\tau_i^x \tau_j^y - \tau_i^y \tau_j^x) + (\quad i,j \to j,k \quad) + (\quad j,k \to k,i \quad) \quad . \qquad (3.16)$$

χ is positive (negative) if the spin turns in the counter-clockwise (clockwise) sense as one moves around a triangular cell in the counter-clockwise sense. Because of the lack of mirror symmetry mentioned above it is not surprising that the two Néel states have different energies: $E_{\text{class}}^A = \frac{3}{2}\tau^2 JN$, $E_{\text{class}}^B =$
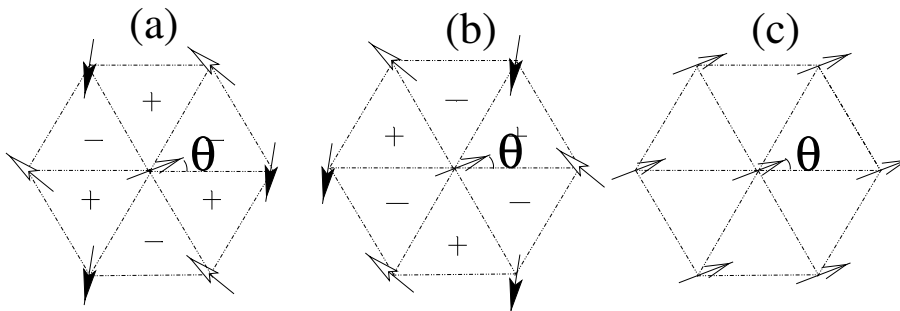
Figure 3.7.   *(a) Classical ground state configuration for $J < 0$ (configure A). (b), (c) Classical ground state configurations for $J > 0$ (configuration B and ferromagnetic configuration). The "+", "-" signs denote the chirality of the triangular plaquettes (see equation 3.16).*

$-\frac{3}{4}\tau^2 J N$. Here, N is the number of sites and the superscripts A and B correspond to the labels of the Néel states in figures 3.7a, b.

More surprisingly the ferromagnetic state is found to be degenerate with the Néel state B in the classical limit, $E_{\text{class}}^{\text{ferro}} = E_{\text{class}}^B$. Furthermore, as is indicated by the angle θ in figures 3.7a, b, the classical energies of the three structures do not depend on their direction relative to the lattice directions. In summary, in the classical approximation the Néel state A is the ground state of model (3.14) for negative coupling, $J < 0$, while for positive J there are at least two classically degenerate ground states, the Néel state B and the ferromagnetic state.

In fact, we have performed a numerical analysis of the 12-spin cell by fixing the direction of every spin to $n\pi/3$ with $n = 0 \cdots 5$, so that there were 6^{12} classical spin configurations. This analysis has revealed that for $J < 0$ there are 6 ground states each of them exhibiting the Néel order of type A (the six fold degeneracy comes from a Z_6 symmetry of our model). The results are dramatically different in the $J > 0$ case, where we have found in total 240 degenerate classical ground states, among which the pure Néel states of type B and ferromagnetic states sum up to a small fraction. For an illustration, see figure 3.8 where two ordered ground states with very large unit cells (figures 3.8b, 3.8d) together with their parent states (figures 3.8a, 3.8c) are presented. Moreover, As will be seen below, the large number of degenerate classical ground states may find its analogue in a large density of low-lying excitations of the quantum version of equation (3.14). This analysis has been extended by [41], where also bigger cells are examined. The results
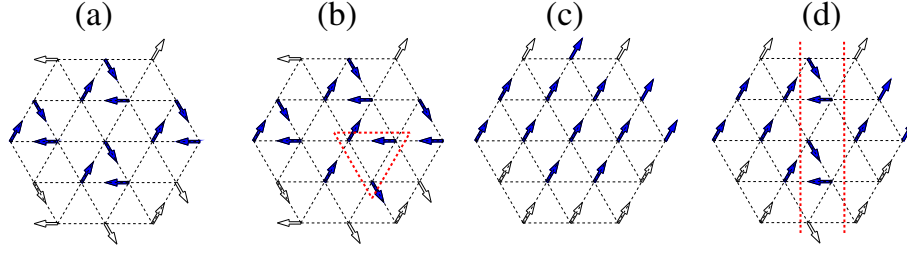
Figure 3.8.   *N=12 spin cell: (a) Configuration B; (b) Localized defect in configuration B marked by the triangular contour. (c) Ferromagnetic configuration; (d) Line defect in ferromagnetic configuration. The open arrows present spins that do not belong to the 12-spin cell. Their orientations are determined by the boundary conditions of the cell.*

can be found in table 3.1.

N	12	15	18	21	24	27
$\mathcal{D}_N$	240	612	1716	4128	11028	30324
$\frac{\ln \mathcal{D}_N}{N}$	0.4567	0.4278	0.4138	0.3965	0.3878	0.3822

Table 3.1.   *$\mathcal{D}_N$ is the number of classical ground states for $J > 0$ on a lattice of size N. In the original version of [41] et al. one angle is fixed. Therefore, they obtain a number of degenerated ground state that is smaller by a factor of 6. The values in the last row are proportional to the entropy per particle. A finite value in the thermodynamic limit would violate the Nernst theorem.*

3.5.4   Effective spin model: spin wave theory

We performed a linear spin wave expansion around the ferromagnetic ground state ($J > 0$) bases on the Holstein-Primakoff expansion [14, 76] and, for the two 120° structures ($J > 0$ and $J < 0$), we closely followed the method derived by Jolicœur and Le Guillou [76, 126].

Including quantum corrections to the ground state energy, the energy per particle in the ferromagnetic case reads:

$$E^{\text{ferro}} = -\frac{3}{4}J[\tau(\tau + 1) - 0.901\tau] \quad , \qquad (3.17)$$

where the magnetization locks in on one of the directions of the triangular lattice ([41] *et al.*), *i. e.* the ferromagnetic ground state becomes sixfold degenerate in accordance with the order of the point group of our model, equation (3.14).

After including the lowest order quantum correction the ground state energy of the state B ($J > 0$) reads:

$$E^B = -\frac{3}{4}J[\tau(\tau + 1) - 1.48\tau] \quad . \tag{3.18}$$

Also here we found sixfold degenerated state. Comparison of equations (3.17) and (3.18) shows that quantum fluctuations lift the degeneracy of the purely classical states. In this semi-classical approach it appears that the ferromagnetic state is the ground state. However, in table 3.1 it is demonstrated that there is a very large manifold of classical ground states.

3.5.5 Numerical results [58]

Numerical method

In order to understand the physics of spinless fermions on a trimerized optical kagomé lattice at filling 2/3 we need to consider the model (3.14) for spin $\tau = 1/2$, *i. e.* in the extreme quantum limit. Questions to be answered for this case are: (*i*) Is the ground state of the model (3.14) an ordered state or is it a spin liquid either of type *I*, *i. e.* a state without broken symmetry, with exponentially fast decaying spin-pair correlations and a gap to the first excitation, or of type *II*, *i. e.* a kagomé like ground state, again without broken symmetry, with extremely short ranged correlations, but with a dense spectrum of excitations adjacent to the ground state. (*ii*) What are the thermal properties of our system? After all, the model can only be realized at finite, albeit low temperatures.

To find answers to these questions we have performed exact diagonalizations of the Hamiltonian (3.14) for cells of $N = 12, 15, 18, 21, 24$ and recently 27 [41] sites using ARPACK routines [1]. The sizes of systems that can be studied by exact diagonalizations are restricted by the amount of memory space that is required for storing the non-zero matrix elements. To reduce this requirement we block-diagonalized the Hamiltonian (3.14) by exploiting its invariance under N-fold translations. This allowed us to reduce the problem of diagonalization of $2^N \times 2^N$ matrix to N *independent* diagonalizations of matrices of size $\sim 2^N/N \times 2^N/N$. The block-diagonalization simplification not only lowers the memory requirements but also greatly reduces the time of calculation, especially when a large number of excited eigenstates is of interest.

Nevertheless, exact diagonalizations of this Hamiltonian remains a demanding task, as in contrast to $SU(2)$ invariant spin models the Hilbert space of the Hamiltonian (3.14) cannot be separated into subspaces of states with fixed total spin and total z-component of the spin. Because of this last circumstance we had to limit our study to systems of at most 27 spins. Fortunately, our results for 21 and 24 spins show qualitative and quantitative resemblance. Therefore, we regard them as representative for larger systems too. In presenting our results we shall mainly confine ourselves to the two largest systems, since the results for smaller systems suffer from strong finite size effects. We remark that only the 12-, 21-, and the 27-site cell can be chosen such that these systems possess the full point group symmetry of the infinite lattice. The lack of this symmetry for the 15- and the 18-site cell adds to the large finite size effects observed in the results for these cells.

Ground state and low temperature properties

For $J < 0$, i. e. for attractive interaction U' between fermions on nearest neighbor trimers, the highest-levels of H_{eff}/J and the corresponding eigenstates are physically most relevant. As will be seen below theses levels are well separated from each other so that we only need to calculate a few of them. The situation is drastically different in the case $J > 0$, where we need the low-lying states of H_{eff}. It turns out that there is an abundance of such low lying states. In this respect the spectrum of H_{eff} is reminiscent of the spectrum of the Heisenberg Hamiltonian on the kagomé lattice [139, 228]. The answer to the question of whether there is a long range order in our model (3.14) is found in table 3.2 and figure 3.13, where we show our numerical results for the spatial spin-spin correlations for the $J < 0$ and $J > 0$ cases, respectively. The cells to which this table and figure refer are shown in figures 3.9a, b, c.

Let us first consider the case $J < 0$ (table 3.2). We did not do a systematic finite-size analysis for these correlations. However, comparing the data for the quantum $\tau = 1/2$ systems with the classical correlations there can be little doubt that in its ground state the system orders in the planar 120° Néel structure. The smallness of the out-of plane correlations lends further support to this conclusion. We have also calculated the expectation values of the chirality χ_{ijk}, equation (3.16), in the ground states of the 12- and of the 21-site cell and have found perfect agreement with the pattern of positive and negative chiralities of the classical configuration, figure 3.7a. Apparently, for $J < 0$ quantum fluctuations have a rather weak effect on the ground state properties of our model (3.14).

For the case $J > 0$ our results for the spin-spin correlations are presented
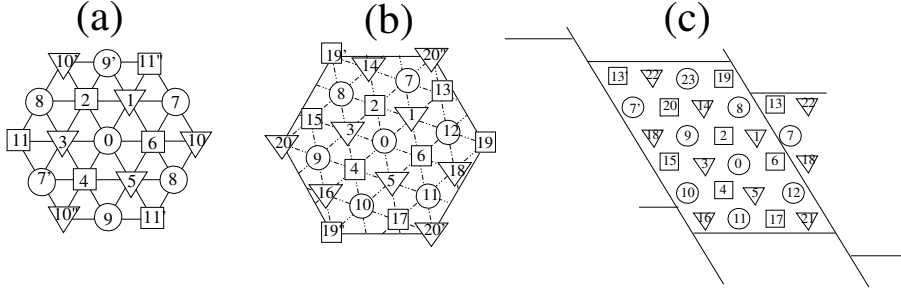
Figure 3.9.   *(a) 12 spin cell, (b) 21 spin cell, (c) 24spin cell.* $\bigcirc$, $\triangledown$, *and* $\square$ *mark the three sub-lattices. Primed sites belong to periodic repetitions of the cell containing the unprimed sites.*

	1st neighbs. $d = 1$	2nd neighbs. $d = \sqrt{3}$	3rd neighbs. $d = 2$	4th neighbs. $d = \sqrt{7}$
classical	-0.125	0.25	-0.125	-0.125
$N = 12$	-0.137	0.251	-0.125	
$N = 21$	-0.134	0.237	-0.117	-0.116
	(-0.029)	(-0.004)	(-0.004)	(-0.003)

Table 3.2.   *Spin-spin correlations,* $\langle \hat{\tau}_0^x \hat{\tau}_j^x + \hat{\tau}_0^y \hat{\tau}_j^y \rangle$ *for* $J < 0$. *In the last row the* $\tau^z - \tau^z$ *correlations are also shown (numbers in parentheses). Owing to the* Z_6 *symmetry of the Hamiltonian (3.14) the correlations depend only on the distance d from the central site* 0 *(see figure 3.9).*

in figure 3.13. As for the case $J < 0$ we have not been able to perform a finite size analysis but again we interpret the data in figure 3.13 as evidence for the existence of planar 120° Néel order in the ground state of our model (3.14). This contradicts the prediction of the linear spin wave analysis according to which one might have expected to find a ferromagnetic ground state (see subsection 3.5.4). However, one must recall that besides the 120° Néel ground state and the ferromagnetic ground state there are many more classical ground states. In a complete linear spin wave analysis one would have to consider every one of these states, a task that is practically impossible to perform. Relative to the in-plane-correlations the magnitude of out-of-plane correlations, which are not displayed in figure 3.13, is even smaller here than in the case $J < 0$. Further support for long-range order in the ground state of the model (3.14) comes from a comparison of the spin-spin correlations

of this model with the same correlations of the $= 1/2$ Heisenberg antiferromagnet on the triangular lattice which we have included in figure 3.13. It is seen there that the ground state correlations of the model (3.14) decay more slowly than those of the ground state of the triangular lattice which is known to possess long range $120°$ Néel order [20, 21].

Additional strong support for existence of a Néel ordered ground state in both $J > 0$ and $J < 0$ cases comes from an investigation of chirality patterns. In both situations the quantum mechanical calculation reveals that there exists a perfectly periodic pattern of chiralities χ_{ijk} as in the classical result. For $J > 0$ we found that $\chi_{ijk} \approx \mp 0.5$ while for $J < 0$ $\chi_{ijk} \approx \pm 0.69$. Both results are obtained in $N = 21$, where the χ_{ijk} was calculated for six triangles located around the central site (figure 3.7). The $\mp, \pm$ notation indicates opposite chiralities between $J > 0$ and $J < 0$ results. A comparison of these values to ∓ 0.65 (Néel B configuration) and ± 0.65 (Néel A configuration), leaves little doubt on the nature of these ground states. Finally, please notice excellent agreement between quantum and classical calculation for $J < 0$.

Values for the spin-spin correlations of the model (3.14) for finite albeit small temperatures are also displayed in figure 3.13. For $T = 0.005J$ about 800 low lying eigenstates were needed to achieve convergence in the data for the correlations. Although these finite temperature correlations are smaller in magnitude than the ground state correlations, they decay as slowly with the distance as the ground state correlations *i. e.* long-range order persists at finite temperatures. This is not surprising since our model (3.14) has *no continuous* symmetry. One thus expects the order to vanish at a finite temperature T_c in a first or second order phase transition. The temperature dependence of spin-spin correlations in $N = 21$ system is depicted in figure 3.10.

The finite size effects affect the correlations very strongly for system sizes $N < 21$. In figure 3.11 we plot the spin-spin correlations for the various system sizes. The data for N=15, 18 are averages of the raw data for fixed lattice distances over the lattice directions. Because of boundary effects the correlations do not show the expected six fold symmetry. As a consequence the data for N=15, 18 cannot be used in a finite-size extrapolation. Nevertheless, despite these large finite size effects, for both cases $J > 0$ and $J < 0$ the ground state energies can be reliably extracted from the data for all the cell sizes including the smaller ones. From the linear fits shown in figure 3.10 we obtain $E_{GS}^A = -0.40|J|$ as the ground state energy in case A. This is to be compared with the classical ground state energy (see subsection 3.5.3): $E_{class}^A = -\frac{3}{2}\tau^2|J| = -0.375|J|$, $(\tau = 1/2)$. In the same way we find $E_{GS}^B = -0.22J$ as the ground state energy per site in case B, which is
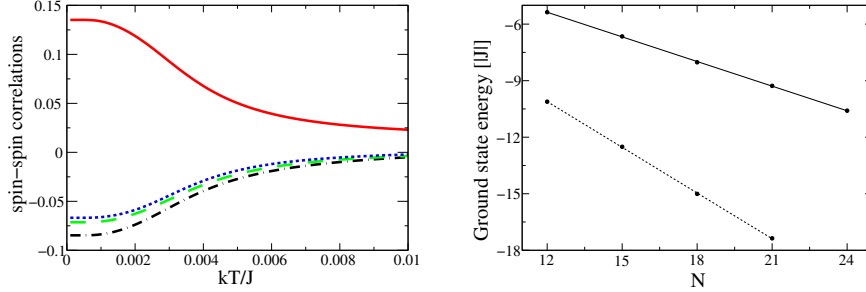
Figure 3.10. *Left picture: The curves from a bottom to top correspond to in-plane spin-spin correlation to the 1st neighbor (black, dash-dotted), 3rd neighbor (green, dashed), 4th neighbor (blue, dotted) and to the 2nd neighbor (red, solid). Two thousand lowest eigenstates were used in this calculation. The system size is $N = 21$.*
Right picture: Ground state energies in units of $|J|$ as a function of the system size N. Solid (dashed) line is a linear fit to $J > 0$ ($J < 0$) data. The fit gives in $J > 0$ case: $-0.22\,J\,N - 0.07\,J$, while in the $J < 0$ case: $0.40\,J\,N + 0.20\,J$.

to be compared to the classical ground state energy (see subsection 3.5.3) $E_{\text{class}}^{B} = -\frac{3}{4}\tau^2 J = -0.1875 J$.

Low energy spectra

Let us finally discuss the energy spectra of our model for both cases $J < 0$ (A), and $J > 0$ (B). Figures 3.12a, b show the accumulated density of states of our model (3.14) for the two cases. On account of the breaking of the discrete symmetries of the Hamiltonian (3.14) by the 120° Néel order the standard expectation would be that the ground state is sixfold degenerate for the *infinite* model and, since there is no continuous symmetry that could be broken, the excitations should be separated from the ground state by a finite gap of the order of J. For *finite* systems the ground state degeneracy will be lifted. Nevertheless, we expected to find six low-lying states in the gap below the lowest excited state. Figure 3.12a, $J < 0$, does not reflect this scenario convincingly. However, there are only a few states with energies substantially below $0.5|J|$. We take this as an indication of a gap of this order of magnitude in the spectrum of the Hamiltonian (3.14) in the thermodynamic limit $N \to \infty$.

Obviously, for $J > 0$ the spectrum differs drastically from the above expectations, see figure 3.12b. There is an abundance of very low-lying exci-
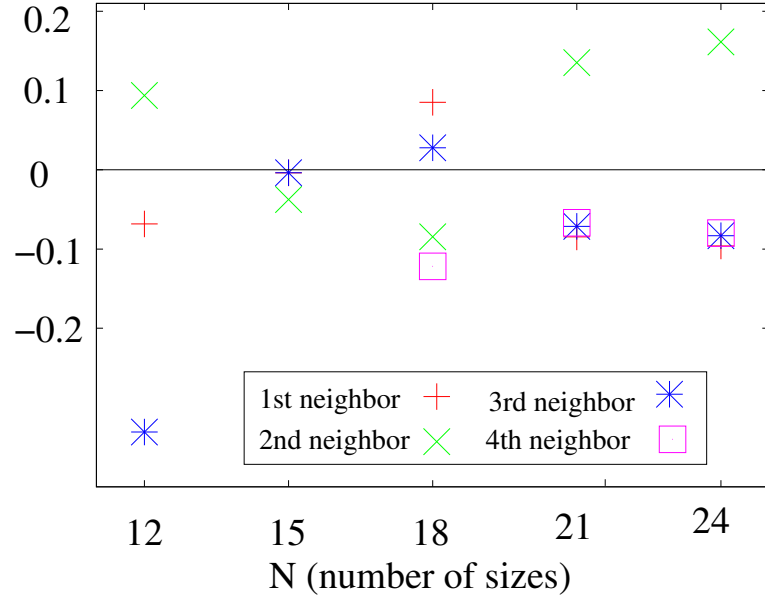
Figure 3.11.   *Spin-spin correlations for the various system sizes. The data for N=15, 18 are averages of the raw data for fixed lattice distances over the lattice directions.*
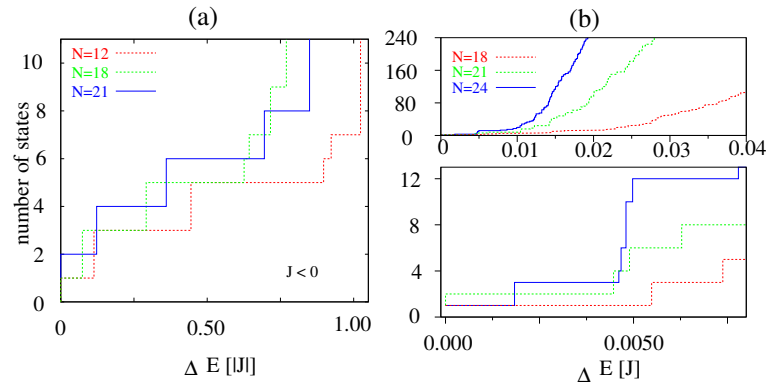

Figure 3.12.   *Accumulated density of states, ı. e. the number of states in the energy interval $\triangle E$ above the ground state for (a) $J < 0$ and (b) $J > 0$*

tations, e. g. for $N = 21$ there are about 2000 (800) states with energies less than $0.09J$ $(0.05J)$ above the ground state. From the perfect symmetry of a finite temperature spin-spin correlations and their relatively slow decay with the temperature, we conclude that the majority of these excited eigenstates support the spin order of the ground state.

Comparison of the lower panel of figure 3.12b with the scenario outlined above suggests that the gap, if any, is smaller than $0.5 \cdot 10^{-2}J$.

Because of the strong finite size effects in the data for $N < 21$ the growth law of the accumulated density of states with the system size N cannot be extracted reliably from our data. They are compatible, however, with an exponential increase of the number of low-lying states with N.

The features of the low-energy part of the spectrum of our model, equation (3.14), are strongly reminiscent of the low-energy part of the spin-1/2 Heisenberg antiferromagnet on the kagomé lattice (HAK) [139, 228]. There is, however, one decisive difference between the two models: while all ground state correlations were found to be extremely short ranged [141] in the HAK there is, by all probabilities, long range spin order in the ground state of our model. The absence of long range order in the HAK led Mila and Mambrini [154, 164] to study the trimerized HAK in the basis consisting of all independent dimer coverings of the lattice by exclusively nearest neighbor singlet pairs. By definition this restricted basis cannot produce any long range order in the ground state of the HAK. Using it in analytical and in numerical calculations Mila and Mambrini were able to reproduce the low-lying part of the spectrum of the HAK. In particular, they were able to determine the constant α in the growth law α^N that describes the increase of the number of low-lying states in the HAK. However, the approach of Mila and Mambrini is not suited for the treatment of our model for at least two reasons: *(i)* in contrast to the HAK our model is not $SU(2)$ invariant. Therefore, a restriction of the full Hilbert space of the model to exclusively singlet states is unwarranted. *(ii)* We need to describe spin-ordered states, and this is not possible in a basis consisting of products of nearest neighbor singlet pairs. We suggest that for our model (3.14) the abundance of low-lying quantum states corresponds to the abundance of classical ground state described in subsection 3.5.3. Zero-point fluctuations lift the degeneracy of the classical states leaving the spin correlations that are built into these classical states qualitatively untouched. On account of its low-energy properties we have proposed the name *quantum spin liquid-crystal* for our system.
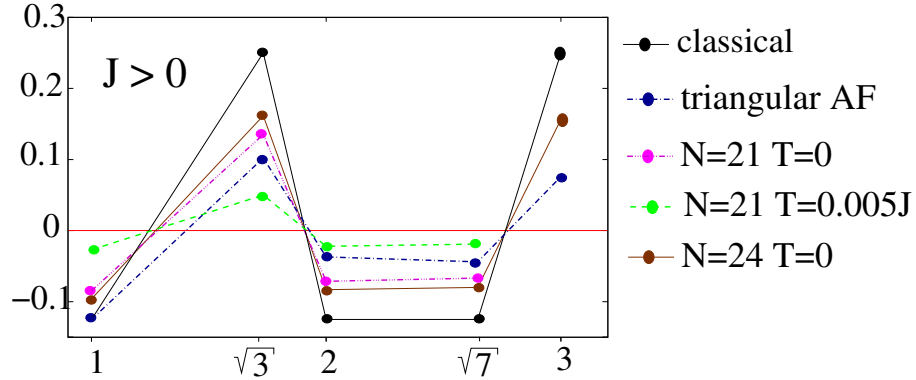
Figure 3.13.   *Spin-spin correlations as in Table I, but for $J > 0$.*

Specific heat

The rapid increase of the accumulated density of states that sets in at excitation energies of this order of magnitude leads to peaks in the specific heat:

$$c_v = \frac{1}{N} \frac{\partial}{\partial T} \frac{\sum_i E_i \exp[-E_i/(kT)]}{\sum_i \exp[-E_i/(kT)]}, \tag{3.19}$$

at the corresponding temperature. We have checked that the peak shifts towards lower temperatures as the size of the system increases. Indeed, in the $N = 24$ system, we found the peak at $kT \approx 2.5 \cdot 10^{-3} J$ while for $N = 21$ it is at $kT \approx 3.6 \cdot 10^{-3} J$, see figure 3.14 for the $N = 21$ results. Recent results for $N = 27$ support this tendency. The precise determination of the peak position and amplitude in the $N = 24$ system requires, however, a calculation based on more excited eigenstates than we have been able to get (~ 7029, see figure 3.12b). The shift of the peak position between these two systems reflects the slightly different behavior of their accumulated density of states. It would be very interesting to know whether this trend continues for larger N, which has consequences for the behavior of the entropy at very low temperatures. The entropy can be obtained using the specific heat:

$$S(t) = \int_0^t \mathrm{d}t' \frac{c_v(t')}{t'} \quad .$$

One possible scenario is that the temperature of the maximal amplitude for the specific heat $t_{\max}$ goes to zero as the system size increases, hence, $\lim_{t \to 0} S(t)$ can have a finite value. A finite entropy per particle at zero temperature violates the Nernst theorem and has been discussed in [144, 166].
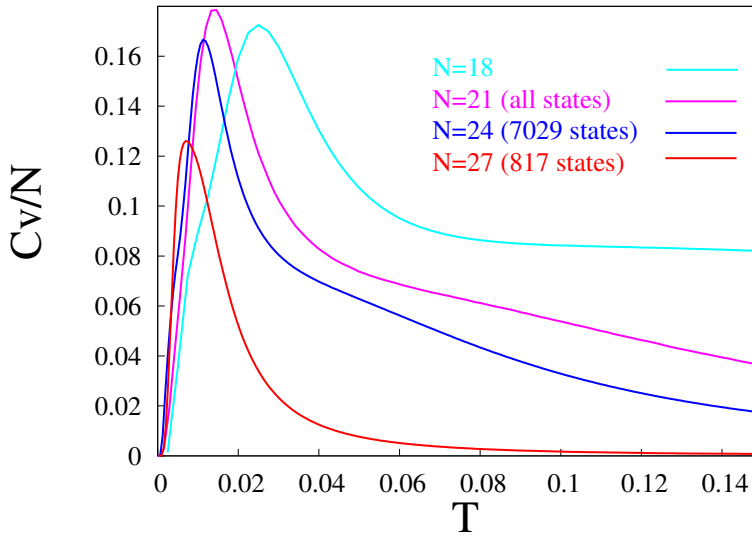
Figure 3.14. *Specific heat for different cell sizes.*

3.6 Bosons

3.6.1 Bose gas in the trimerized kagomé lattice

In order to facilitate the calculations, we add to the Hamiltonian (3.4) a term of the form $-\mu \sum_i n_i$, where μ is the chemical potential, that controls the average particle number of the system. In the trimerized kagomé lattice, the couplings t_{ij} take the values t, t' for intra- and inter-trimer hopping, respectively. We set also $U_{ij} = V$, $= V'$, for intra- and inter-trimer interactions, respectively.

In reference [198] we have considered the limiting case of hard core bosons, when U was much larger than any other energy scale, i.e. two bosons were not allowed at the same site. We have shown then that in the strongly trimerized case $(t', V' \ll V < t)$ the system will enter a trimerized Mott phase with the ground state corresponding to the product over (independent) trimers. Depending on the particular value of $\bar{\mu} \equiv (\mu - V)/(2t + V)$ we may have 0 $(\bar{\mu} < -1)$, 1 $(-1 \leq \bar{\mu} < 0)$, 2 $(0 \leq \bar{\mu} < 1)$ or 3 $(1 \leq \bar{\mu})$ bosons per trimer, i.e. filling factors $\nu = 0$, 1/3, 2/3 or 1 boson per site. For fractional filling, the atoms within a trimer minimize the energy forming a, so-called, W-state [72]: $|W\rangle = (|001\rangle + |010\rangle + |100\rangle)/\sqrt{3}$ for $\nu = 1/3$, and $|W\rangle = (|110\rangle + |101\rangle + |011\rangle)/\sqrt{3}$ for $\nu = 2/3$. It is worth noticing that W-states themselves have interesting applications for quantum information theory (c.f. [128]).

Figure 3.15. *Left picture: Mott phases (denoted by the corresponding particle numbers per trimer) of the state with lowest energy in the $t - (\mu + 2t)$ plane for zero inter-trimer hopping $t' = 0$.*
Right picture: Phase boundaries between Mott insulator and superfluid phase in parameter space of the hopping elements t, t' and the chemical potential μ. Below the loops the state is in a Mott phase, where the number of bosons per trimer is displayed in the diagram.
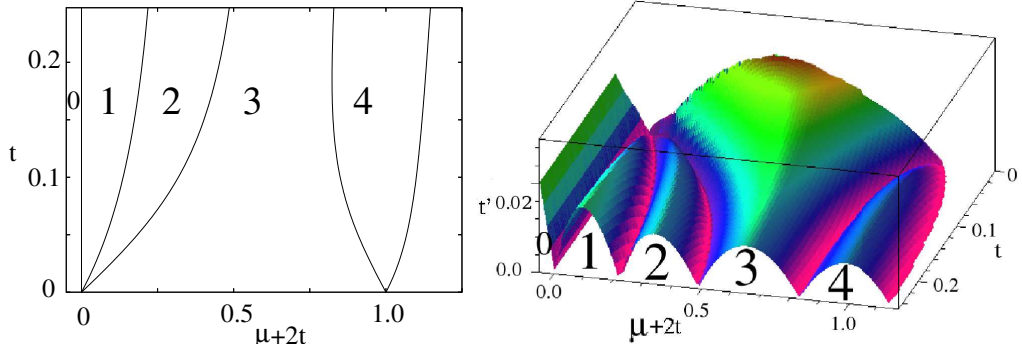
Generalizing the mean-field theory of Ref. [80], we have obtained the phase diagram in the $\bar{t}' \equiv t'/(2t + V)$ and $\bar{\mu}$ plane with characteristic lobes describing the boundaries of the Mott phases, given by $\bar{t}' = (|\bar{\mu}| - 1)/2$ for $|\mu| \geq 1$, and $\bar{t}' = (3/2)|\bar{\mu}|(1 - |\bar{\mu}|)/(4 - |\bar{\mu}|)$ for $|\mu| < 1$. Observations of this Mott transition require temperatures T of the order of t', i.e. smaller than t and V. Assuming that U is of the order of few recoil energies [100, 101], this requires T to be in the range of tens of nK. The results for $t < V$ are qualitatively similar.

In this section we present a method to generalize these results to the case when the bosons are not necessarily hard core, i.e. U may be comparable with t. For simplicity we set $U_{ij} = 0$, so that the Hamiltonian is still described by the three parameters: t, t' for intra- and inter-trimer hopping, and U for the on-site interactions. Obviously, for vanishing inter-trimer hopping, $t' = 0$, the system is in a Mott insulating state with a fixed number of particles per trimer. The corresponding Mott states are displayed in the phase diagram in the $t - (\mu + 2t)$ plane in figure 3.15. As t' is increased the system undergoes a phase transition into a superfluid state. To obtain the phase diagram for this transition, figure 3.15, we have used a generalization of the mean-field approach of Fisher *et al.* [80, 195, 218], also investigated in [36, 37]. Details of the method can be found in the subsection 3.6.2. In our calculations we have confined ourselves to values of the chemical potential such that the particle

number per trimer does not exceed four. In figure 3.15, further lobes with higher particle numbers will occur along the μ-axes for higher values of μ than those shown. Instead of calculating the, so-called, superfluid order parameter $\psi = \langle b_i \rangle = \langle b_i^\dagger \rangle$ self-consistently, a fully analytical expressions describing the boundaries in figure 3.15 can be obtained, as it is shown in the subsection 3.6.2. We mention that by using a cell strong coupling perturbative expansion [38, 86] the phase boundary can be obtained with relatively little numerical effort with the accuracy of a Quantum Monte Carlo simulation.

3.6.2 Mean-field theory for a bosonic gas

The boundaries between Mott insulator and superfluid phases can be obtained by means of a mean-field approach similar as that employed in reference [142]. We consider only on-site contact-interaction terms, but contrary to reference [142] we do not restrict ourselves to the hard-core limit. The system is governed by a Bose-Hubbard Hamiltonian of the form: $H = H_{\text{tr}} + H_{\text{hop}}$, with:

$$H_{\text{tr}} = = -t \sum_{\langle ij \rangle} (b_i^\dagger b_j + h.c.)$$

$$+ \frac{1}{2} \sum_i n_i (n_i - 1) - \mu \sum_i n_i \quad , \tag{3.20}$$

$$H_{\text{hop}} = -t' \sum_{\langle \alpha\beta \rangle} (b_\alpha^\dagger b_\beta + h.c.), \tag{3.21}$$

where t, t' (denoting the intra- and inter-trimer hopping) and μ are measured in units of the on-site interaction potential U. Greek indices denote inter-trimer hopping.

Assuming a fixed number of atoms n per trimer, we consider all possible Fock-states of the form $|n_1 n_2 n_3\rangle$ with $n_1 + n_2 + n_3 = n$. For example, for one particle per trimer the Hilbert-space contains the Fock-states $|100\rangle$, $|010\rangle$ and $|001\rangle$. Since the model is invariant under rotation of $2\pi/3$ the eigenstates are of the form $|W_1\rangle = (|100\rangle + z|010\rangle + z^2|001\rangle)/\sqrt{3}$, with $z \in \{1, \exp(i\frac{2}{3}\pi), \exp(-i\frac{2}{3}\pi)\}$, implying states with zero, left- and right-chirality, also known as W states [72]. We denote $z_\pm = \exp(\pm i2\pi/3)$ and introduce the operators $B_\pm = (b_1 + z_\pm b_2 + z_\pm^2 b_3)/\sqrt{3}$, $B_0 = (b_1 + b_2 + b_3)/\sqrt{3}$. Their commutation relations are $\left[B_\alpha, B_\beta^\dagger \right] = \delta_{\alpha\beta}$, where $\alpha, \beta \in \{0, +, -\}$. The chirality operator is defined as $\chi = (B_+^\dagger B_+ - B_-^\dagger B_-) \mathbf{mod} 3$. Equation (3.20)

can be rewritten in the form:

$$
\begin{aligned}
H_{\mathrm{tr}} &= -t3B_0^\dagger B_0 + (t-\mu)\left\{ B_0^\dagger B_0 + B_+^\dagger B_+ + B_-^\dagger B_- \right\} \\
&+ \frac{1}{6}\left\{ \left(B_0^{\dagger 2} + 2B_+^\dagger B_-^\dagger\right)\left(B_0^2 + 2B_+ B_-\right) \right. \\
&+ \left(B_+^{\dagger\,2} + 2B_0^\dagger B_-^\dagger\right)\left(B_+^2 + 2B_0 B_-\right) \\
&+ \left. \left(B_-^{\dagger\,2} + 2B_0^\dagger B_+^\dagger\right)\left(B_-^2 + 2B_0 B_+\right) \right\}.
\end{aligned}
\tag{3.22}
$$

One sees that $\left[\exp\mathrm{i}2\pi(B_+^\dagger B_+ - B_-^\dagger B_-)/3, H_{\mathrm{tr}}\right] = 0$, and hence, the chirality of a state is a conserved quantity. It can be shown that the ground state has chirality zero, and therefore we restrict ourselves henceforth to these states.

For a given number of particles n per trimer, we denote by $|W_n^\mu\rangle$ states that are symmetrized with respect to the occupation numbers n_1, n_2 and n_3 of the trimer. The subscript μ specifies a particular one of these non-chiral states. For instance, for two different states of this kind exist: $|W_2^1\rangle = (|110\rangle + |101\rangle + |011\rangle)/\sqrt{3}$ and $|W_2^2\rangle = (|200\rangle + |020\rangle + |002\rangle)/\sqrt{3}$. We can then diagonalize the Hamiltonian H_{tr} in this basis, $H_n^{\alpha\beta} = \langle W_n^\alpha|H_{\mathrm{tr}}|W_n^\beta\rangle$, obtaining the eigenenergies ϵ_n^l and eigenstates $|\psi_n^l\rangle$, where $0 \le l \le n$. The lowest energies ϵ_n^0 for each particle number n have to be compared to obtain the ground state in the $(t\text{-}\mu)$-phase space.

If the inter-trimer hopping t' is small, the phase boundaries in the t-t'-μ phase diagram can be well estimated by using a mean-field approach [80, 195, 218]. We introduce the superfluid order parameter $\psi = \langle b_i\rangle = \langle b_i^\dagger\rangle$, for every site i. Neglecting fluctuations of b_i, $b_j^\dagger$ in the second order, we can substitute $b_j^\dagger b_i = \psi(b_j^\dagger + b_i) - \psi^2$. H_{hop} can then be decomposed into a sum of single-site Hamiltonians of the form: $H_{\mathrm{hop}} \approx 6t'\psi^2 - 2\sqrt{3}t'\psi(B + B^\dagger)$. The Hamiltonian H is then decomposed into two parts $H = H_0 + V$, with $H_0 = H_{\mathrm{tr}} + 6t'\psi^2$ and $V = -2t'\sqrt{3}\psi(B_0 + B_0^\dagger)$, where H_0 is perturbed by V. In second order perturbation theory, the energy takes the form $E = \epsilon_n^0 + r\psi^2$, where:

$$
r = 6t' + \sum_{m=n\pm1,i} \frac{|\langle \psi_n^0 V \psi_m^i\rangle|^2}{\epsilon_n^0 - \epsilon_m^i} \quad .
\tag{3.23}
$$

The Mott insulator to superfluid transition is identified by setting $r = 0$: for $r > 0$ the energy is minimized for ψ^2 is zero (Mott insulator), while for $r < 0$ ψ acquires a finite value (superfluid state). The equation $r = 0$ defines a 2D manifold in the t'-t-μ-parameter space.

As an example, we determine the expression for the boundaries of the Mott phase with one particle per trimer. Due to the form of equation (3.23) this calculation demands the knowledge of the eigenenergies and eigenfunctions for $n = 1$ and $n = 2$. For $n = 1$,
$|\psi_1^0\rangle = (|001\rangle + |010\rangle + |100\rangle)/\sqrt{3} = B^\dagger|\psi_0\rangle$, and $\epsilon_1^0 = \langle\psi_1^0|H_{\mathrm{tr}}|\psi_1^0\rangle = -\mu - 2t$. For $n = 2$:

$$\epsilon_2^{0,1} = \frac{1}{2}\left(1 \mp \sqrt{(1+2t)^2 + 32t^2}\right) - t - 2\mu, \qquad (3.24)$$

and $|\psi_2^{0,1}\rangle = \cos\phi_{0,1}|W_2^2\rangle + \sin\phi_{0,1}|W_2^1\rangle$, with:

$$\tan\phi_{0,1} = \frac{1}{4\sqrt{2}t}\{(1+2t) \mp \sqrt{(1+2t)^2 + 32t^2}\}. \qquad (3.25)$$

At $t' = 0$ the region of 1 particle per trimer is provided by the condition $0 \le \epsilon_1^0 \le \epsilon_2^0$, i.e. when $-2t \le \mu \le t + (1 - \sqrt{(1+2t)^2 + 32t^2})/2$.

After a straightforward but tedious calculation, we can then calculate the sum in equation (3.23):

$$\sum_{m=0,2,i} \frac{|\langle\psi_1^0|V|\psi_m^i\rangle|^2}{\epsilon_1^0 - \epsilon_m^i}$$
$$= 4t'^2\psi^2\left(\frac{(6\mu - 24t - 4)}{\mu^2 - \mu(2t+1) - 8t^2} - \frac{3}{2t+\mu}\right). \qquad (3.26)$$

Hence, solving for $r = 0$, we obtain the value of t' at the phase boundary:

$$t' = \frac{1/2\,(\mu^2 - \mu(2t+1) - 8t^2)\,(2t+\mu)}{(\mu + 8t)(2t + 1/3) - \mu^2 - 8t^2}.$$

The results of this and further Mott loops are depicted in figure 3.15.

3.7 Fermion-fermion mixtures

Finally, we consider a fermion-fermion mixture with half filling for each species, i.e. a spin 1/2 Hubbard model:

$$H_{FF} = -\sum_{\langle ij\rangle} t_{ij}(f_i^\dagger f_j + \tilde{f}_i^\dagger \tilde{f}_j + \mathrm{h.c.}) + \sum_i V n_i \tilde{n}_i, \qquad (3.27)$$

where the operators f_i and $f_i^\dagger$ ($\tilde{f}_i$ and $\tilde{f}_i^\dagger$) are the creation and annihilation operators for the two components, $n_i = f_i^\dagger f_i$ ($\tilde{n}_i = \tilde{f}_i^\dagger \tilde{f}_i$), and, as above,

$t_{ij} = t_0$ (t'_0) for intra- (inter-) trimer hopping. In the strong coupling limit, $t_0, t'_0 \ll V$ [14], H_{FF} reduces to the Heisenberg antiferromagnet:

$$H = J \sum_{\langle i,j \rangle_{intra}} \vec{s}_i \cdot \vec{s}_j + \bar{J}' \sum_{\langle i,j \rangle_{inter}} \vec{s}_i \cdot \vec{s}_j, \tag{3.28}$$

where $J = 4t_0^2/V$, and $J' = 4t'^2_0/V$, and $\vec{s} = (s_x, s_y, s_z)$, with $n - \tilde{n} = 2s_z$, $f^\dagger \tilde{f} = s_x + \mathrm{i}s_y$, and $\tilde{f}^\dagger f = s_x - \mathrm{i}s_y$.

In the strongly trimerized limit [154, 164], the total spin of an individual trimer takes the minimal value, i.e. $1/2$. There are four degenerate states having $s_z = \pm 1/2$ and left or right chirality. The spectrum of the system in the singlet sector consists of a narrow band of low energy states of the width of order J', separated from the higher singlet (triplet) bands by a gap of order $3J/4$ $(2J'/3)$.

3.8 Conclusions

We have discussed in detail the physics of ultra-cold gases in trimerized kagomé lattices. The observation of this kind of physics, and detection of the predicted effects requires various steps: preparation of the trimerized lattice, loading of the considered gases into the lattice, and detection. The first step, i.e. the preparation of the kagomé lattice, has been discussed in detail in section 3.2.

Probably the easiest experiment to perform is the observation of the novel Mott phases of the Bose gas. Temperature requirements ($\simeq 100$nK) are rather moderate. The challenge here is to achieve a filling of $1/3$, $2/3$, $\cdots$ atoms per trimer. In principle physics should do it for us, since the "exotic" Mott phases are the thermodynamic phases of the system at zero temperature. There is, however, another elegant method of preparing such phases. To this aim one should start with a triangular lattice and achieve a Mott state with 1, 2, 3, ... atoms per site. Then one should deform the lattice to a trimerized kagomé. The detection of such Mott phases can be done simply by releasing the atoms from the lattice, as in reference [100, 101]. Coherence on the trimer level will then be visible in the appearance of interference fringes in time-of-flight images, which should reflect the on-trimer momentum distribution $\sim \sum_{i,j} \cos \vec{k}(\vec{r}_i - \vec{r}_j)$, where $\vec{r}_i$ are the positions of the minima in a trimer. In spite of the appearance of these fringes, the Mott insulator nature of the state would be apparent in the presence of a gap for the excitations, which can be observed by tilting experiments as those of reference [100, 101]. The opening of the gap should be analyzed as a function of the trimerization degree t'/t, which can be controlled as it has been discussed in section 3.2.

The experiment with a fermion-fermion mixture is more demanding. The main problem is, of course, the preparation of the states in the low energy singlet sector. A possible way to prepare a singlet state in the trimerized kagomé lattice with $T < 3J/4$ could employ the recently obtained Bose-Einstein condensates of molecules consisting of two fermionic atoms [102, 125] at temperatures of the order of 10 nK. Such BEC's should be loaded onto an ideal and weak kagomé lattice. Note that the molecules formed after sweeping across a Feshbach resonance, are in a singlet state of the pseudo-spin $\vec{s}$. This can be easily seen, because the two Fermions enter the resonance from the s-wave scattering channel (i.e. in the symmetric state with respect to the spatial coordinates), and thus are in a singlet state of the pseudo-spin (i.e. antisymmetric state with respect to exchange of electronic and nuclear spins). Since the interaction leading to the spin flipping at the Feshbach resonance [213] is symmetric under the simultaneous interchange of both nuclear and electronic spin, then the formed molecule remains in a pseudo-spin singlet state. The typical size of the molecule is of the order of the s-wave scattering length a, and thus can be modified at the resonance [184], which can be comparable to the lattice period. By increasing the lattice amplitude the molecule will be broken into two separate fermionic atoms, which occupy neighboring lattice sites and which are in a singlet pseudo spin state. In this way, a singlet covering of the kagomé lattice may be achieved, allowing for the direct generation of a Resonance Valence Bond Crystal [12].

Assuming that we can prepare the system in a singlet state at $t' < T < t$, then the density of states of the low lying singlet levels can be obtained by repeated measurements of the system energy. The latter can be achieved by simply releasing the lattice, so that all of the interaction energy in excess of the zero point energy is transformed into kinetic energy.

In a similar way we can measure the mean value and the distribution of any nearest neighbor two-spin correlation functions. To this aim one has to apply at the moment of the trap release an appropriately chosen nearest neighbor two-spin Hamiltonian and keep it acting during the cloud expansion (for details see [89, 90]). In a similar manner one can measure the spectrum of triplet excitation, by using a combination of super-lattice methods and laser excitation on can flip spins [27]. The measurement of the singlet-triplet gap requires a resolution better than J'.

A similar type of measurements can be performed in the ideal kagomé lattice, when $t = t'$. In this case, the singlet-triplet gap is filled with singlet excitations [228]. By varying ϕ, one can change the lattice quasi-statically from a strongly trimerized to the ideal kagomé lattice, for which the final value of J will be smaller than the initial J, but larger than the initial J'. The system should remain within the lowest set of 1.15^N states that originally

formed the lowest singlet band. The singlet-triplet gap, if any, is estimated to be $\leq J/20$, and should be measurable using the methods described above.

The observation of properties of the spinless interacting Fermi gas is also experimentally very challenging. The first step is to create the interacting Fermi gas, obviously. As we discussed it in subsection 3.3 this can be achieved either with dipolar particles, or composite fermions. Both of these possibilities are challenging themselves, although the rapid progress in cooling and trapping of dipolar atoms [104] and molecules allows one to hope that interacting spinless Fermi gases will be routinely available in the near future.

Preparing of the 2/3 filling is also a challenge. The low energy states may be prepared by employing quasi-static changes of the degree of trimerization of the lattice. For instance one can start with a completely trimerized lattice; the filling $\nu = 2/3$ may be achieved then by starting with $\nu = 1$, and eliminating 1 atom per trimer using, for instance, laser excitations. One can then increase t' and U' slowly, on the time scale slower than the final $1/J$ ($\simeq$seconds). Alternatively, one could start with $\nu \simeq 2/3$ in the moderately trimerized regime. As in reference [100, 101], the inhomogeneity of the lattice due to the trapping potential, would then allow to achieve the Mott state with $\nu = 2/3$ per trimer in the center of the trap. Nearly perfect 2/3 filling can be achieved by loading a BEC of molecules formed by 2 fermions into a triangular lattice, generating an MI state, quasi-statically transforming the lattice to a trimerized kagomé one, "dissociating" the molecules by changing the scattering length to negative values, and by finally optically pumping the atoms into a single internal state. Preparing $\nu = 2/3$ might involve undesired heating (due to optical pumping), which can be overcome by using laser, or phonon cooling afterwards (cf. [55]). Note that the imperfections of ν can be described by a "$t - J$"-kind of model, and are of interest themselves.

Yet another challenge is to measure the predicted properties of the "*quantum spin liquid-crystal*". One quantity which should be possible to measure relatively easy, is the energy of the system. This can be done simply by opening the lattice; by repeated measurement of the energy $E(T)$ at (definite) finite temperatures one would get in this way an access to the density of modes, i.e. one could compare the results with figure 3.12. From such measurements one could infer the existence of a gap E_{gap}, since, if E_{gap} is large enough, $E(T)$ becomes T-independent for $kT \leq E_{\text{gap}}$.

CHAPTER 4

WIGNER CRYSTALS IN DIPOLAR GASES

4.1 Introduction

Phenomena appearing in many-particle systems with interactions were already described in the early days of Quantum Mechanics [82, 111]. For instance, in 1934 Wigner concluded that interacting electrons occupy localized states [237]. In the eighties, another example of true many-body effects was given by the seminal discovery of the Fractional Quantum Hall Effect [188, 214] in an 2D electron gas in a strong magnetic field. To explain this phenomenon, Laughlin [138] proposed a trial wave function describing an incompressible quantum fluid with fractional charged quasi-particle excitations. Moreover, for sufficiently small densities of electrons, it is expected that this so called Laughlin state terminates into a Wigner crystal [199]. In the case when higher Landau levels are occupied, the ground state behavior of the system is more subtle and exhibits different new phases such as charge density waves called stripes and bubble phases [83]. Experimental evidence for the phase transition between a bubble phase and a Wigner crystal at a filling factor of approximately $\nu = 4.22$ is the detection of two resonances in the real diagonal microwave conductivity of a 2D electron system [143].

Nowadays, similar phenomena are being examined in ultracold atomic gases. Examples are the appearance of the fractional quantum Hall effect for a filling factor of $\nu = 1/3$ in rapidly rotating fermionic dipolar gases [15] or the integer quantum Hall effect with atomic fermions [173].

Creating true Coulomb forces in ultracold quantum gases is rather difficult, since any ionization process implies heating. Another approach for studying gases with long-range interactions would be using dipole-dipole forces. A promising setup of this kind, using condensed bosonic Chromium atoms with a magnetic dipole momentums of $6\mu_B$, has been employed to observe the effect caused by dipole-dipole interactions [208]. On the other hand, the magnitude of the interaction strength is much higher with electrical

dipoles, which appear in ultracold heteronuclear molecules, which inspired efforts towards the creation of dipolar molecular gases [23, 123]. In this line of research, a scheme of accumulating NH-radicals in a magnetic trap has been presented in references [23, 216, 217]. In the case of bosons, another way of obtaining a heteronuclear condensate is with optical lattices [60]. Each lattice site contains two atoms, one of each species: molecules are created via photo-association (e.g. see [205]) and, when the lattice potential is quasi statically ramped down, the superfluid phase is entered.

A useful tool when working with dipolar gases is the creation of a gauge field by rapidly rotating the gas. This gauge field is equivalent to that of a magnetic field parallel to the rotation axis, which allows us to transfer the results known for electrons in the lowest Landau level to fermionic rotating dipolar gases. In this framework, the appearance of a Laughlin wavefunction as a ground state at a filling factor of $\nu = 1/3$ was predicted, and an quasi-particle excitation spectrum was calculated in reference [15]. In this chapter we discuss the possibility of the formation of a Wigner crystal in a "magnetic field". It is expected [148, 149] that above a critical filling factor the crystal melts down.

In the first part we will compare the energies of a Laughlin state and a Wigner crystal taking into account a finite extension of the wavefunction in the axial direction. In the second part we discuss the effect of anharmonicity, which results in the melting of the crystal. For a growing filling factor the mean deviation of particles from their lattice points increases until the crystal melts. Knowing the melting point we are now able to a formulate a Lindemann criterion [145] for the Wigner crystal. The Lindemann criterion was formulated for classical crystals and says that when the amplitude of the particle oscillations exceeds a critical value, the crystal melts down. In quantum systems the oscillation amplitude is replaced by the deviation of mean value for the particle position.

4.2   The Wigner crystal

4.2.1   The system

In this chapter we consider ultracold dipolar fermionic gases in a quasi-2D system. The dipole moments are orientated perpendicular to the system plane, which can be achieved using either a strong electric field for electrical dipoles or, correspondingly, in the case of magnetic dipoles with a strong magnetic field, both fields being parallel to the axial direction, thus ensures an isotropic interparticle interaction in the 2D-plane. Additionally, the system

is examined in a fast rotating frame. Effectively, the rotation can be mapped onto a model of a charged particle in a magnetic field.

4.2.2 Classical energy

It is essential for all later considerations to know the lattice type of a Wigner crystal with dipolar interaction. Finding the configuration with the lowest energy also determines the phonon interaction behavior and decisively influences the melting parameter.

Generally, if the dipolar particles are placed at positions $\mathbf{r}_i$ the energy per particle reads:

$$E = \frac{d^2}{N} \sum_{i>j} \frac{1}{|\mathbf{r}_i - \mathbf{r}_j|^3} \quad , \tag{4.1}$$

where d is the dipole moment and N the particle number. For charged particles it is known that, compared to all other configuration, the triangular lattice structure has the lowest energy [29]. Following the lines of reference [29] it is possible to show that this is also true for dipolar particles. In the following, we will demonstrate that for dipolar particles the triangular lattice structure is at least a stable configuration. First we restrict ourselves to basis vectors with equal length, and we show that by varying the angle the triangular lattice is the energetically preferred structure. Then, by fixing the angle and varying the length of the vectors, we show that basis vectors with equal length minimize the energy.

A set of basis vectors with the length a can be characterized by the angle β:

$$\mathbf{b}_1 = a \begin{pmatrix} 0 \\ 1 \end{pmatrix} \quad \mathbf{b}_2 = a \begin{pmatrix} \sin \beta \\ \cos \beta \end{pmatrix} \quad . \tag{4.2}$$

If we trap the N dipoles in a fixed area, meaning the density n is constant, a depends on β. In the case of $\beta = \pi/2$ the density is $n = 1/a^2$. Varying the angle the density does not change, $n = 1/(\sin \beta a^2)$, therefore $a = 1/\sqrt{n \sin \beta}$. A particular position is $\mathbf{r} = l_x \mathbf{b}_x + l_y \mathbf{b}_y$, where l_x and l_y are integer numbers running, for infinity big lattices, from $-\infty$ to ∞. Using the parameterization in equation (4.2) the energy takes the form:

$$E = \frac{d^2}{2} n^{\frac{3}{2}} \sin^{\frac{3}{2}} \beta \sum_{l_x l_y \neq 0} \frac{1}{(l_x^2 + l_y^2 + 2l_x l_y \cos \beta)^{\frac{3}{2}}} \tag{4.3}$$

$$= d^2 n^{\frac{3}{2}} \sin^{\frac{3}{2}} \beta \left(\sum_{l_x l_y > 0} \frac{1}{(l_x^2 + l_y^2 - 2l_x l_y \cos \beta)^{\frac{3}{2}}} + \frac{1}{(l_x^2 + l_y^2 + 2l_x l_y \cos \beta)^{\frac{3}{2}}} + 2\zeta(3) \right) \quad .$$

Extrema of this expression correspond to the zeros of its derivative with respect to β:

$$\frac{\partial E}{\partial \beta} = \frac{3}{2} d^2 n^{\frac{3}{2}} \left\{ \sin \beta^{\frac{1}{2}} \cos \beta \left[\left(\sum_{l_x l_y > 0} \frac{1}{\left(l_x^2 + l_y^2 + 2 l_x l_y \cos \beta \right)^{\frac{3}{2}}} \right) \right. \right.$$

$$+ \left(\sum_{l_x l_y > 0} \frac{1}{\left(l_x^2 + l_y^2 - 2 l_x l_y \cos \beta \right)^{\frac{3}{2}}} \right) + 2\zeta(3) \right] + \sin \beta^{\frac{5}{2}} l_x l_y$$

$$\left. \times \left[\left(\sum_{l_x l_y > 0} \frac{1}{\left(l_x^2 + l_y^2 + 2 l_x l_y \cos \beta \right)^{\frac{5}{2}}} \right) - \left(\sum_{l_x l_y > 0} \frac{1}{\left(l_x^2 + l_y^2 - 2 l_x l_y \cos \beta \right)^{\frac{5}{2}}} \right) \right] \right\} .$$

We obtain extrema for two values of β:

$$\frac{\partial E}{\partial \beta} \Big|_{\beta = \frac{\pi}{2}} = 0$$

$$\frac{\partial E}{\partial \beta} \Big|_{\beta = \frac{\pi}{3}} = \frac{3}{4} d^2 n^{\frac{3}{2}} \sqrt{\frac{\sqrt{3}}{2}} \left[\sum_{l_x l_y > 0} \frac{1}{\left(l_x^2 + l_y^2 + l_x l_y \right)^{\frac{3}{2}}} \left(1 + 3 \frac{l_x l_y}{\left(l_x^2 + l_y^2 + l_x l_y \right)} \right) \right.$$

$$\left. + \frac{1}{\left(l_x^2 + l_y^2 - l_x l_y \right)^{\frac{3}{2}}} \left(1 - 3 \frac{l_x l_y}{\left(l_x^2 + l_y^2 - l_x l_y \right)} \right) + 2\zeta(3) \right]$$

$$= 0 \quad .$$

In order to determine a stable configuration we need to calculate the second derivative:

$$\frac{\partial^2 E}{\partial \beta^2} = \frac{3}{2} d^2 n^{\frac{3}{2}} \left[\left(\frac{1}{2} \frac{\cos^2 \beta}{\sin \beta^{\frac{1}{2}}} - \sin \beta^{\frac{3}{2}} \right) 2\zeta(3) \sum_{l_x, l_y > 0} \left\{ \left(\frac{1}{2} \frac{\cos^2 \beta}{\sin \beta^{\frac{1}{2}}} - \sin \beta^{\frac{3}{2}} \right) \right. \right.$$

$$\times \left(\frac{1}{\left(l_x^2 + l_y^2 + 2 l_x l_y \cos \beta \right)^{\frac{3}{2}}} + \frac{1}{\left(l_x^2 + l_y^2 - 2 l_x l_y \cos \beta \right)^{\frac{3}{2}}} \right)$$

$$\times 8 \sin \beta^{\frac{3}{2}} \cos \beta l_x l_y \left(\frac{1}{\left(l_x^2 + l_y^2 + 2 l_x l_y \cos \beta \right)^{\frac{5}{2}}} - \frac{1}{\left(l_x^2 + l_y^2 - 2 l_x l_y \cos \beta \right)^{\frac{5}{2}}} \right)$$

$$\times 10 \sin \beta^{\frac{7}{2}} l_x^2 l_y^2 \left(\frac{1}{\left(l_x^2 + l_y^2 + 2 l_x l_y \cos \beta \right)^{\frac{7}{2}}} + \frac{1}{\left(l_x^2 + l_y^2 - 2 l_x l_y \cos \beta \right)^{\frac{7}{2}}} \right) \left. \left. \right\} \right] \quad .$$

For $\beta = \pi/2$ the result is:

$$\frac{\partial^2 E}{\partial \beta^2}\Big|_{\beta=\frac{\pi}{2}} = 3d^2 n^{\frac{3}{2}} \left[\sum_{l_x, l_y > 0} \left(\frac{1}{\left(l_x^2 + l_y^2\right)^{\frac{3}{2}}} \left(10 \frac{l_x^2 l_y^2}{\left(l_x^2 + l_y^2\right)^2} - 1 \right) \right) - \zeta(3) \right]$$

$$= -0.9925 d^2 n^{\frac{3}{2}} \quad,$$

which indicates a local maximum. For $\beta = \pi/3$ the second derivative is positive:

$$\frac{\partial^2 E}{\partial \beta^2}\Big|_{\beta=\frac{\pi}{3}}$$

$$= \frac{3}{2} d^2 n^{\frac{3}{2}} \left[2 \left(\frac{1}{8} \sqrt{\frac{2}{\sqrt{3}}} - \left(\frac{\sqrt{3}}{2} \right)^{\frac{3}{2}} \right) \zeta(3) \right.$$

$$+ \sum_{l_x, l_y > 0} \left\{ \left(\frac{1}{8} \sqrt{\frac{2}{\sqrt{3}}} - \left(\frac{\sqrt{3}}{2} \right)^{\frac{3}{2}} \right) \left(\frac{1}{\left(l_x^2 + l_y^2 + l_x l_y\right)^{\frac{3}{2}}} + \frac{1}{\left(l_x^2 + l_y^2 - l_x l_y\right)^{\frac{3}{2}}} \right) \right.$$

$$+ 4 \left(\frac{\sqrt{3}}{2} \right)^{\frac{3}{2}} \left(\frac{1}{\left(l_x^2 + l_y^2 + l_x l_y\right)^{\frac{5}{2}}} - \frac{1}{\left(l_x^2 + l_y^2 - l_x l_y\right)^{\frac{5}{2}}} \right)$$

$$\left. \left. + 10 \left(\frac{\sqrt{3}}{2} \right)^{\frac{10}{2}} \left(\frac{1}{\left(l_x^2 + l_y^2 + l_x l_y\right)^{\frac{7}{2}}} + \frac{1}{\left(l_x^2 + l_y^2 - l_x l_y\right)^{\frac{7}{2}}} \right) \right\} \right]$$

$$= d^2 n^{\frac{3}{2}} 2.2219 \quad,$$

and therefore, the configuration $\beta = \pi/3$ corresponds to a local minimum.

Now we fix the angle $\beta = \pi/3$ and vary the lattice length which we can parameterize with the factor a and the angle α:

$$\mathbf{b}_1 = a \cos \alpha \begin{pmatrix} 0 \\ 1 \end{pmatrix} \quad \mathbf{b}_2 = \frac{a}{2} \sin \alpha \begin{pmatrix} \sqrt{3} \\ 1 \end{pmatrix} \quad . \tag{4.4}$$

The area per unit cell is $a^2 \sin 2\alpha$. To keep the density constant we set $a^2 = n/\sin 2\alpha$, where n is the density. The energy now becomes:

$$E = \frac{d^2}{2} \frac{n^{\frac{3}{2}}}{\sin^{\frac{3}{2}} 2\alpha} \sum_{l_x l_y \neq 0} \frac{1}{\left(\cos^2 \alpha l_x^2 + \sin^2 \alpha l_y^2 + \sin \alpha \cos \alpha l_x l_y\right)^{\frac{3}{2}}} \quad .$$

We calculate the first derivative and set $\alpha = \pi/4$, which corresponds to triangular lattice:

$$\frac{\partial E}{\partial \alpha}\big|_{\alpha=\frac{\pi}{4}} = \frac{d^2}{2}\left(\frac{n}{2}\right)^{\frac{3}{2}} 32 \sum_{l_x l_y \neq 0} \frac{l_y^2 - l_x^2}{\left(l_x^2 + l_y^2 + l_x l_y\right)^{\frac{5}{2}}}$$
$$= 0 \quad .$$

The second derivative at the angle $\alpha = \pi/4$ reads:

$$\frac{\partial^2 E}{\partial \alpha^2}\big|_{\alpha=\frac{\pi}{4}} = \frac{d^2}{2}\left(\frac{n}{2}\right)^{\frac{3}{2}} 24 \sum_{l_x l_y \neq 0} \frac{7l_x^4 + 6l_x^3 l_y - 2l_x^2 l_y^2 + 6l_x l_y^3 + 7l_y^4}{\left(l_x^2 + l_y^2 + l_x l_y\right)^{\frac{7}{2}}}$$
$$> 0 \quad .$$

The odd powers in l_x and l_y will sum up to zero and the remaining parts are always positive, hence we conclude that the energy has a local minimum when the basis vectors have the same length.

Using numerical methods, it can be rigorously shown that the triangular lattice has the lowest energy. Hence, in the classical limit the energy per particle, given equation (4.3), reads:

$$E = \frac{d^2}{a^3} 5.513 \quad .$$

4.3   Phonons in a non-rotating dipolar gas

Classically, the point-like dipoles are arranged in a triangular lattice and placed at the position $\mathbf{r}(\mathbf{l}_i)$. Allowing small displacements $\mathbf{u}(\mathbf{l}_i)$ from $\mathbf{r}(\mathbf{l}_i)$ (figure 4.1), the dipole-dipole interaction energy of equation (4.1) can be expanded in a Taylor series:

$$\Phi = d^2 \sum_{\mathbf{l}_i, \mathbf{l}_j \neq \mathbf{l}_i} \frac{1}{|(\mathbf{r}(\mathbf{l}_i) + \mathbf{u}(\mathbf{l}_i) - \mathbf{r}(\mathbf{l}_j) - \mathbf{u}(\mathbf{l}_j)|^3}$$
$$= \Phi_0 + \sum_{n=1}^{\infty} \frac{1}{n!} \sum_{\alpha_1 \ldots \alpha_n} \sum_{\mathbf{l}_1 \ldots \mathbf{l}_n} \Phi_{\alpha_1 \ldots \alpha_n}(\mathbf{l}_1 \ldots \mathbf{l}_n) u_{\alpha_1}(\mathbf{l}_1) \ldots u_{\alpha_n}(\mathbf{l}_n), \qquad (4.5)$$

where

$$\Phi_{\alpha_1 \ldots \alpha_n}(\mathbf{l}_1 \ldots \mathbf{l}_n) = \frac{\partial^n \Phi}{\partial u_{\alpha_1}(\mathbf{l}_1) \ldots \partial u_{\alpha_n}(\mathbf{l}_n)}\bigg|_{\mathbf{u}=0} \quad .$$

With $\alpha_i \in \{x, y\}$ and $u_\alpha(\mathbf{l}_i)$ denotes the $x(y)$-component of the vector $\mathbf{u}(\mathbf{l}_i)$, while the vector $\mathbf{l} = (l_x, l_y)^T$, containing integer components, labels every site on the lattice. Since the dipoles are placed in potential minima, the first order term vanishes. Moreover, the harmonic term depends on the difference $\mathbf{r}_i - \mathbf{r}_j$. The second derivative of the potential can be found in the appendix (B.1) and is used to calculate the force acting on a displaced dipole. Newtons second law reads:

$$m\frac{\mathrm{d}^2}{\mathrm{d}t^2}u_\alpha(\mathbf{l}) = -\sum_{\alpha'\mathbf{l}'} \Phi_{\alpha\alpha'}(\mathbf{l} - \mathbf{l}')u_{\alpha'}(\mathbf{l}') \quad , \tag{4.6}$$

where $\Phi_{\alpha\alpha'}(\mathbf{l} - \mathbf{l}')/m$ is called the dynamical matrix [31]. We consider a system with periodic boundary conditions and express the displacements in the Fourier space:

$$\mathbf{u}(\mathbf{l}, t) = \frac{1}{\sqrt{\pi}} \sum_{\mathbf{k}} \int_\infty^\infty \mathrm{d}\omega \tilde{\mathbf{u}}(\mathbf{k}, \omega) \, \mathrm{e}^{\mathrm{i}(\mathbf{kr}-\omega t)} \quad .$$

In such a case, equation (4.6) becomes:

$$\omega^2 \sum_{\mathbf{k}} \tilde{u}_\alpha(\mathbf{k}, \omega)\mathrm{e}^{-\mathrm{i}\mathbf{kl}} = \frac{1}{m} \sum_{\alpha'\mathbf{l}'\mathbf{k}} \Phi_{\alpha\alpha'}(\mathbf{l} - \mathbf{l}')\tilde{u}_{\alpha'}(\mathbf{k}, \omega)\mathrm{e}^{-\mathrm{i}\mathbf{kl}'}$$

$$= \frac{1}{m} \sum_{\alpha'\mathbf{k}} \omega_d^2 F_{\alpha\alpha'}(\mathbf{k}) \, \mathrm{e}^{-\mathrm{i}\mathbf{kl}} \tilde{u}_{\alpha'}(\mathbf{k}, \omega)$$

$$\Rightarrow \omega_\alpha^2(\mathbf{k})\tilde{u}_\alpha(\mathbf{k}) = \omega_d^2 \sum_{\alpha'} F_{\alpha\alpha'}(\mathbf{k})\tilde{u}_{\alpha'}(\mathbf{k}) \quad ,$$

where $\omega_d^2 = d^2 n^{3/2}/(a^2 m)$ and

$$\omega_d^2 F_{\alpha\alpha'}(\mathbf{k}) = \sum_{\mathbf{l}} \Phi_{\alpha\alpha'}(\mathbf{l})\mathrm{e}^{\mathrm{i}\mathbf{k}(\mathbf{l})}$$

are the Fourier transformations of the second derivatives. The approximate expression for $F_{\alpha\alpha'}(\mathbf{k})$ is given in the appendix (B.7). For a given $\mathbf{k}$, the problem is reduced to the diagonalization of a 2×2-matrix $F_{\alpha\alpha'}(\mathbf{k})$. The eigenvalues give the two branches of the phonon dispersion relation $\omega_i^2(\mathbf{k})$, and the corresponding eigenvectors $\vec{e}_i$ illustrate the polarization:

$$\omega_i^2(\mathbf{k})\vec{e}_{i,\alpha} = \omega_d^2 \sum_{\alpha'} F_{\alpha\alpha'}(\mathbf{k}) \, \vec{e}_{i,\alpha'}(\mathbf{k}) \quad , \tag{4.7}$$

where the $\omega_i(\mathbf{k})$ is the dispersion relation of the phonons in the lattice.
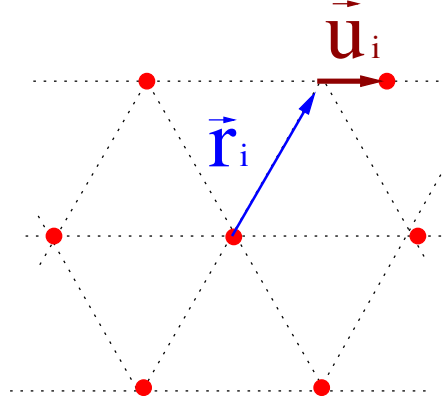
Figure 4.1.   *The particle sites on the ith lattice point with coordinate $\mathbf{r}_i$. The displacement of the particle from this lattice point is given by the vector $\mathbf{u}_i$.*

4.3.1   The phonon Hamiltonian

The dynamics of the phonons are described by the Hamiltonian:

$$H = H_0 + H_2 + H_3 + \cdots \quad ,$$

where up to the second order the form of H is:

$$H = \sum_{\alpha \mathbf{l}} \frac{p_\alpha^2(\mathbf{l})}{2m} + \frac{1}{2} \sum_{\alpha \beta} \sum_{\mathbf{l}\mathbf{l}'} \Phi_{\alpha\beta}(\mathbf{l}\mathbf{l}') u_\alpha(\mathbf{l}) u_\beta(\mathbf{l}') \quad ,$$

with the commutation relation:

$$[u_\alpha(\mathbf{l}), p_{\alpha'}(\mathbf{l}')] = \mathrm{i}\hbar \delta_{\mathbf{l}\mathbf{l}'} \delta_{\alpha\alpha'} \quad .$$

All other commutation relations are zero. Using the eigenvalues of the dynamical matrix (4.7) we express the coordinates:

$$u_\alpha(\mathbf{l}, t) = a\sqrt{\frac{\omega_0}{2}} \sum_{\mathbf{k}i} \vec{e}_{i\alpha}(\mathbf{k}) \frac{\mathrm{e}^{\mathrm{i}\mathbf{k}\mathbf{x}}}{\sqrt{\omega_i(\mathbf{k})}} \left(b_i(\mathbf{k}) \mathrm{e}^{-\mathrm{i}\omega_i(\mathbf{k})t} + b_i^\dagger(-\mathbf{k}) \mathrm{e}^{\mathrm{i}\omega_i(\mathbf{k})t} \right)$$

$$p_\alpha(\mathbf{l}, t) = \frac{\hbar}{a} \frac{1}{\sqrt{2\mathrm{i}\omega_0}} \sum_{\mathbf{k}i} \vec{e}_{i\alpha}(\mathbf{k}) \sqrt{\omega_i(\mathbf{k})} \, \mathrm{e}^{\mathrm{i}\mathbf{k}\mathbf{x}} \left(b_i(\mathbf{k}) \mathrm{e}^{-\mathrm{i}\omega_i(\mathbf{k})t} + b_i^\dagger(-\mathbf{k}) \mathrm{e}^{\mathrm{i}\omega_i(\mathbf{k})t} \right) \quad ,$$

$$(4.8)$$

with $\omega_0 = \hbar/(a^2 m)$. Now the Hamiltonian takes the compact from:

$$H = \sum_{\mathbf{k}i} \hbar \omega_i(\mathbf{k}) \left(b_i^\dagger(\mathbf{k}) b_i(\mathbf{k}) + \frac{1}{2} \right) \quad .$$

In the ground state we sum up the zero-point oscillations to get the correction of the energy:

$$\Delta E = \frac{\hbar}{2} \sum_{\mathbf{k}i} \omega_i(\mathbf{k}) \quad .\tag{4.9}$$

4.3.2 The dispersion relation

For every momentum $\mathbf{k}$ in equation (4.7) one gets two eigenvalues $\omega_i^2(\mathbf{k})$, $i \in \{T, L\}$, denoting the transversal and the longitudinal mode.

The elements of the dynamical matrix $\Phi_{\alpha\alpha'}/m$ decay with $\mathbf{r}^{-5}$. Therefore, one gets a very good approximation for the dispersion relation, when calculating the Fourier transform of the dynamical matrix, summing only the terms with the smallest $\mathbf{r}$ (see appendix (B.7)). The results for the different components of the Fourier transform take the form:

$$F_{xx}(\mathbf{k}) \approx \omega_d^2 \left\{ -\frac{3}{2} \left(\cos \mathbf{k}\mathbf{r}_1 + \cos \mathbf{k}\left(\mathbf{r}_1 - \mathbf{r}_2\right) \right) - 24 \cos \mathbf{k}\mathbf{r}_2 + 27 \right\}$$

$$F_{xy}(\mathbf{k}) = F_{yx}(\mathbf{k}) \approx \omega_d^2 \left\{ -15\frac{\sqrt{3}}{2} \left(\cos \mathbf{k}\mathbf{r}_1 - \cos \mathbf{k}\left(\mathbf{r}_1 - \mathbf{r}_2\right) \right) \right\}$$

$$F_{yy}(\mathbf{k}) \approx \omega_d^2 \left\{ -\frac{33}{2} \left(\cos \mathbf{k}\mathbf{r}_1 + \cos \mathbf{k}\left(\mathbf{r}_1 - \mathbf{r}_2\right) \right) + 6 \cos \mathbf{k}\mathbf{r}_2 + 27 \right\}, \tag{4.10}$$

where $\mathbf{r}_1$ and $\mathbf{r}_2$ are the basis vectors. Now the two branches of the dispersion relation could be expressed as:

$$\omega_{1,2}(\mathbf{k}) = \left(\frac{F_{xx}(\mathbf{k}) + F_{yy}(\mathbf{k})}{2} \pm \sqrt{\frac{\left(F_{xx}(\mathbf{k}) - F_{yy}(\mathbf{k})\right)^2}{4} + F_{xy}^2(\mathbf{k})} \right)^{\frac{1}{2}} ,$$

and are visualized in figure 4.2. The quantum correction of equation (4.9) to the energy is $\Delta E = \hbar\omega_d 3.22$.

4.3.3 Existence of a crystal

Placed at their lattice points, the dipoles oscillate around their potential minimum. If the amplitude of the ground state oscillation exceeds a critical value, anharmonic terms leading to phonon-phonon interactions are not negligible. The phonon-phonon interactions yield imaginary frequencies and the crystal starts to melt. We parameterize the problem with the modified melting parameter used in references [148, 149, 150]:
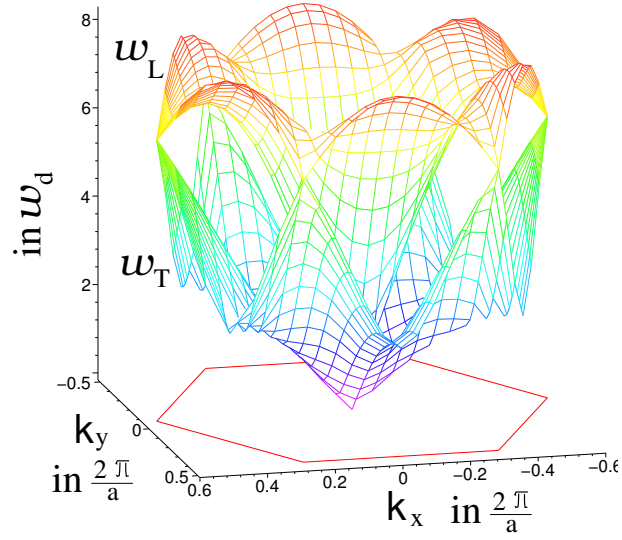
Figure 4.2. *Dispersion relation of the phonon Hamiltonian.*

$$\gamma = \frac{1}{a^2} \sum_\alpha \langle (u_\alpha(\mathbf{l}, 0) - u_\alpha(\mathbf{l} + \mathbf{a}, 0))^2 \rangle$$

$$= \frac{1}{a^2} \sum_\alpha \left(2\langle u_\alpha^2(\mathbf{l}, 0) \rangle - \langle u_\alpha(\mathbf{l}, 0) u_\alpha^\dagger(\mathbf{l} + \mathbf{a}, 0) \rangle - \langle u_\alpha(\mathbf{l} + \mathbf{a}, 0) u_\alpha^\dagger(\mathbf{l}, 0) \rangle \right)$$

$$= \frac{2}{a^2} \sum_\alpha \left(\langle u_\alpha^2(0, 0) \rangle - \langle u_\alpha(0, 0) u_\alpha^\dagger(\mathbf{a}, 0) \rangle \right) \quad ,$$

where the vector $\mathbf{a}$ points to the neighbored lattice cell. We can perform the last step due to the invariance under discreet lattice translations. Using equation (4.8) we get:

$$\gamma = \frac{2}{a^2} \sum_\alpha \left(\langle u_\alpha^2(0, 0) \rangle - \langle u_\alpha(0, 0) u_\alpha^\dagger(\mathbf{a}, 0) \rangle \right)$$

$$= \frac{\omega_0}{N^2} \sum_\alpha \sum_{\mathbf{k}\mathbf{k}'ii'} \frac{\vec{e}_{i\alpha}(\mathbf{k}) \vec{e}_{i'\alpha}(\mathbf{k}')}{\sqrt{\omega_i(\mathbf{k}) \omega_{i'}(\mathbf{k}')}} \left(1 - e^{i\mathbf{k}'\mathbf{a}} \right)$$

$$\times \left(\langle b_i(\mathbf{k}) b_{i'}^\dagger(-\mathbf{k}') \rangle + \langle b_i^\dagger(-\mathbf{k}) b_{i'}(\mathbf{k}') \rangle \right) \quad .$$

Since in the Fourier transformed dynamical matrix in equations (4.10) the quasi-momentum appears only as an argument in even functions, the dispersion relations and the polarization vectors are the same for a particular $\mathbf{k}$

and $-\mathbf{k}$. We rewrite the modified melting parameter:

$$\gamma = 2\frac{\omega_0}{N}\sum_{\mathbf{k}i}\frac{1-\cos\mathbf{ka}}{\omega_i(\mathbf{k})} \quad .$$

Because $\omega_i(\mathbf{k})$ scales with ω_d, the modified melting parameter grows with $\gamma \propto \sqrt{a}$. Apparently, the deviation is small for small a. According to Lindemanns law [145], a lattice is only stable for a sufficiently small lattice constant a. In experiments this is only possible up to a certain extent. If a becomes too small, the long range approximation of the dipole-dipole interaction is not valid, or the field strength to align the dipoles has to be extremely large.

4.4 Rotating frame

Alternatively, one can consider the experiment in a rotating frame. Rotating BEC's already have been examined quite extensively [2, 33, 45, 50, 153, 160, 203]. They show the well pronounced feature of vortices formations, which are quantized circulations of BEC's. In order to realize a rotating gas, it has to be trapped in an external potential which is approximately harmonic for small r. The effective potential vanishes if the rotational frequency approaches the trap potential frequency. Even faster rotational frequencies can be performed by applying non-harmonic higher order terms of the trapping potential [33].

A system in a rotational frame, rotating with frequency Ω, and trapped in an external harmonic potential with the trap frequency $\omega_\perp$, is described with the Hamiltonian:

$$\begin{aligned}
H &= -\frac{\hbar^2}{2m}\Delta + \frac{1}{2}\omega_\perp^2\mathbf{r}^2 - \Omega L_z + H_{DD} \\
&= -\frac{\hbar^2}{2m}\Delta + \frac{1}{2}\omega_\perp^2\mathbf{r}^2 - \mathrm{i}\Omega\hbar\left(y\partial_x - x\partial_y\right) + H_{DD} \\
&= \frac{1}{2m}\left(-\mathrm{i}\hbar\vec{\nabla} - \frac{q}{c}\vec{A}\right)^2 + \frac{1}{2}\left(\omega_\perp^2 - \Omega^2\right)\mathbf{r}^2 + H_{DD} \quad ,
\end{aligned} \qquad (4.11)$$

with

$$\vec{A} = m\Omega\frac{c}{q}\begin{pmatrix} -y \\ x \end{pmatrix} \quad .$$

Here H_{DD} is the interparticle interaction energy caused by the dipole-dipole potential. The Hamiltonian (4.11) describes a model of a particle carrying

a charge q in a magnetic field with the corresponding cyclotron frequency $\omega_c = 2\Omega$. In the case of non-interacting particles, $H_{DD} = 0$ and in the regime of the critical rotation $\omega_\perp = \Omega$, the properties of the Hamiltonian (4.11) are well known. The corresponding energy levels are called Landau levels:

$$E_n = \hbar\omega_c \left(n + \frac{1}{2} \right) \quad .$$

One level has a degeneracy (per unit area) that reads:

$$n_B = \frac{1}{2\pi l_B^2} \quad ,$$

where $l_B = \sqrt{\hbar/(qB)}$ is the magnetic length. Henceforth, we express a length in the unit of l_B ($l_B = 1$). The filling factor is defined as:

$$\nu = \frac{n}{n_B} \quad ,$$

where n is the particle density in the system. Increasing the "magnetic field" at a constant density leads to lower filling factors. In the following we consider only states in the lowest Landau level. The contribution to the energy, coming from the non-interacting part of the Hamiltonian, are the same for all single particle wavefunctions. Subsequently, we deal with product states of single particle wavefunctions and, therefore, only consider the interaction energy.

4.5   Laughlin wavefunction

In the presence of interparticle interaction, finding the ground state of the system becomes difficult. For an electronic system in the completely filled lowest Landau level ($\nu = 1$), an approach based on trial wavefunctions is known to be very successfully. Among many trial wavefunctions the most known are Laughlin wavefunctions which are close to the ground state at a filling factor of $\nu = 1/3$ [188].

In order to describe the observed fractional quantum Hall effect, Laughlin suggested a variational state fulfilling the constraints:

- The many-body wavefunction is comprised of solely single-body wave-functions lying in the lowest Landau level.

- This wavefunction is entirely antisymmetric.

- The wavefunction is an eigenstate of the total angular momentum.

Inspired by an approximate solution for small particle numbers, he suggested a form that is:

$$\psi_M(z_1 \dots z_N) = \prod_{j<k}^{N} (z_j - z_k)^M e^{-\frac{1}{4}\sum_{l=1}^{N}|z_l|^2} \quad , \tag{4.12}$$

here N is the particle number, $M \in 1, 3, 5, \dots$ corresponds to the inverse of the filling factor, and z_i is the complex representation of the point in a 2D-plane. In this expression we ignore the normalization. For filling factors around $\nu = 1/3$, the Laughlin wavefunction is a very good approximation and it was suggested to appear also in dipolar systems [15]. On the other hand, it has been shown for systems with Coulomb interaction that, while reducing the filling factor, the ground state becomes a charge density wave, for instance a Wigner crystal [95, 124].

4.5.1 Energy of the Laughlin state

We have calculated the energy of the Laughlin wavefunction at different filling factors. The interaction energy reads:

$$U_L = \frac{d^2}{2M} \int_0^{\infty} \mathrm{d}r\, r \frac{g(r)}{r^3} \quad , \tag{4.13}$$

where r is measured in units of l_B, and $g(r)$ is the pair correlation function:

$$g(z_1 - z_2) = \frac{2\pi M N(N-1)}{\langle \psi | \psi \rangle} \int \mathrm{d}z_3 \dots \mathrm{d}z_N |\psi(z_1, z_2; z_3 \dots z_N)|^2 \quad . \tag{4.14}$$

For $\nu = 1$ the correlation function can be analytically obtained in the thermodynamical limit [188] and reads:

$$g(\mathbf{r}) = 1 - e^{-\frac{r^2}{2}} \quad .$$

Therefore, the interaction energy is $U = d^2\sqrt{2\pi}/4 \approx d^2 0.627$. For other values of M, the pair-correlation function $g(r)$ can only be approximately calculated [94]. We present the results of our Monte-Carlo calculation in subsection 4.5.2.

Energy corrections due to the extension in the third dimension

The quasi-2D regime is achieved by strongly confining the gas in one dimension, e.g. in the ξ-direction. Nevertheless, the gas has a finite Gauss shaped extension in this direction, which depends on the trap frequency in ξ-direction. For sufficiently strong confinement in the ξ-direction the wavefunction can be rewritten in the form:

$$\psi_{3D}(\{z_i, \xi_i\}) = \psi_{2D}(\{z_i\}) \left(l\sqrt{\pi}\right)^{-\frac{N}{2}} e^{-\frac{1}{4l^2}\sum_i \xi_i^2} \quad,$$

where l determines the extension in ξ-direction. The trial extend in the ξ-direction will modify the interparticle interaction in the 2D-plane. Assuming that two dipoles have a distance r in a 2D-plane, the interaction energy is:

$$\begin{aligned}
v_{2D}(r) &= \frac{d^2}{l^2\pi} \int_{-\infty}^{\infty} d\xi_1 d\xi_2 e^{-\frac{\xi_1^2 + \xi_2^2}{l^2}} \left((\xi_1 - \xi_2)^2 + r^2\right)^{-\frac{3}{2}} \left(1 - \frac{3(\xi_1 - \xi_2)^2}{(\xi_1 - \xi_2)^2 + r^2}\right) \\
&= \frac{d^2}{l^3\sqrt{2\pi}} \int_0^{\infty} d\xi e^{-\xi \frac{r^2}{2l^2}} \sqrt{\frac{\xi}{(\xi + 1)^3}} \quad.
\end{aligned} \tag{4.15}$$

In the limit of $r \gg l$ the potential behaves like:

$$v_{2D}(r \gg l) \approx \frac{d^2}{r^3} \quad.$$

The effective potential is shown in figure 4.3. It appears that $v_{2D}(r)$ is always smaller than d^2/r^3. However, the difference $v_{2D}(r) - d/r^3$ only becomes noticeable for small values of $r < l_B$, and is therefore important for filling fractions of the order unity or larger.

4.5.2   Monte-Carlo integration

In this subsection we want to obtain the pair correlation function (4.14). With the help of a Monte Carlo method [188] we perform an integration over $(2N - 4)$ dimensions where N is the particle number.

Numerical treatment

We calculated the pair correlation $g(r)$ function for filling factors from 1 down to 1/19 where the number of particles in our computation is 512. In order to perform the integration we use the "Plasma analogy" [138, 188]. The density of the Laughlin wavefunction in equation (4.12) reads:

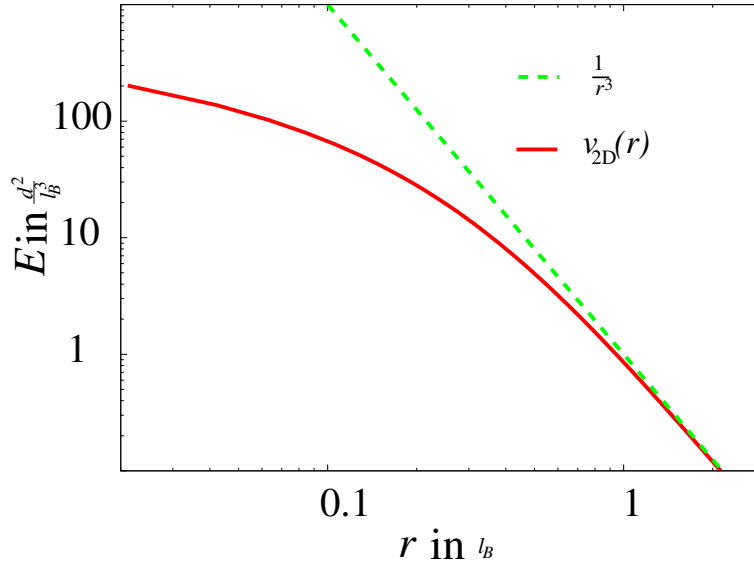$$\rho(\{z_i\}) = e^{-\sum_{i>j} 2M \ln|z_i - z_j| + \sum_i |z_i|^2} \quad.$$

Figure 4.3. *The effective potential* v_{2D} *in a* log-log *plot. For big r the potential approaches* $1/r^3$.

The integration of ρ over all variables is formally equivalent to the canonical partition sum of a 2D plasma gas in a harmonic trap at the temperature $T = M$. This problem can be solved with standard algorithms. We use importance sampling by performing a Marcov chain with 2^{32} sample points which are obtained by a Metropolis algorithm.

In our algorithm one particle is pinned at the origin. We randomly choose one of the other particles and change the position by a random value either in the x or in y direction. The update is certainly accepted to be the new configuration if the "energy of the plasma gas" is decreased. If the energy is increased the probability of accepting the update is:

$$p = e^{-\beta \Delta E} \quad ,$$

where ΔE is the energy difference between the old configuration and the update and $\beta = 1/T$ is the filling factor. This procedure is known to provide the proper statistics for the importance sampling. In order to measure the pair correlation function, the plane is divided into rings with equal width as demonstrated in figure 4.4. After every interaction step, the number of particles in each ring is counted. In the end the result in each ring is averaged over all iterations. The number of rings in our calculation is 640, where the outer radius of the last ring is $r_{640} = 1.1 R_M$, with $R_M \approx \mu 2NM l_B$ being radius of the Laughlin wavefunction. The width of the ring is small, but
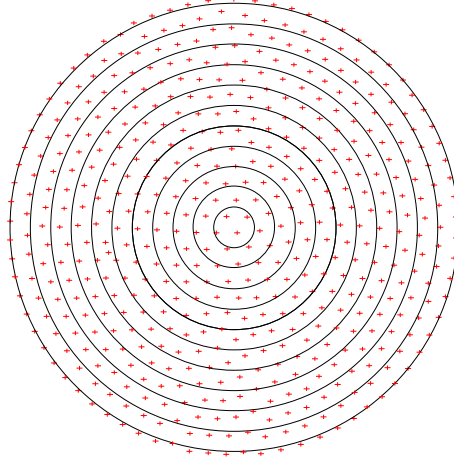
Figure 4.4.   *The plane is divided into rings. In every realization the particles within a particular ring are counted.*

finite, Hence, one has to estimate the mean radius corresponding to the ring. The value of the radius is limited by the inner and outer radii of this ring. In order to estimate the radius, we consider the distribution of counted points within the ring. If the rings are sufficiently narrow, we can approximate the distribution linearly as $g(r) \approx c + \lambda r$, where r is in the range of the considered ring. We calculate the expectation value for the radius that reads:

$$\langle r \rangle = \frac{\int_{r_R - \delta r}^{r_R} \mathrm{d}r \, g(r) r^2}{\int_{r_R - \delta r}^{r_R} \mathrm{d}r \, g(r) r} \quad ,$$

where r_R is the outer radius of the ring and δr is the width of the ring. Using the approximate form of $g(r)$, the expectation value radius for this ring reads:

$$\langle r \rangle = \frac{\lambda r_R^3 + r_R^2 \left(c - \frac{3}{2}\lambda dr \right) - r_R dr \left(c - \lambda dr \right) + dr^2 \left(\frac{1}{3}c - \frac{1}{4}\lambda dr \right)}{\lambda r_R^2 + r_B \left(c - \lambda dr \right) - dr \left(\frac{1}{2}c - \frac{1}{3}\lambda dr \right)} \quad . \quad (4.16)$$

In order to get the proper amplitude of the pair correlation function, we also allow the center particle to move within the frame of a "plasma gas" analogy [138, 188]. The outcome would be the density distribution of the Laughlin state, which is known to be $\rho(r) = 1 / \left(2\pi M l_B^2 \right)$ where we set $l_B = 1$. On the other hand, an unpinned center particle does not sufficiently change the distribution far away from the origin. Consequently, we have to multiply our results with $2\pi M$. In our calculations the pair-correlation functions have the amplitude of $g(r) \approx 1$, for r sufficiently far away from the center and the edge.

For lower filling factors the oscillation amplitude is less dumped (see figure 4.5). In order to calculate the pair correlation functions for filling factors below 1/19, one has to choose a particle number above $N = 512$ which is numerically demanding. As a check we calculate the interaction energy of an electronical system. The corresponding energy (see [136]) for $\nu = 1/5$ is:

$$U_{\text{el}} = \frac{e^2}{2Ml_B} \int_0^\infty (drg(r) - 1)$$
$$= -\frac{e^2}{l_B} 0.32756 \quad,$$

which is in a good agreement with earlier outcomes [136] where the energy is $U_{\text{el}} = -e^2/l_B(0.3277 \pm 0.0002)$. Here e is the charge of the electron.

Accuracy

The sources for inaccuracy are:

- the finite system size,

- the finite resolution,

- the finite number of realization.

We considered a system with 512 particles, therefore, the radius of the Laughlin state is $R_M \approx \sqrt{2NM}\, l_B \approx 71l_B$. Albeit the system is relatively huge, it suffers from finite size effects, which are responsible for oscillation with an amplitude of $\Delta g(r) \approx 0.005$. Therefore, the upper border of integration determines the result of the interaction energy, which oscillates with an amplitude of $\Delta U_{\text{el}}^1 \approx 0.0003$. The deviation of the expectation value is $\sigma_{\text{el}} = 0.00022$.

In order to interpolate the discrete points we are using the Cubic Spline Interpolation [81]. The resolution is the width of the rings which is $\approx 0.12l_B$. The inaccuracy coming from this routine depends on the 4th order Taylor expansion of the pair correlation function. With a typical oscillation length of the pair-correlation function of $\approx 5l_B$, the error coming from the Spline routine is $\Delta U_{\text{el}}^2 < 0.0001$. We want to emphasize that choosing the right values for the radii of the rings, which is given by equation (4.16), has the same effect as taking a higher resolution. Since our function is relatively smooth, we can safely assume that the error of values for λ is less than 10%, hence the resulting error is $\Delta U_{\text{el}}^3 < 0.00002$ which we can neglect. The error for c is based on the numerical inaccuracy of the metropolis algorithm. It turns out that this error is $\Delta U_{\text{el}}^4 < 0.00002$.

In order to estimate the inaccuracy coming from the finite number of samples in the metropolis algorithm, we need to consider the correlation length between the realizations. Starting from a particular realization, we only get reliable results if the correlation to the subsequent realizations is decaying exponentially with consecutive iteration steps. The correlation of two realizations that are separated by l steps reads:

$$\langle r_t r_{t+l} \rangle = e^{-\frac{l}{\gamma}} \quad ,$$

here r_t is the realization at the step t and $\langle r_t r_{t+l} \rangle$ is a scalar product between realizations. The effective uncertainty reads [25]:

$$\sigma_{\text{eff}} = \sigma \sqrt{\frac{1+2\gamma}{N}} \quad ,$$

whereas $N = 2^{32}$ is the number of realizations and σ is the deviation:

$$\sigma^2 = \langle n_R^2 \rangle - \langle n_R \rangle^2 \quad .$$

$\langle n_R \rangle$ is the averaged number of particles in the ring R, divided by the area of the particular ring and multiplied with $2\pi M$ respectively; $\langle n_R^2 \rangle$ corresponds to the averaged square of the counted particle numbers. The deviation in the energy $\Delta U_{\text{el}}^5 \approx 0.0001$. Our final result is $U_{\text{el}} = -0.32756 \pm 0.00036$ and it agrees with the result of [136].

4.6   Energy correction of the Wigner crystal

In the classical limit the energy is a sum of all interaction energies of point like particles. This limit neglects the finite size of the dipole wavefunction in both the x-y-plane and the extension into the ξ-direction. Due to the anisotropy of a dipole-dipole potential both corrections have different signs and we consider them separately.

For low filling factors $\nu < 1/3$ the dipoles are sufficiently separated. Therefore, the wavefunction is a product state of eigenfunctions in the lowest Landau level, centered at the positions where the classical energy is minimized. The state reads:

$$\psi_W = \mathcal{A} \prod_j \phi_{\mathbf{R}_j}(\mathbf{z}_j) \quad ,$$

where $\mathcal{A}$ is the antisymmetrization operator. The eigenfunction of the lowest Landau level takes the form:

$$\phi_{\mathbf{R}} = \frac{1}{\sqrt{2\pi l_B^2}} e^{-\frac{1}{4l_B^2}|\mathbf{z}-\mathbf{R}|^2 - \frac{1}{4l_B^2}(\mathbf{z}\mathbf{R}^* - \mathbf{z}^*\mathbf{R})} \quad .$$
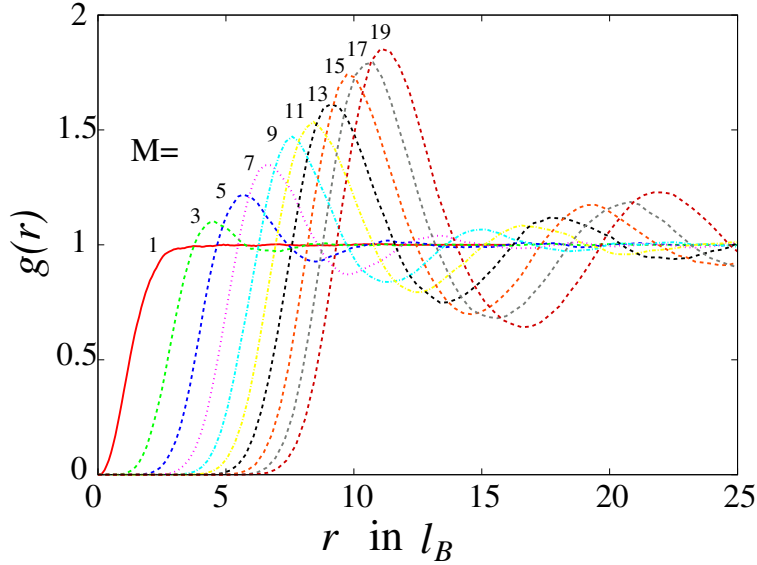
Figure 4.5. *The figure shows the pair correlation functions of a Laughlin state at different filling factors.*

In appendix (B.1) it is demonstrated that for sufficiently low filling factors the antisymmetrization can be omitted. Hence, the energy between two 2D wave-packages $\phi(x, y)$, separated by the vector $\mathbf{R} = (0, aR)$, reads:

$$E_{12} = \int_{\infty}^{\infty} dx_1 dx_2 dy_1 dy_2 \phi_0(x_1, y_1)^2 \phi_{\mathbf{R}}(x_2, y_2)^2 v_{2D}\left(\sqrt{(x_1 - x_2)^2 + (y_1 - y_2)^2}\right)$$

$$= \frac{1}{l_B^2 4\pi} \int_{\infty}^{\infty} dx dy \, e^{-\frac{(x - aR)^2 + y^2}{4l_B^2}} v_{2D}\left(\sqrt{(x - aR)^2 + y^2}\right) \quad . \tag{4.17}$$

$v_{2D}(r)$ is the effective 2D potential and a is the lattice constant, and $R \geq 1$ is dimensionless. In the pure 2D case the potential is $v(r) = 1/r^3$. If we omit the antisymmetrization, the integrand of the second line has a non integrable pole at $\mathbf{r}_1 = \mathbf{r}_2$, where $\mathbf{r}_i = (x_i, y_i)$. On the other hand, the antisymmetric wavefunction vanishes at this point, hence the density wave function grows quadratically in the difference $\mathbf{r}_1 - \mathbf{r}_2$. The pole in the integrand is of the first order, and is therefore integrable. However, the main distribution of the integral comes from the vicinity of $\mathbf{r}_1 = \mathbf{r}_2 - \mathbf{R}$.

The extension in the ξ-direction

Taking into account the extension in the ξ-direction, the effective 2D potential in the case of fully polarized dipoles is given in equation (4.15) and

reads:

$$v_{2D}(r) = \frac{d^2}{l^3\sqrt{2\pi}} \int_0^\infty d\xi e^{-\xi\frac{r^2}{2l^2}} \sqrt{\frac{\xi}{(\xi+1)^3}} \quad ,$$

with $r^2 = x^2 + y^2$. We assume that the extension in ξ direction is smaller than the interparticle distance $l \ll aR$. Now, we can expand the integrand around $\xi = 0$ and get:

$$v_{2D}(r) \approx \frac{d^2}{l^3\sqrt{2\pi}} \int_0^\infty d\xi e^{-\xi\frac{r^2}{2l^2}} \left(\sqrt{\xi} - \frac{3}{2}\xi^{\frac{3}{2}} + \frac{15}{8}\xi^{\frac{5}{2}} - \frac{35}{16}\xi^{\frac{7}{2}} \cdots \right)$$

$$= \frac{d^2}{r^3} \left(1 - \frac{9}{2}\left(\frac{l}{r}\right)^2 + \frac{225}{8}\left(\frac{l}{r}\right)^4 - \frac{3675}{16}\left(\frac{l}{r}\right)^6 + \cdots \right) \quad .$$

As expected, in the limit of vanishing l the potential is $v_{2D}(r) = 1/r^3$.

The extension in the x-y-plane

We develop the effective potential $v_{2D}(\sqrt{(x-a)^2 + y^2})$ around $x = 0$ and $y = 0$ and solve the integral in equation (4.17):

$$E_{12} \approx \frac{d^2}{(aR)^3} \left(1 + 9\frac{1}{R^2}\left[\frac{l_B}{a}\right]^2 \beta + \frac{255}{2}\frac{1}{R^4}\left[\frac{l_B}{a}\right]^4 \beta^2 \right.$$

$$\left. + \frac{3675}{2}\frac{1}{R^6}\left[\frac{l_B}{a}\right]^6 \beta^3 + \frac{297675}{8}\frac{1}{R^8}\left[\frac{l_B}{a}\right]^8 \beta^4 + \cdots \right) \quad ,$$

with

$$\beta = 1 - \frac{1}{2}\left[\frac{l}{l_B}\right]^2 \quad .$$

With $(l_B/a)^2 = \sqrt{3}/(4\pi M)$ and summing over all lattice sites we finally get:

$$U_W \approx \frac{d^2}{M^{3/2}} \left\{ 0.2823 + 0.2146\frac{\beta}{M} + 0.3388\frac{\beta^2}{M^2} \right.$$

$$\left. + 0.7456\frac{\beta^3}{M^3} + 2.0676\frac{\beta^4}{M^4} + \cdots \right\} \quad .$$

In figure 4.6 the interparticle interaction energy of a Laughlin state and a Wigner crystal at different extensions in the ξ-direction are compared. In figure 4.7 a phase diagram is presented in the M-l plane. Comparing a Laughlin state and a Wigner crystal, the state with a lower interparticle interaction energy is shown. For low filling factors the Wigner crystal is energetically favorable.
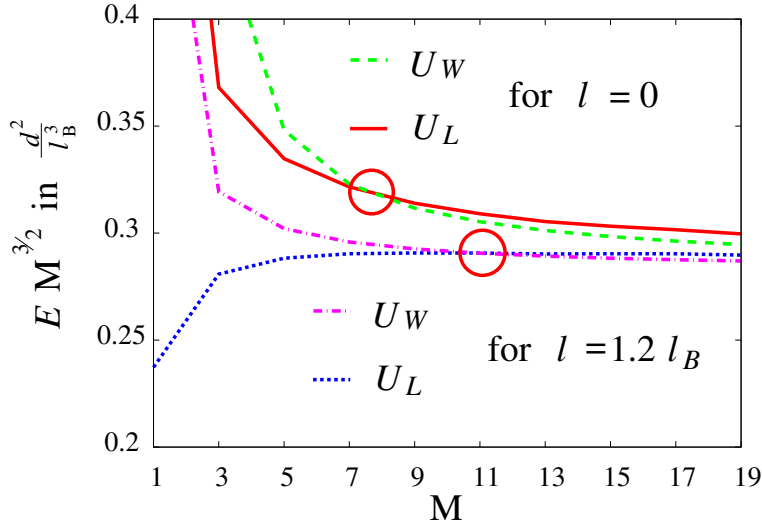
Figure 4.6.   *Interaction energies of a Laughlin state and of a Wigner crystal without extension in ξ-direction (l = 0) and with a finite extension (l = 1.2l_B). The red circles denote the phase transition.*

4.7 Phonons in a rotating crystal

4.7.1 The Bogoliubov transform

In order to examine the spectrum, we diagonalize the Hamiltonian in a "magnetic field", effectively caused by the rotation. The desired shape of the Hamiltonian is:

$$H = \hbar \sum_{\mathbf{k}} \sum_{m=-,+} \omega_m(\mathbf{k}) \left(b_m^\dagger(\mathbf{k}) b_m(\mathbf{k}) + \frac{1}{2} \right) \quad ,$$

here − and + are two modes. The commutation relations for the annihilation and creation operators $b_m(\mathbf{k})$ and $b_m^\dagger(\mathbf{k})$ read:

$$\left[b_i(\mathbf{k}), b_j^\dagger(\mathbf{k}') \right] = \delta_{i,j} \delta_{\mathbf{k},\mathbf{k}'}$$

$$[b_i(\mathbf{k}), b_j(\mathbf{k}')] = \left[b_i^\dagger(\mathbf{k}), b_j^\dagger(\mathbf{k}') \right] = 0$$

$$\Rightarrow [b_m(\mathbf{k}), H] = \hbar \omega_m(\mathbf{k}) b_m \quad . \tag{4.18}$$
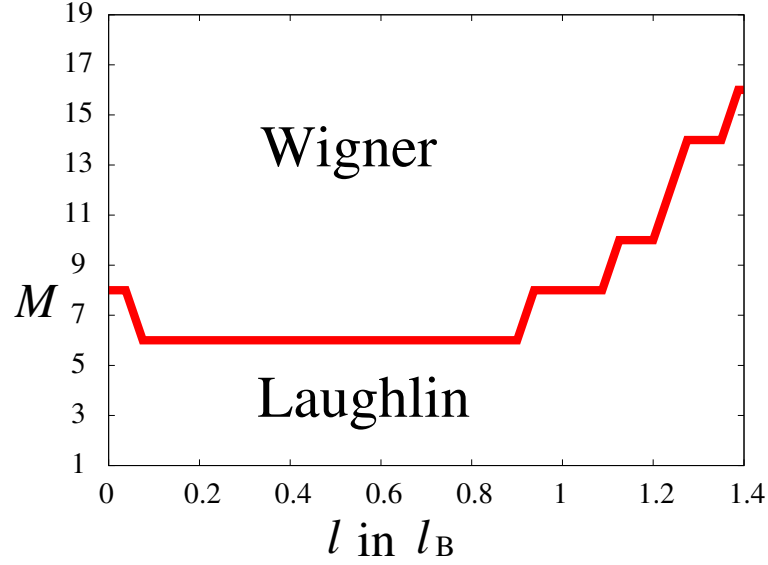
Figure 4.7.   *For physical systems ($M = 1, 3, \cdots$) the interparticle interaction energies of a Wigner crystal and a Laughlin state are compared. The red line denotes a phase transition. For lower filling factors the Laughlin state has a higher interparticle interaction energy than the Wigner crystal. The transition depends on the extension in the ξ-direction.*

The operators are obtained by a Bogoliubov transformation [26, 87, 150], generally written as:

$$b_m(\mathbf{k}) = \mathbf{w}_m(\mathbf{k})\mathbf{u}(\mathbf{k}) + \mathbf{v}_m(\mathbf{k})\mathbf{p}(\mathbf{k})$$
$$b_m^\dagger(\mathbf{k}) = \mathbf{w}_m^*(\mathbf{k})\mathbf{u}(\mathbf{k}) + \mathbf{v}_m^*(\mathbf{k})\mathbf{p}(\mathbf{k}) \quad . \tag{4.19}$$

The right hand site contains scalar products of two component vectors. Using the commutation relation for components of $\mathbf{q}$ and $\mathbf{p}$, we obtain a condition for the vectors $\mathbf{v}_m$ and $\mathbf{w}_m$. We recalculate the commutator of $b_i(\mathbf{k})$ and $b_j^\dagger(\mathbf{k})$ using equation (4.19) and obtain:

$$\Rightarrow \left[b_m(\mathbf{k}), b_{m'}^\dagger(\mathbf{k}')\right] = [\mathbf{w}_m(\mathbf{k})\mathbf{u}(\mathbf{k}) + \mathbf{v}_m(\mathbf{k})\mathbf{p}(\mathbf{k}), \mathbf{w}_{m'}^*(\mathbf{k}')\mathbf{u}(\mathbf{k}') + \mathbf{v}_{m'}^*(\mathbf{k}')\mathbf{p}(\mathbf{k}')]$$
$$= \mathrm{i}\hbar\delta_{\mathbf{k},\mathbf{k}'}\delta_{m,m'}\left(\mathbf{w}_m(\mathbf{k})\mathbf{v}_m^*(\mathbf{k}) - \mathbf{w}_m^*(\mathbf{k})\mathbf{v}_m(\mathbf{k})\right)$$
$$= \delta_{\mathbf{k},\mathbf{k}'}\delta_{m,m'} \quad ,$$

and get the condition:

$$\mathbf{w}_m(\mathbf{k})\mathbf{v}_m^*(\mathbf{k}) - \mathbf{w}_m^*(\mathbf{k})\mathbf{v}_m(\mathbf{k}) = 1 \quad . \tag{4.20}$$

We express the original Hamiltonian (4.11) using the Fourier transformed $\mathbf{p}$ and $\mathbf{u}$ and it reads:

$$H = \sum_{\mathbf{k}} \frac{\mathbf{p}^2(\mathbf{k})}{2m} + \frac{\omega_c}{2} \left(p_T(\mathbf{k})u_L(\mathbf{k}) - p_L(\mathbf{k})u_T(\mathbf{k}) \right)$$

$$+ \frac{m}{2} \left(\omega_T^2(\mathbf{k})u_T^2(\mathbf{k}) + \omega_L^2(\mathbf{k})u_L^2(\mathbf{k}) + \frac{\omega_c^2}{4}\mathbf{u}^2(\mathbf{k}) \right) \quad,$$

where the frequencies $\omega_T(\mathbf{k})$ and $\omega_L(\mathbf{k})$ are the dispersion relations along the wave vector $\mathbf{k}$. We obtain additional conditions for $\mathbf{v}_m$ and $\mathbf{w}_m$, when we compute the commutation relations of $\mathbf{u}$ and $\mathbf{p}$ with H:

$$[u_i(\mathbf{k}), H] = \mathrm{i}\hbar \left(\frac{p_i(\mathbf{k})}{m} + \frac{\omega_c}{2}\epsilon_{ij}u_j(\mathbf{k}) \right)$$

$$[p_i(\mathbf{k}), H] = -\mathrm{i}\hbar \left(m \left(\omega_i^2(\mathbf{k}) + \frac{\omega_c^2}{4} \right) u_i(\mathbf{k}) - \frac{\omega_c}{2}\epsilon_{ij}p_j(\mathbf{k}) \right) \quad,$$

where $\epsilon_{ij} = -\epsilon_{ji}$ is the antisymmetric tensor. We again calculate the commutator of b_m and H using equation (4.19) and omit the argument $(\mathbf{k})$:

$$\frac{1}{\hbar}[b_m, H] = \frac{1}{\hbar}[w_{mT}u_x + w_{mL}u_y + v_{mT}p_x + v_{mL}p_y, H]$$

$$= \mathrm{i} \left(w_{mT} \left(\frac{p_x}{m} - \frac{\omega_c}{2}u_y \right) + w_{mL} \left(\frac{p_y}{m} + \frac{\omega_c}{2}u_x \right) \right.$$

$$\left. -m \left(v_{mT} \left(\omega_T + \frac{\omega_c^2}{4} \right) + v_{mL} \left(\omega_L + \frac{\omega_c^2}{4} \right) \right) - \frac{\omega_c}{2}\left(v_{mT}p_y - v_{mL}p_x \right) \right)$$

$$= \omega_m b_m$$

$$= \omega_m \left(w_{mT}u_x + w_{mL}u_y + v_{mT}p_x + v_{mL}p_y \right) \quad.$$

By identifying the terms containing only u_x (respectively with u_y, p_x and p_y) one gets equations for v and w:

$$\mathrm{i}\left(\frac{w_{mT}}{m} + v_{mL}\frac{\omega_c}{2} \right) = \omega_m v_{mT}$$

$$\mathrm{i}\left(\frac{w_{mL}}{m} - v_{mT}\frac{\omega_c}{2} \right) = \omega_m v_{mL}$$

$$\mathrm{i}\left(w_{mL}\frac{\omega_c}{2} - v_{mT}m\left(\omega_T^2 + \frac{\omega_c^2}{4} \right) \right) = \omega_m w_{mT}$$

$$-\mathrm{i}\left(w_{mT}\frac{\omega_c}{2} + v_{mL}m\left(\omega_L^2 + \frac{\omega_c^2}{4} \right) \right) = \omega_m w_{mL} \quad. \tag{4.21}$$

The first two lines of equation (4.21) can be rewritten in the form:

$$\begin{pmatrix} w_{mT} \\ w_{mL} \end{pmatrix} = m \begin{pmatrix} -\mathrm{i}\omega_m & -\frac{\omega_c}{2} \\ \frac{\omega_c}{2} & -\mathrm{i}\omega_m \end{pmatrix} \begin{pmatrix} v_{mT} \\ v_{mL} \end{pmatrix} \quad, \tag{4.22}$$

where the third and the fourth line lead to:

$$m \begin{pmatrix} \omega_T^2 + \frac{\omega_c^2}{4} & 0 \\ 0 & \omega_L^2 + \frac{\omega_c^2}{4} \end{pmatrix} \mathbf{v}_m = \begin{pmatrix} i\omega_m & \frac{\omega_c}{2} \\ -\frac{\omega_c}{2} & i\omega_m \end{pmatrix} \mathbf{w}_m$$

$$= m \begin{pmatrix} i\omega_m & \frac{\omega_c}{2} \\ -\frac{\omega_c}{2} & i\omega_m \end{pmatrix} \begin{pmatrix} -i\omega_m & -\frac{\omega_c}{2} \\ \frac{\omega_c}{2} & -i\omega_m \end{pmatrix} \mathbf{v}_m \quad .$$

(4.23)

Combining equations (4.22) and (4.23) we obtain:

$$\begin{pmatrix} \omega_T^2 + \frac{\omega_c^2}{4} & 0 \\ 0 & \omega_L^2 + \frac{\omega_c^2}{4} \end{pmatrix} \mathbf{v}_m = \begin{pmatrix} \omega_m^2 + \frac{\omega_c^2}{4} & -i\omega_c\omega_m \\ i\omega_m\omega_c & \omega_m^2 + \frac{\omega_c^2}{4} \end{pmatrix} \mathbf{v}_m \quad .$$

Hence, we get the relation:

$$v_{mT} = i\frac{\omega_m^2 - \omega_L^2}{\omega_m\omega_c} v_{mL}$$

$$v_{mL} = -i\frac{\omega_m^2 - \omega_T^2}{\omega_m\omega_c} v_{mT}$$

$$w_{mT} = -im\frac{\omega_m^2 + \omega_T^2}{2\omega_m} v_x$$

$$w_{mL} = -im\frac{\omega_m^2 + \omega_L^2}{2\omega_m} v_y \quad ,$$

hence:

$$\left(\omega_m^2 - \omega_L^2\right)\left(\omega_m^2 - \omega_T^2\right) = \omega_m^2\omega_c^2 \quad .$$

Therefore, the two branches of the corresponding dispersion relation are:

$$\omega_\pm^2 = \frac{\omega_T^2 + \omega_L^2 + \omega_c^2}{2} \pm \sqrt{\frac{(\omega_T^2 + \omega_L^2 + \omega_c^2)^2}{4} - \omega_T^2\omega_L^2} \quad .$$

(4.24)

For huge magnetic fields $\omega_c^2 \gg \omega_{L,T}^2(\mathbf{k})$ the branches are, compared to the gap between the branches, almost flat with $\omega_-^2(\mathbf{k}) \approx 0$ and $\omega_+^2(\mathbf{k}) \approx \omega_c^2$. Using the normalization condition we get:

$$v_{mT}v_{mT}^* = \frac{1}{m\hbar}\left(\frac{\omega_m}{\omega_m^2 - \omega_T^2}\right)\left(\frac{\omega_c^2\omega_m^2}{(\omega_m^2 + \omega_T^2)(\omega_m^2 - \omega_L^2) + (\omega_m^2 - \omega_T^2)(\omega_m^2 + \omega_L^2)}\right)$$

$$= \frac{1}{2\hbar m}\frac{\omega_m^2\omega_c^2}{(\omega_m^2 - \omega_T^2)}\frac{\omega_m}{(\omega_m^4 - \omega_T^2\omega_L^2)}$$

$$= \frac{\omega_m}{\hbar m}\frac{(\omega_m^2 - \omega_L^2)}{(\omega_m^4 - \omega_T^2\omega_L^2)} \quad ,$$

(4.25)

and

$$v_{mL}v_{mL}^* = \frac{\omega_m}{2\hbar m}\frac{(\omega_m^2 - \omega_T^2)}{(\omega_m^4 - \omega_T^2\omega_L^2)} \quad . \tag{4.26}$$

Due to the form of the dispersion relations $\omega_{L,T}(\mathbf{k})$, v_{mT} and v_{mL} are symmetric functions in $\mathbf{k}$. If we choose v_{mT} to be real, v_{mL} will have to be purely imaginary. The position and momentum operators can now be constructed and takes the form:

$$\mathbf{u}(\mathbf{k}) = -\mathrm{i}\hbar \sum_{m=+,-} \left(-\mathbf{v}_m^* b_m + \mathbf{v}_m b_m^\dagger\right)$$

$$\mathbf{p}(\mathbf{k}) = -\mathrm{i}\hbar \sum_{m=+,-} \left(\mathbf{w}_m^* b_m - \mathbf{w}_m b_m^\dagger\right) \tag{4.27}$$

or

$$\mathbf{u}(\mathbf{r},t) = -\mathrm{i}\frac{\hbar}{\sqrt{N}} \sum_{m\mathbf{k}} \mathrm{e}^{\mathrm{i}\mathbf{kr}} \left(-\mathbf{v}_m^*(\mathbf{k})b_m(\mathbf{k})\mathrm{e}^{-\mathrm{i}\omega_m(\mathbf{k})t} + \mathbf{v}_m(-\mathbf{k})b_m^\dagger(-\mathbf{k})\mathrm{e}^{\mathrm{i}\omega_m(\mathbf{k})t}\right)$$

$$= \sum_{m\mathbf{k}} \mathrm{e}^{\mathrm{i}\mathbf{kr}} \left(\xi_m(\mathbf{k},t) + \xi^\dagger(-\mathbf{k},t)\right) \quad . \tag{4.28}$$

4.8 The Green's function in a magnetic field

The anharmonic parts of the potential in equation (4.5) influence the phonon dispersion relation. They can lead to imaginary frequencies, which is a signature for the melting of the crystal. Moreover, the deviation of the dipoles from their lattice points, classically interpreted as the oscillation around the potential minima, is increased when amplifying the anharmonic parts.

We incorporate the 3$^{\mathrm{rd}}$ and the 4$^{\mathrm{th}}$ order of the Taylor expansion perturbatively:

$$H = H_0 + H_3 + H_4 \quad .$$

In order to treat this problem, we introduce the Green's function as the time ordered two point correlation function of the displacements:

$$\mathcal{D}_{\alpha\alpha'}(\mathbf{r},t) = \mathrm{i}\begin{cases} \langle u_\alpha(\mathbf{r},t)u_{\alpha'}(0,0)\rangle & t > 0 \\ \langle u_{\alpha'}(0,0)u_\alpha(\mathbf{r},t)\rangle & t < 0 \end{cases} \quad . \tag{4.29}$$

In the harmonic case we can use the equation (4.27) to express the Green's function and obtain:

$$\mathcal{D}_{\alpha\alpha'}(\mathbf{r},t) = \mathrm{i}\frac{\hbar^2}{N} \sum_{\mathbf{k}m} \mathrm{e}^{\mathrm{i}\mathbf{kr}}\begin{cases} v_{m\alpha}^*(\mathbf{k})v_{m\alpha'}(\mathbf{k})\mathrm{e}^{-\mathrm{i}\omega_m(\mathbf{k})t} & t > 0 \\ v_{m\alpha'}^*(\mathbf{k})v_{m\alpha}(\mathbf{k})\mathrm{e}^{\mathrm{i}\omega_m(\mathbf{k})t} & t < 0 \end{cases} \quad .$$

The Fourier transform in space and time variables reads:

$$\mathcal{D}_{\alpha\alpha'}(\mathbf{k}, \omega) = -2\hbar^2 \sum_m v_{m\alpha}^*(\mathbf{k}) v_{m\alpha'}(\mathbf{k}) \frac{\omega_m}{\omega^2 - \omega_m^2} \quad .$$

Using equations (4.25) and (4.26) the components of the matrix $\mathcal{D}_{\alpha\alpha'}$ has the form:

$$\mathcal{D}_{TT}(\mathbf{k}, \omega) = -a^2 \omega_0 \sum_{m=\pm} \frac{(\omega_m^2 - \omega_L^2)}{(\omega_m^4 - \omega_T^2 \omega_L^2)} \frac{\omega_m^2}{(\omega^2 - \omega_m^2)}$$

$$\mathcal{D}_{LL}(\mathbf{k}, \omega) = -a^2 \omega_0 \sum_{m=\pm} \frac{(\omega_m^2 - \omega_T^2)}{(\omega_m^4 - \omega_T^2 \omega_L^2)} \frac{\omega_m^2}{(\omega^2 - \omega_m^2)}$$

$$\mathcal{D}_{LT}(\mathbf{k}, \omega) = \pm i a^2 \omega_0 \sum_{m=\pm} \frac{\sqrt{(\omega_m^2 - \omega_T^2)(\omega_m^2 - \omega_L^2)}}{(\omega_m^4 - \omega_T^2 \omega_L^2)} \frac{\omega \omega_m}{(\omega^2 - \omega_m^2)}$$

$$= \pm i a^2 \omega_0 \sum_{m=\pm} \frac{\omega_c \omega_m^2}{(\omega_m^4 - \omega_T^2 \omega_L^2)} \frac{\omega}{(\omega^2 - \omega_m^2)} \quad .$$

In the Cartesian coordinates the Green's function takes the form:

$$\mathcal{D}^0(\mathbf{k}, \omega) = a^2 \omega_0 \sum_{m=\pm} \frac{\omega_m^2(\mathbf{k})}{(\omega_m^4(\mathbf{k}) - \omega_T^2(\mathbf{k})\omega_L^2(\mathbf{k}))} \frac{1}{(\omega^2 - \omega_m^2(\mathbf{k}))}$$
$$\left(\hat{\mathcal{M}}_T(\mathbf{k}) \omega_L^2(\mathbf{k}) + \hat{\mathcal{M}}_L(\mathbf{k}) \omega_T^2(\mathbf{k}) - \omega_m^2(\mathbf{k}) + i \hat{\epsilon} \omega_c \omega \right) \quad , \quad (4.30)$$

where $\hat{\mathcal{M}}_{0,1}(\mathbf{k})$ are the projectors to the eigenvectors of the real part of $\mathcal{D}^0(\mathbf{k})$ and ϵ is the antisymmetric tensor. The form of the inverse Green's function is relatively simple and is:

$$\left(\mathcal{D}^0 \right)^{-1}(\mathbf{k}, \omega) = \frac{1}{a^2 \omega_0} \left(\hat{\mathcal{M}}_T(\omega_T^2(\mathbf{k}) - \omega^2) + \hat{\mathcal{M}}_L(\omega_L^2(\mathbf{k}) - \omega^2) - i \hat{\epsilon} \omega_c \omega \right) \quad .$$
$$(4.31)$$

4.8.1   Green's functions in anharmonic systems

Non-vanishing anharmonic terms change the form of the Green's function defined in equation (4.29). A common approach to this problem is to treat the anharmonic terms H_3 and H_4 perturbatively (see e.g. [3]).

We assume that the perturbative part is turned on at $t = -T$ and turned off at $t = T$, where $T \to \infty$. For $t > T$ or $t < -T$ the system is described with the harmonic Hamiltonian. In order to examine the Green's function

for all relevant times, one has to introduce the time evolution operator:

$$\mathcal{S} = \mathcal{T} \exp{-\frac{i}{\hbar} \int_{-\infty}^{\infty} dt \, (H_3(t) + H_4(t))}$$

$$= 1 + \mathcal{T} \sum_{n=1}^{\infty} \frac{1}{n!} \left(-\frac{i}{\hbar}\right)^n \int dt_1 \dots dt_n \, (H_3(t_1) + H_4(t_1)) \dots (H_3(t_n) + H_4(t_n)),$$

$$(4.32)$$

where the exponential description is an abbreviation of the sum. $\mathcal{T}$ denotes that the product is time ordered.

The Green's function can then be expressed with the formula:

$$\mathcal{D}_{\alpha\alpha'}(\mathbf{r}, t) = \frac{i}{\langle \mathcal{S} \rangle} \langle \mathcal{T} u_\alpha(\mathbf{r}, t) u_{\alpha'}(0, 0) \mathcal{S} \rangle \quad , \qquad (4.33)$$

which can be expanded as a sum. The addenda of H_3 contain an odd number of creation and annihilator operators (see appendix (B.5)), hence, the first non-vanishing term in the sum (4.32) is the second order term of H_3. The H_4 term is developed up to the first order. It turns out that for large magnetic fields ($\omega_c \gg \omega_0$) the amplitude of these two contributions are proportional to the filling factor ν, while all other nontrivial contributions are of higher order.

4.8.2 Self-consistent solution of the Dyson equation

The phonon-phonon interaction has to be treated in a perturbative expansion. This can be done by including the sum in equation (4.32) into the expression for the Green's function (4.33). Schematically, the addenda of the perturbation series can be expressed as Feynman diagrams. A phonon Green's function is denoted with a thin line ——— . We illustrate the final exact Green's function in equation (4.33) with a thick line ▬▬ . The self-energy block, which contains all one-particle irreducible loops, is depicted with: ⊣Σ⊢ .
Remarkably, the exact expression for the Green's function can be obtained using the Dyson equation:

$$\left(\blacksquare \right)^{-1} = \left(\text{———} \right)^{-1} - \boxed{\Sigma} \quad ,$$

where $\boxed{\Sigma}$ is the self-energy block without the two external "legs". One-particle irreducible, non-trivial loops of the lowest order are the second order

of the three phonon vortex:

and the first order of the fourth phonon vortex: .

Now we approximate the self-energy block by taking only into account these loops:

$$\boxed{\Sigma} \approx \bigcirc + \bigcirc \quad .$$

Since we sum up only loops of the lowest order in ν, the self-energy block $\boxed{\Sigma}$ is an approximation. However, we can increase the accuracy of our outcome by solving the Dyson equation self-consistently. In the first iteration we obtain the Green's functions up to the lowest order:

$$\left(\text{——}\right)^{-1} = \left(\text{——}\right)^{-1} - \boxed{\Sigma} \quad . \tag{4.34}$$

We use the approximation ▬▬ to recalculate the lowest order loops, and the self-energy block respectively:

$$\boxed{\Sigma} \approx \bigcirc + \bigcirc \quad ,$$

already represented without legs. In the next iteration step, the Dyson equation reads:

$$\left(\text{▬▬}\right)^{-1} = \left(\text{——}\right)^{-1} - \boxed{\Sigma} \quad .$$

We repeat this scheme until we reach convergence or until we have to stop, for instance due to the appearance of imaginary frequencies.

4.8.3   The first iteration for the Green's function

Using the Green's function in equation (4.31), we solve the Dyson equation when performing the first iteration step:

$$
\begin{aligned}
a^2 w_0 \left(\mathcal{D}^1\right)^{-1}(\mathbf{k}, \omega) &= a^2 w_0 \left(\left(\mathcal{D}^0\right)^{-1}(\mathbf{k}, \omega) - \Sigma(\mathbf{k}, \omega)\right) \\
&= \hat{\mathcal{M}}_T \left(\omega_T^2(\mathbf{k}) - \omega^2\right) + \hat{\mathcal{M}}_L \left(\omega_L^2(\mathbf{k}) - \omega^2\right) - a^2 w_0 \Sigma(\omega, \mathbf{k}),
\end{aligned}
\tag{4.35}
$$

where we only consider the real part and neglect corrections coming from the imaginary part which are of higher order. Now we like to express $\mathcal{D}_1^{-1}(\mathbf{k}, \omega)$

using a form that is similar to the one of $\mathcal{D}_0^{-1}(\mathbf{k}, \omega)$, thus allowing us to perform further iteration steps. We are going to approximate equation (4.35) with:

$$a^2 w_0 \left(\mathcal{D}^1\right)^{-1} \approx A_0^{-1}\tilde{\mathcal{M}}_T \left(\tilde{\omega}_T^2(\mathbf{k}) - \omega^2\right) + A_1^{-1}\tilde{\mathcal{M}}_L \left(\tilde{\omega}_L^2(\mathbf{k}) - \omega^2\right) \quad , \quad (4.36)$$

where the inverse of A_0 and A_1 are amplitudes, $\tilde{\mathcal{M}}_i$ are projectors and $\tilde{\omega}_i(\mathbf{k})$ are the branches of the renormalized dispersion relation. We want to find values for these quantities that approximate the exact solution (4.35) as good as possible. This approximation is a reasonable choice, because the biggest contribution in the loops comes from the Green's function around the poles. First, we calculate the eigenvalues of $\mathcal{D}_1^{-1}(\mathbf{k}, \omega)$:

$$a^2 w_0 \left(\mathcal{D}^1\right)^{-1}(\mathbf{k}, \omega) = \tilde{\mathcal{M}}_T(\mathbf{k}, \omega)\lambda_T(\mathbf{k}, \omega) + \tilde{\mathcal{M}}_L(\mathbf{k}, \omega)\lambda_L(\mathbf{k}, \omega) \quad .$$

It turned out that for a particular frequency $\omega = \omega_{0,i}$ one eigenvalue $\lambda_i(\mathbf{k}, \omega)$ is zero. Terms linear in ω do not appear in the Dyson equation (4.34), hence, we develop $\lambda_i(\mathbf{k}, \omega)$ around $\omega_{0,i}^2$ linear in ω^2:

$$\lambda_i(\mathbf{k}, \omega) \approx A_i^{-1}(\mathbf{k}) \left(\omega_{0,i}^2 - \omega^2\right) \quad , \quad (4.37)$$

for $i \in \{T, L\}$. We can obtain the desired form of equation (4.36) if we set the dispersion relations to:

$$\tilde{\omega}_i^2(\mathbf{k}) = \omega_{0,i}^2 \quad . \quad (4.38)$$

The projector matrices are obtained at $\omega^2 = \tilde{\omega}_{T,L}^2(\mathbf{k})$. Due to the amplitudes the form of the new Green's function is more complex, on the other hand, the following iteration steps can be performed in the same way as in equation (4.35).

4.9 The melting parameter

4.9.1 Criteria for a stable crystal

We would like to determine the condition for a stable Wigner crystal. Therefore we consider the following questions:

- Is the energy of the Wigner crystal below the energy of other trial wavefunctions, in particular of the Laughlin wavefunction?

- Are the renormalized phonon frequencies real?

- Do we have a converging self-consistent solution?

The first point was already answered in section 4.5. For reasonably high filling factors $\nu > 1/5$ the Laughlin wavefunction has a lower energy (see figure 4.7), so that a Wigner crystal cannot appear. Moreover, by performing an exact diagonalization for a small number of particles at a filling factor of $\nu = 1/3$ it can be shown that the overlap of the ground state with Laughlin state is almost one [179], which is consistent with our observation. Below a critical value for the filling factor ($\nu < 1/7$ for $l = 0$) the Wigner crystal has a lower energy.

Going from lower to higher filling factors, the contribution coming from the phonon-phonon interaction becomes important. We are taking these anharmonic effects into account by solving the Dyson equation self-consistently. Performing an iteration step in the self-consistent Dyson equation leads to renormalized dispersion relations (see equation (4.38)). A signature for melting is the appearance of imaginary frequencies at low quasi-momenta, which leads to a decay of the phonon modes. The highest filling factor, for which we do not observe imaginary frequencies after solving the Dyson equation self-consistently, defines the critical filling factor, and for smaller values we have a stable Wigner crystal. At this critical filling factor we can determine the modified melting parameter as shown in equation (B.11). We perform 13 iterations and show that the convergence is reached. Figure 4.8 shows the modified melting parameter at different filling factors. Moreover, it shows the points where we obtain imaginary frequencies corresponding to the iteration. In figure 4.9 the critical modified melting parameter γ and inverse filling M are plotted against the iteration steps.

4.9.2   The Lindemann criterion

The question whether we can formulate a Lindemann criterion depends on the universality of our results. We have three typical system parameters, which we can vary: ω_0, ω_d, and ω_c. Without losing the generality, we can fix $\omega_d = 1$ and express ω_0 and ω_c in the units of ω_d. Then, for every set of $\{\omega_0, \omega_c\}$ we can check the stability of the crystal. For a given ω_c we determine ω_0 at which the crystal melts and compute the critical inverse filling factor with the formula:

$$ M = \frac{1}{2\pi\sqrt{3}} \frac{\omega_c}{\omega_0} \quad . $$

Of course, the critical inverse filling factor depends on ω_c. In figure 4.10 it is shown that for very large values of ω_c the critical inverse filling factor
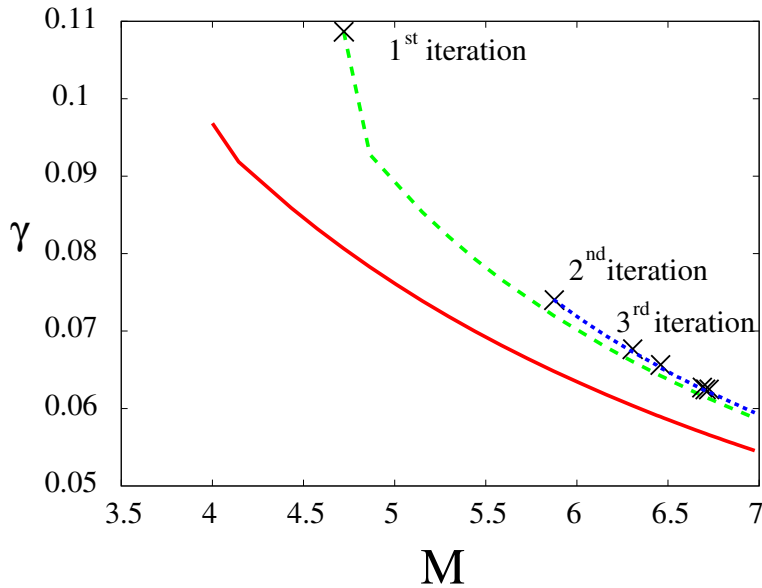
Figure 4.8. The modified melting parameter $\gamma = \langle \mathbf{u}(\mathbf{r}_1, 0)\mathbf{u}(0, 0)\rangle/a^2$ is plotted against the inverse filling factor $M = 1/\nu$. $\mathbf{r}_1$ is the vector pointing to the neighbored lattice site. The red line shows the modified melting parameter, when the anharmonicity is omitted. The orange crosses denote, corresponding to the iteration step, the appearance of imaginary frequencies.
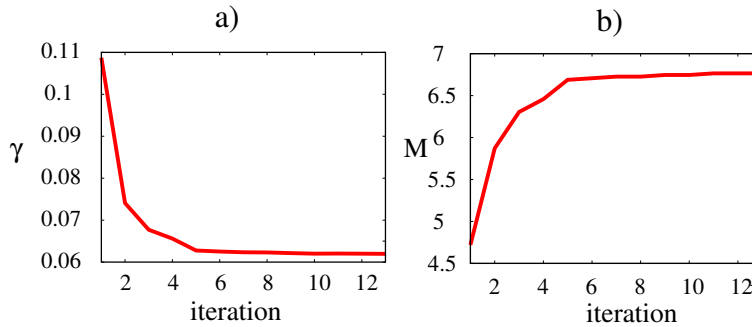

Figure 4.9. Figure a) shows the critical modified melting parameter while in figure b) the critical inverse filling factor is depicted. Both graphs are plotted against the iteration step and show a clear convergence.
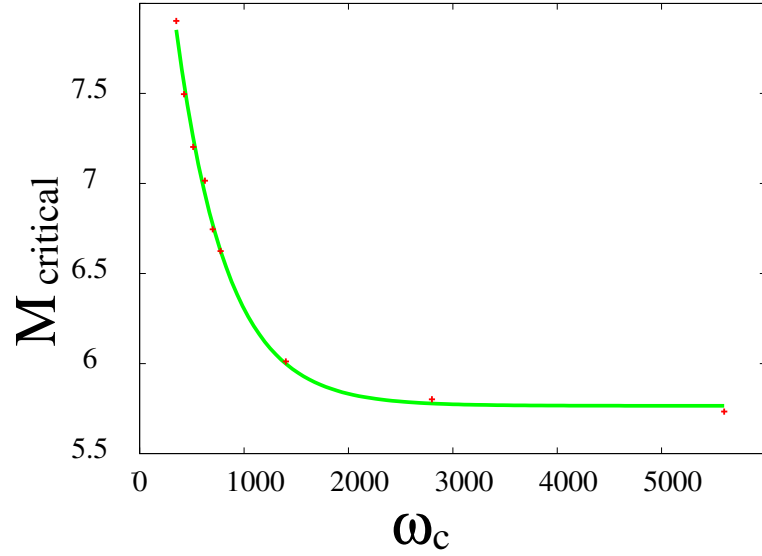
Figure 4.10.   *The red dots are the critical melting parameter versus ω_c. The green line is obtained by a least square fit. The functions reads: $M_{cr}(\omega_c) \approx 4.33 \mathrm{e}^{-0.00209\omega_c} + 5.77$.*

converges to a constant. Hence, we can formulate the Lindemann criterion for a large magnetic field, where the crystal melts at a modified melting parameter of $\gamma \simeq 0.077$ which corresponds to a filling factor of $\nu = 0.174$. Both γ and ν are independent of ω_c for large magnetic fields.

4.10   Conclusion

We have discussed the occurrence of a Wigner crystal in a rapid rotating 2D gas. Comparing the Laughlin state with the Wigner crystal, the Laughlin state has a lower energy for filling factors $1/5 \leq \nu \leq 1$, while below a critical value of the filling factor, the Wigner crystal is the energetically preferred state. Figure 4.7 shows the transition point depends on the extension in the ξ-direction, which is parameterized by l. For example at $l = 0$ the Laughlin state has a lower energy for $\nu \geq 1/7$.

We also considered the stability of a Wigner crystal. At very low filling factors the system behaves harmonically. However, contributions coming the from phonon-phonon interactions become important close to the critical filling factor. We examined the influence of these phonon-phonon interactions on the dispersion relation by taking into account the second order of the 3-

vertex loop and the first order of a 4-vertex loop in the self-energy. The amplitude of both contributions is proportional to the filling factor ν. It turns out that in the 2D limit and for large values of the "magnetic field", the Wigner crystal is stable below a filling factor of $\nu < 0.174$, which is in a good agreement with the energetic observation, where for $l = 0.2l_B$ the transition takes place at $0.2 \geq \nu \geq 0.142$.

So far we only compared two trial wave functions. In electronic systems it was shown that in some ranges of the filling factors a Laughlin-Jastrow correlated Wigner crystal [239] has the lowest energy. Principally, such considerations can also be extended to the system of rotating dipolar gases and it can be expected that a crystal structure has a lower energy than the Laughlin state even for slightly higher filling factors.

In order to observe a Wigner crystal one has to prepare a dipolar Fermi gas, which is a challenging task. Efforts in this direction have been made theoretically [16, 60, 97] and experimentally [23, 123, 208, 216, 217]. The dipoles are polarized in a strong magnetic field or an electric field perpendicular to the radial direction. In the next step the gas has to be transmitted into a rotating frame, which nowadays can be achieved by using standard techniques [2, 33, 45, 50, 153, 160, 203]. The model of a particle in a rotating frame is equivalent to the model of a charged particle in a magnetic field, with a cyclotron frequency being twice as big as the rotation frequency ($\omega_c = 2\Omega$). Close to the critical rotation frequency, when the value of frequency is close to the radial trap frequency, the effective trapping potential becomes shallow. The system is considered to be in the homogeneous limit. Any "magnetic field" can be created by increasing the value of the rotation frequency, if at the same time, the value of the trap frequency $\omega_\perp$ is increased and is always above $\Omega < \omega_\perp$.

By changing the "magnetic field" or manipulating the density by modifications of the external potential, one can control the filling factor. With this tool it is possible to sweep from a filling factor where the Laughlin state is energetically favorable, towards a filling factor where we expect the Wigner crystal to be stable.

Unfortunately, the key signature of the Wigner crystal, the density modulation, cannot be directly observed by an absorption image. The profile of a time of flight image corresponds to the momentum distribution in the gas and will be a featureless Gaussian. On the other hand, Hanbury Brown and Twiss demonstrated [34] that noise correlations can be used to examine the properties of a particle source. It has been shown that the density distribution of a Mott insulator [84] can be recovered, which reflects the underlying ordering in the 3D optical lattice. Similarly, this method has been used to measure the phase coherence length of an elongated Bose-Einstein

condensate [112]. The observation of the quantum noise correlation could also be an appropriate tool to discover the density modulation in the Wigner crystal. Since the particle number in the Wigner crystal is relatively small, the noise/signal ratio is big. Because the gas contains fermionic dipoles, the peaks in the quantum noise correlation function will have a negative sign. On the other hand, a Laughlin state has a homogeneous density distribution, and hence, we do not expect peaks in the quantum noise correlation profile at this point. By preparing states with different filling factors, one can determine the transition point.

APPENDIX A

COMPOSITE FERMIONS

A.1 Proof of the fermionic properties of the composite fermions

In order to proof that the operator $\tilde{f}_i = \left(b_i^\dagger\right)^s f_i$ has Fermionic properties we are using the complete induction. Assumed that for a certain s the relation:

$$\frac{(\tilde{n}_s - s)!}{\tilde{n}_s!}\{\left(b_i^\dagger\right)^s f_i, b_j^s f_j^\dagger\} = \delta_{i,j} \quad , \tag{A.1}$$

holds. The conservation low $n(m) + sm = n$ is crucial for the proof. It is a straight forward calculation to show that this is also true for $s + 1$:

$$\{\left(b_i^\dagger\right)^{s+1} f_i, b_j^{s+1} f_j^\dagger\}$$

$$= b_i^\dagger b_j\{\left(b_i^\dagger\right)^s f_i, b_j^s f_j^\dagger\} - b_i^\dagger[b_j, \left(b_i^\dagger\right)^s f_i]b_j^s f_j^\dagger - [b_i^\dagger, b_j^{s+1} f_j^\dagger]\left(b_i^\dagger\right)^s f_i$$

$$= \delta_{i,j}\left(n(m)\frac{(n(m) + ms)!}{n(m) + (m-1)s!} - s\left(b_i^\dagger\right)^s b_i^s f_i f_j^\dagger + (s+1)b_j^s\left(b_i^\dagger\right)^s f_j^\dagger f_i\right)$$

$$= \delta_{i,j}\left(n(m)\frac{(n(m) + ms)!}{n(m) + (m-1)s!}\right.$$

$$\left. + s(m-1)\frac{n(m)!}{(n(m) - s)!} + (s+1)m\frac{(n(m) + s)!}{n(m)!}\right) \tag{A.2}$$

Since m is either 0 or 1, equation (A.2) can be decomposed:

$$\{\left(b_i^\dagger\right)^{s+1} f_i, b_j^{s+1} f_j^\dagger\}$$

$$= \delta_{i,j}\left(m\{(n(m)+(s+1)m\}\frac{(n(m)+ms)!}{n(m)!}\right.$$

$$\left.+(1-m)\{n(m)-s\}\frac{n(m)!}{(n(m)-s)!}\right)$$

$$= \delta_{i,j}\left(m\frac{(n(m)+(s+1)m)!}{n(m)!}+(1-m)\frac{n(m)!}{(n(m)-(s+1))!}\right) \qquad \text{(A.3)}$$

$$= \delta_{i,j}\frac{(\tilde{n}_{s+1}-(s+1))!}{\tilde{n}_{s+1}!} \qquad \text{(A.4)}$$

$$\Rightarrow \frac{\tilde{n}_{s+1}!}{(\tilde{n}_{s+1}-(s+1))!}\{\left(b_i^\dagger\right)^{s+1} f_i, b_j^{s+1} f_j^\dagger\} \quad = \quad \delta_{i,j} \quad ,$$

where $\tilde{n}_{s+1} = n(m) + (s+1)m$. Equation (A.3) can be summarized to equation (A.4), because the left part is zero for $m = 0$ while the right part is zero for $m = 1$. Since for $s = 0 \quad \Rightarrow \quad \{f_i, f_j^\dagger\} = \delta_{i,j}$ is true by definition, the equation (A.1) must hold for any s.

A.2   Homogeneity

Without the kinetic part, which couples different cells, the solution of the Bose-Fermi-Hubbard Hamiltonian is a product state of single cell solutions, that reads:

$$|\psi\rangle = \prod_k \sum_{n,m} c_{n,m}^k |nm\rangle_k \quad .$$

In the case of inhomogeneity the ground state is degenerated. Without altering the energy, a homogeneous results can be formed by a linear combination of the degenerated ground states. Of course, switching on the hopping the entire Hilbert space has to be considered, but in the mean-field picture we examine only product states. Homogeneity means that, for a particular n and m, all $c_{n,m}^i$ are independent of i. In this case the kinetic energy reads:

$$-t_B \sum_{\langle ij\rangle}\langle\psi|b_i^\dagger b_j + h.c.|\psi\rangle = -t_B N 2d \sum_{n=1}^\infty n\left(c_n c_{n-1}^* + h.c.\right) \quad ,$$

where d is the dimension of the system. In order to simulate inhomogeneity we modify in the coefficients for two particular cells. Now, the product state

reads: :

$$|\psi(\delta)\rangle = \sum_{n,m} c^i_{n,m}|nm\rangle_i \sum_{n,m} c^j_{n,m}|nm\rangle_j \prod_{k\neq i,j} \sum_{n,m} c_{n,m}|nm\rangle \quad .$$

For example, the following coefficients are altered by a small δ:

$$c^{i\,2}_{n1,m1} = c^2_{n1,m1} + \delta$$
$$c^{i\,2}_{n2,m2} = c^2_{n2,m2} - \delta$$
$$c^{j\,2}_{n1,m1} = c^2_{n1,m1} - \delta$$
$$c^{j\,2}_{n2,m2} = c^2_{n2,m2} + \delta \quad .$$

This assures, that both, the particle number and the normalization of Fock coefficients, remain constant. If the cells i and j are not neighbored the energy difference reads:

$$\Delta E = -t2d \left(\left(c_{n_1-1}n_1 + c_{n_1+1}(n_1+1) \right) c_{n_1} \left(2 - \sqrt{1-\delta/c^2_{n_1}} - \sqrt{1+\delta/c^2_{n_1}} \right) \right.$$
$$\left. + \left(c_{n_2-1}n_2 + c_{n_2+1}(n_2+1) \right) c_{n_2} \left(2 - \sqrt{1-\delta/c^2_{n_2}} - \sqrt{1+\delta/c^2_{n_2}} \right) \right) \quad ,$$

which grows monotonically with δ. The calculation is the same if $n_1 \neq n_2 \pm 1$. Considering only the altered cells and if, for instance, $n = n_1 = n_2 + 1$ the energy difference is:

$$\Delta E = -t \left(n \left(4c_n c_{n-1} - \sqrt{c^2_n + \delta} - \sqrt{c^2_n - \delta} - \sqrt{c^2_{n-1} + \delta} - \sqrt{c^2_{n-1} - \delta} \right) \right.$$
$$+ (n+1)c_n c_{n+1} \left(2 - \sqrt{1-\delta/c^2_n} - \sqrt{1+\delta/c^2_n} \right)$$
$$\left. + (n-1)c_{n-1}c_{n-2} \left(2 - \sqrt{1-\delta/c^2_{n-1}} - \sqrt{1+\delta/c^2_{n-1}} \right) \right) \quad ,$$

which again grows with monotonically with δ. This example shows, that any small deviation from a homogeneous product increases the energy. In general, if the self-interaction becomes dominant, inhomogeneous states lower the energy.

A.3   Mean-field consideration

The mean-field calculation for composite fermions is quite straight forward. The perturbation Hamiltonian reads:

$$\mathcal{W} = -t_B d\psi \left(b^\dagger_i + b_i \right) \quad .$$

The second order correction for the energy reads:

$$E_2 = \psi^2 \sum_n \left\{ \frac{|\langle \tilde{n}, 0|\mathcal{W}|n, 0\rangle|^2}{E_0(\tilde{n}, 0) - E_0(n, 0)}(1 - \rho_F) \right.$$
$$\left. + \frac{|\langle \tilde{n} - s, 1|\mathcal{W}|n, 1\rangle|^2}{E_0(\tilde{n} - s, 1) - E_0(n, 1)}\rho_F \right\} \quad . \tag{A.5}$$

Due to the form of $\mathcal{W}$ only addenda with either $n = \tilde{n} \pm 1$ or $n = \tilde{n} - s \pm 1$ contribute to the correction. The four possibilities are:

$$\frac{|\langle \tilde{n}, 0|b^\dagger|\tilde{n} - 1, 0\rangle|^2}{E_0(\tilde{n}, 0) - E_0(\tilde{n} - 1, 0)} = \frac{\sqrt{\tilde{n}}}{\tilde{n} - \tilde{\mu}_B - 2}$$

$$\frac{|\langle \tilde{n}, 0|b|\tilde{n} + 1, 0\rangle|^2}{E_0(\tilde{n}, 0) - E_0(\tilde{n} + 1, 0)} = -\frac{\sqrt{\tilde{n} + 1}}{\tilde{n} + \tilde{\mu}_B}$$

$$\frac{|\langle \tilde{n} - s, 1|b^\dagger|\tilde{n} - s - 1, 1\rangle|^2}{E_0(\tilde{n} - s, 1) - E_0(\tilde{n} - s - 1, 1)} = \frac{\sqrt{\tilde{n} - s}}{\tilde{n} - s - \tilde{\mu}_B + \alpha}$$

$$\frac{|\langle \tilde{n} - s, 1|b|\tilde{n} - s + 1, 1\rangle|^2}{E_0(\tilde{n} - s, 1) - E_0(\tilde{n} - s - 1, 1)} = -\frac{\sqrt{\tilde{n} - s + 1}}{\tilde{n} - s + \tilde{\mu}_B - \alpha} \quad .$$

Therefore, the correction to the energy reads:

$$E_2 = -\psi^2 t_B d \left[(1 - \rho_F) \left(\frac{\left(\sqrt{\tilde{n}} - \sqrt{\tilde{n} + 1}\right)(\tilde{n} - \mu_B) + \sqrt{\tilde{n} + 1}}{(\tilde{n} - \tilde{\mu}_B - 1)(\tilde{n} - \mu_B)} \right) \right.$$
$$\left. + \rho_F \left(\frac{\left(\sqrt{\tilde{n} - s} - \sqrt{\tilde{n} - s + 1}\right)(\tilde{n} - s + \alpha - \mu_B) + \sqrt{\tilde{n} - s + 1}}{(\tilde{n} - s + \alpha - \tilde{\mu}_B - 1)(\tilde{n} - s + \alpha - \mu_B)} \right) \right] \quad .$$

A.4 Commutation relation between fermionic operators

In this appendix we discuss some technical details concerning the simple man's Gutzwiller ansatz for fermions, consisting in writing the variational wavefunction as a product of on-site Fermi operators, and neglecting the anticommutation relations between Fermi operators in different sites.

Formally, our variational approach is equivalent to replacing the Fermionic annihilation and creation operators $\tilde{f}_i, \tilde{f}_i^\dagger$ by spin $1/2$ operators $\sigma(i), \sigma^\dagger(i)$. This approach can be justified using the exact Jordan-Wigner transformation in 2D and 3D ([74, 85, 116], see also [215]). In the case of 2D this

transformation acquires the form:

$$S^+(j) = \tilde{f}_j^\dagger e^{i\sum_{k\neq j} \arg(k,j)\tilde{f}_k^\dagger \tilde{f}_k} \quad , \tag{A.6}$$

$$S^-(j) = e^{-i\sum_{k\neq j} \arg(k,j)\tilde{f}_k^\dagger \tilde{f}_k} \tilde{f}_j \quad , \tag{A.7}$$

$$S_z(j) = \tilde{f}_j^\dagger \tilde{f}_j - \frac{1}{2} \quad , \tag{A.8}$$

where $\arg(k,j)$ is the angle between $\mathbf{k} - \mathbf{j}$ and an arbitrary space direction on the lattice, which we choose as x. The Fermionic Hamiltonian of equation (2.8) becomes then:

$$H_{eff} = J_{eff} \sum_{\langle i,j\rangle} S^+(j)e^{iA(i,j)}S^-(i) + h.c.$$

$$+ K_{eff} \sum_{\langle i,j\rangle} \left(S_z(i) + \frac{1}{2}\right)\left(S_z(j) + \frac{1}{2}\right), \tag{A.9}$$

where the "magnetic vector potential":

$$A(i,j) = \sum_{k\neq i,j} [\arg(k,i) - \arg(k,j)](S_z(k) + 1/2) \quad . \tag{A.10}$$

The simple man's Gutzwiller approximation corresponds on this level to i) a variational ansatz for the ground state wavefunction in the form of product of on-site spin states, and ii) substitution of the "magnetic potential" by its average, which under assumption of mirror reflection symmetry with respect to the lattice axes is zero.

APPENDIX B

WIGNER CRYSTAL

B.1 Effect of antisymmetrizing two dipoles

The antisymmetric wavefunction of two particle, separated by the distance R, in a magnetic field reads:

$$
\Phi(x_1, y_1, x_2, y_2) = \left(2\pi l_B^2 \sqrt{2} \sqrt{1 - e^{-\frac{R^2}{2l_B^2}}} \right)^{-1}
$$

$$
\left(e^{-\frac{x_1^2 + y_1^2}{4l_B^2}} e^{-\frac{x_2^2 + (y_2 - R)^2}{4l_B^2}} e^{-i\frac{Rx_2}{2l_B^2}} - e^{-\frac{x_2^2 + y_2^2}{4l_B^2}} e^{-\frac{x_1^2 + (y_1 - R)^2}{4l_B^2}} e^{-i\frac{Rx_1}{2l_B^2}} \right),
$$

which is normalized to unity. If the two particles interact with an potential $v_{2D}(r)$ the energy reads:

$$
U_{12} = \left(4\pi^2 l_B^4 \left(1 - e^{-\frac{R^2}{2l_B^2}} \right) \right)^{-1} \int dx_1 dx_2 dy_1 dy_2 \left\{ e^{-\frac{x_1^2 + y_1^2 + x_2^2 + (y_2 - R)^2}{2l_B^2}} \right.
$$

$$
\left. - e^{-\frac{x_1^2 + y_1^2 + x_2^2 + y_2^2 - R(y_1 + y_2)}{2l_B^2}} \cos \frac{R(x_2 - x_1)}{2l_B^2} \right\} v_{2D} \left(\sqrt{(x_1 - x_2)^2 + (y_1 - y_2)^2} \right).
$$

We substitute $\tilde{x}_1 = \frac{1}{2}(x_1 + x_2)$, $\tilde{x}_2 = (x_1 - x_2)$, $\tilde{y}_1 = \frac{1}{2}(y_1 + y_2)$ and $\tilde{y}_2 = (y_1 - y_2)$. The integral becomes:

$$
\begin{aligned}
U_{12} &= \frac{1}{4\pi^2 l_B^4} \frac{1}{1 - e^{-\frac{R^2}{2l_B^2}}} \int d\tilde{x}_1 d\tilde{x}_2 d\tilde{y}_1 \tilde{d}y_2 \left(e^{-\frac{2\tilde{x}_1^2 + 2\tilde{y}_1^2 + \frac{1}{2}(\tilde{x}_2^2 + \tilde{y}_2^2) + R^2 - 2R(\tilde{y}_1 - \frac{1}{2}\tilde{y}_2)}{2l_B^2}} \right. \\
&\quad \left. - e^{-\frac{2\tilde{x}_1^2 + 2\tilde{y}_1^2 + \frac{1}{2}(\tilde{x}_2^2 + \tilde{y}_2^2) - 2R\tilde{y}_1}{2l_B^2}} \cos\left(\frac{R\tilde{x}_2}{2l_B^2}\right) \right) v_{2D}(\sqrt{\tilde{x}_2^2 + \tilde{y}_2^2}) \\
&= \frac{1}{2\pi l_B^2} \frac{1}{1 - e^{-\frac{R^2}{2l_B^2}}} \int dx dy \left(e^{-\frac{x^2 + (y+R)^2}{4l_B^2}} \right. \\
&\quad \left. - e^{-\frac{x^2 + y^2}{4l_B^2}} e^{-\frac{R^2}{4l_B^2}} \cos\left(\frac{Rx}{2l_B^2}\right) \right) v_{2D}(\sqrt{x^2 + y^2}).
\end{aligned}
$$

The left part is known from the symmetric wave function. The right hand side is an exponential small contribution due to the antisymmetrization.

B.2   Expansion of Φ

With displacements $\mathbf{u}(\mathbf{l})$ of the dipoles at positions $\mathbf{r}(\mathbf{l})$ in the lattice, the potential reads (equation (4.5)):

$$
\Phi = d^2 \sum_{\mathbf{l}, \mathbf{l}' \neq \mathbf{l}} \frac{1}{|\mathbf{r}(\mathbf{l}) + \mathbf{u}(\mathbf{l}) - \mathbf{r}(\mathbf{l}') - \mathbf{u}(\mathbf{l}')|^3} \quad .
$$

The first derivative of Φ with respect to $u_\alpha(\mathbf{l})$ is:

$$
\frac{\partial \Phi}{\partial u_\alpha(\mathbf{l})} = -d^2 3 \sum_{\mathbf{l}' \neq \mathbf{l}} \frac{r_\alpha(\mathbf{l}) + u_\alpha(\mathbf{l}) - r_\alpha(\mathbf{l}') - u_\alpha(\mathbf{l}')}{|\mathbf{r}(\mathbf{l}) + \mathbf{u}(\mathbf{l}) - \mathbf{r}(\mathbf{l}') - \mathbf{u}(\mathbf{l}')|^5} \quad .
$$

Since the dipoles are in the potential minimum, the first order part is supposed to be zero. If $\mathbf{l} \neq \mathbf{l}'$ the second derivative reads:

$$
\begin{aligned}
&\frac{\partial^2 \Phi}{\partial u_\alpha(\mathbf{l}) \partial u_{\alpha'}(\mathbf{l}')} \\
&= -d^2 n^{\frac{3}{2}} \left(15 \frac{(r_\alpha(\mathbf{l}) + u_\alpha(\mathbf{l}) - r_\alpha(\mathbf{l}') - u_\alpha(\mathbf{l}'))(r_{\alpha'}(\mathbf{l}) + u_{\alpha'}(\mathbf{l}) - r_{\alpha'}(\mathbf{l}') - u_{\alpha'}(\mathbf{l}'))}{|\mathbf{r}(\mathbf{l}) + \mathbf{u}(\mathbf{l}) - \mathbf{r}(\mathbf{l}') - \mathbf{u}(\mathbf{l}')|^7} \right. \\
&\quad \left. - 3 \frac{\delta_{\alpha\alpha'}}{|\mathbf{r}(\mathbf{l}) + \mathbf{u}(\mathbf{l}) - \mathbf{r}(\mathbf{l}') - \mathbf{u}(\mathbf{l}')|^5} \right) \quad .
\end{aligned}
$$

In order to get the harmonic part of the potential we set $\mathbf{u}(\mathbf{l}) = 0$. In a short notation it is:

$$\Phi_{\alpha_1\alpha_2}(\mathbf{l} - \mathbf{l}') = \left.\frac{\partial^2\Phi}{\partial u_\alpha(\mathbf{l})\partial u_{\alpha'}(\mathbf{l}')}\right|_{\mathbf{u}=0}$$

$$= -\frac{d^2}{|\mathbf{r}(\mathbf{ll}')|^5}\left(\frac{15}{|\mathbf{r}(\mathbf{ll}')|^2}\mathbf{r}_\alpha(\mathbf{ll}')\,\mathbf{r}_{\alpha'}(\mathbf{ll}') - 3\delta_{\alpha\alpha'}\right) \quad, \qquad \text{(B.1)}$$

with $\mathbf{r}_{\alpha_i}(\mathbf{ll}') = \mathbf{r}_{\alpha_i}(\mathbf{l}) - \mathbf{r}_{\alpha_i}(\mathbf{l}')$ and $|\mathbf{r}(\mathbf{ll}')| = |\mathbf{r}(\mathbf{l}) - \mathbf{r}(\mathbf{l}')|$ is the distance is the distance between two dipoles. Similarly one obtains for the differentiation at the same position $\mathbf{l}$:

$$\left.\frac{\partial^2\Phi}{\partial u_\alpha(\mathbf{l})\partial u_{\alpha'}(\mathbf{l})}\right|_{\mathbf{u}=0} = -\sum_{\mathbf{l}'\neq\mathbf{l}}\Phi_{\alpha_1\alpha_2}(\mathbf{l} - \mathbf{l}') \quad.$$

The examination of non-harmonic terms requires higher derivative of Φ. One can already see in equation (B.1) that higher derivative must vanish, if the derivatives with respect of $\mathbf{u}(l)$ are taken on three different lattice positions $\mathbf{l}_1 \neq \mathbf{l}_2 \neq \mathbf{l}_3$. For example, we set $\mathbf{l}_1 = \mathbf{l}_2 = \mathbf{l}$ and $\mathbf{l}_3 = \mathbf{l}'$:

$$\Phi_{\alpha_1\alpha_2\alpha_3}(\mathbf{l} - \mathbf{l}') = \left.\frac{\partial^3\Phi}{\partial u_{\alpha_1}(\mathbf{l})\partial u_{\alpha_2}(\mathbf{l}')u_{\alpha_3}(\mathbf{l})}\right|_{\mathbf{u}=0}$$

$$= \frac{d^2 n^{\frac{3}{2}}}{|\mathbf{r}(\mathbf{ll}')|^7}\left(105\frac{(r_{\alpha_1}(\mathbf{ll}'))\,(r_{\alpha_2}(\mathbf{ll}'))\,(r_{\alpha_3}(\mathbf{ll}'))}{|\mathbf{r}(\mathbf{ll}')|^2}\right.$$

$$\left. - 15\left\{\delta_{\alpha_1\alpha_2}r_{\alpha_3}(\mathbf{ll}') + \delta_{\alpha_1\alpha_3}r_{\alpha_2}(\mathbf{ll}') + \delta_{\alpha_2\alpha_3}r_{\alpha_1}(\mathbf{ll}')\right\}\right) \quad. \qquad \text{(B.2)}$$

The expression on the left hand side is symmetric under permutation of the α's. The derivative with respect to equal $\mathbf{l}$ reads:

$$\left.\frac{\partial^3\Phi}{\partial u_{\alpha_1}(\mathbf{l})\partial u_{\alpha_2}(\mathbf{l})u_{\alpha_3}(\mathbf{l})}\right|_{\mathbf{u}=0} = -\sum_{\mathbf{l}\neq\mathbf{l}'}\Phi_{\alpha_1\alpha_2\alpha_3}(\mathbf{l} - \mathbf{l}') \quad.$$

The fourth derivative is:

$$
\Phi_{\alpha_1\cdots\alpha_4}(\mathbf{l}-\mathbf{l}') = \frac{\partial^4\Phi}{\partial u_{\alpha_1}(\mathbf{l})\partial u_{\alpha_2}(\mathbf{l})u_{\alpha_3}(\mathbf{l})u_{\alpha_4}(\mathbf{l}')}\Big|_{\mathbf{u}=0}
$$

$$
= -\frac{d^2 n^{\frac{3}{2}}}{|\mathbf{r}(\mathbf{ll}')|^7}\Bigg\{ 945\frac{\mathbf{r}_{\alpha_1}(\mathbf{ll}')\mathbf{r}_{\alpha_2}(\mathbf{ll}')\mathbf{r}_{\alpha_3}(\mathbf{ll}')\mathbf{r}_{\alpha_4}(\mathbf{ll}')}{|\mathbf{r}(\mathbf{ll}')|^4}
$$

$$
-\frac{105}{|\mathbf{r}(\mathbf{ll}')|^2}\left\{\delta_{\alpha_1\alpha_2}\left(\mathbf{r}_{\alpha_3}(\mathbf{ll}')\right)\left(\mathbf{r}_{\alpha_4}(\mathbf{ll}')\right)+\delta_{\alpha_1\alpha_3}\left(\mathbf{r}_{\alpha_2}(\mathbf{ll}')\right)\left(\mathbf{r}_{\alpha_4}(\mathbf{ll}')\right)\right.
$$

$$
+\delta_{\alpha_1\alpha_4}\left(\mathbf{r}_{\alpha_2}(\mathbf{ll}')\right)\left(\mathbf{r}_{\alpha_3}(\mathbf{ll}')\right)+\delta_{\alpha_2\alpha_3}\left(\mathbf{r}_{\alpha_1}(\mathbf{ll}')\right)\left(\mathbf{r}_{\alpha_4}(\mathbf{ll}')\right)
$$

$$
+\delta_{\alpha_2\alpha_4}\left(\mathbf{r}_{\alpha_1}(\mathbf{ll}')\right)\left(\mathbf{r}_{\alpha_3}(\mathbf{ll}')\right)+\delta_{\alpha_3\alpha_4}\left(\mathbf{r}_{\alpha_1}(\mathbf{ll}')\right)\left(\mathbf{r}_{\alpha_2}(\mathbf{ll}')\right)\big\}
$$

$$
\left.+15\left(\delta_{\alpha_1\alpha_2}\delta_{\alpha_3\alpha_4}+\delta_{\alpha_1\alpha_3}\delta_{\alpha_2\alpha_4}+\delta_{\alpha_1\alpha_4}\delta_{\alpha_2\alpha_3}\right)\right\} \quad , \tag{B.3}
$$

and the derivative with respect to $\mathbf{u}\left(\mathbf{l}\right)$ at the same position $\mathbf{l}$ reads:

$$
\frac{\partial^4\Phi}{\partial u_{\alpha_1}(\mathbf{l})\partial u_{\alpha_2}(\mathbf{l})u_{\alpha_3}(\mathbf{l})u_{\alpha_4}(\mathbf{l})}\Big|_{\mathbf{u}=0} = -\sum_{\mathbf{l}\neq\mathbf{l}'}\Phi_{\alpha_1\alpha_2\alpha_3\alpha_4}(\mathbf{l}-\mathbf{l}') \quad .
$$

All derivatives depend only on the difference between $\mathbf{r}\left(\mathbf{l}\right)-\mathbf{r}\left(\mathbf{l}'\right)$.

B.3   Three-phonon interaction H_3

As it is well-known, the quadratic term describes phonons, whereas higher order corrections are responsible for phonon-phonon interaction. In this section, we examine the Hamiltonian for the third order part H_3 that reads:

$$
H_3 = \frac{1}{3!}\sum_{\alpha_1\alpha_2\alpha_3}\sum_{\mathbf{l}_1\mathbf{l}_2\mathbf{l}_3}\Phi_{\alpha_1\alpha_2\alpha_3}(\mathbf{l}_1,\mathbf{l}_2,\mathbf{l}_3)u_{\alpha_1}(l_1)u_{\alpha_2}(l_2)u_{\alpha_3}(l_3) \quad , \tag{B.4}
$$

where $\mathbf{u}\left(\mathbf{l}\right)$ are the phonon operators (see equation (4.28)).

$$
u_\alpha(\mathbf{l}) = \sum_{m\mathbf{k}}\mathrm{e}^{\mathrm{i}*\mathbf{k}\mathbf{r}_l}\left(\xi_{m\alpha}(\mathbf{k})+\xi^\dagger_{m\alpha}(-\mathbf{k})\right) \quad .
$$

If in the sum in equation (B.4) all $\mathbf{l}_i$ are different $\mathbf{l}_1 \neq \mathbf{l}_2 \neq \mathbf{l}_3$, then $\Phi_{\alpha_1\alpha_2\alpha_3}(\mathbf{l}_1\mathbf{l}_2\mathbf{l}_3)=0$. Therefore, we have to consider two cases:

- All $\mathbf{l}_i$ are equal, $\mathbf{l}_1 = \mathbf{l}_2 = \mathbf{l}_3 = l$.

- Two of the $\mathbf{l}_i$ are equal and the third one is different, for example, $l_1 = l_2 = l$ and $l_3 = l' \neq l$.

The contribution of the first case reads:

$$\frac{1}{3!} \sum_{\mathbf{l}} \Phi_{\alpha_1\dots\alpha_3}(\mathbf{lll}) u_{\alpha_1}(\mathbf{l}) u_{\alpha_2}(\mathbf{l}) u_{\alpha_3}(\mathbf{l})$$

$$= -\frac{1}{N^3} \sum_{\mathbf{l}} \sum_{\mathbf{k}_1\dots\mathbf{k}_3} \sum_{m_1\dots m_3} \left(\xi_{m_1\alpha_1}(\mathbf{k}_1) + \xi_{m_1\alpha_1}^{\dagger}(-\mathbf{k}_1)\right)\left(\xi_{m_2\alpha_2}(\mathbf{k}_2) + \xi_{m_2\alpha_2}^{\dagger}(-\mathbf{k}_2)\right)$$

$$\left(\xi_{m_3\alpha_3}(\mathbf{k}_3) + \xi_{m_3\alpha_3}^{\dagger}(-\mathbf{k}_3)\right) e^{i\mathbf{l}(\mathbf{k}_1+\mathbf{k}_2+\mathbf{k}_3)} \sum_{\mathbf{l}'\neq\mathbf{l}} \Phi_{\alpha_1\dots\alpha_3}(\mathbf{l}-\mathbf{l}')$$

$$= -\frac{\omega_d^2 m}{3!aN^3} \sum_{\mathbf{k}_1\dots\mathbf{k}_3} \sum_{m_1\dots m_3} \left(\xi_{m_1\alpha_1}(\mathbf{k}_1) + \xi_{m_1\alpha_1}^{\dagger}(-\mathbf{k}_1)\right)\left(\xi_{m_2\alpha_2}(\mathbf{k}_2) + \xi_{m_2\alpha_2}^{\dagger}(-\mathbf{k}_2)\right)$$

$$\left(\xi_{m_3\alpha_3}(\mathbf{k}_3) + \xi_{m_3\alpha_3}^{\dagger}(-\mathbf{k}_3)\right) \delta_{\mathbf{k}_1+\mathbf{k}_2+\mathbf{k}_3} F_{\alpha_1\dots\alpha_3}(0) \quad.$$

where $F_{\alpha_1\dots\alpha_3}(\mathbf{k})$ is computed in equation (B.8). In the second case for $\mathbf{l}_1 = \mathbf{l}_2 = l$, respectively $l_3 = \mathbf{l}' \neq l$ we have:

$$\sum_{\mathbf{l}\neq\mathbf{l}'} \Phi_{\alpha_1\dots\alpha_3}(\mathbf{lll}') u_{\alpha_1}(\mathbf{l}) u_{\alpha_2}(\mathbf{l}) u_{\alpha_3}(\mathbf{l}')$$

$$= \frac{1}{3!N^3} \sum_{\mathbf{l}} \sum_{\mathbf{k}_1\dots\mathbf{k}_3} \sum_{m_1\dots m_3} \left(\xi_{m_1\alpha_1}(\mathbf{k}_1) + \xi_{m_1\alpha_1}^{\dagger}(-\mathbf{k}_1)\right)\left(\xi_{m_2\alpha_2}(\mathbf{k}_2) + \xi_{m_2\alpha_2}^{\dagger}(-\mathbf{k}_2)\right)$$

$$\left(\xi_{m_3\alpha_3}(\mathbf{k}_3) + \xi_{m_3\alpha_3}^{\dagger}(-\mathbf{k}_3)\right) e^{i\mathbf{l}(\mathbf{k}_1+\mathbf{k}_2+\mathbf{k}_3)} \sum_{\mathbf{l}'\neq\mathbf{l}} \Phi_{\alpha_1\dots\alpha_3}(\mathbf{l}-\mathbf{l}') e^{i\mathbf{k}_3(\mathbf{l}-\mathbf{l}')}$$

$$= \frac{\omega_d^2 m}{3!aN^3} \sum_{\mathbf{k}_1\dots\mathbf{k}_3} \sum_{m_1\dots m_3} \left(\xi_{m_1\alpha_1}(\mathbf{k}_1) + \xi_{m_1\alpha_1}^{\dagger}(-\mathbf{k}_1)\right)\left(\xi_{m_2\alpha_2}(\mathbf{k}_2) + \xi_{m_2\alpha_2}^{\dagger}(-\mathbf{k}_2)\right)$$

$$\left(\xi_{m_3\alpha_3}(\mathbf{k}_3) + \xi_{m_3\alpha_3}^{\dagger}(-\mathbf{k}_3)\right) \delta_{\mathbf{k}_1+\mathbf{k}_2+\mathbf{k}_3} \tilde{F}_{\alpha_1\dots\alpha_3}(\mathbf{k}_3) \quad.$$

The other two possibilities can be obtained in a similar way. After combining all combinations, we obtain for H_3 the formula:

$$H_3 = \frac{\omega_d^2 m}{3!a} \sum_{\mathbf{k}_1\dots\mathbf{k}_3} \sum_{m_1\dots m_3} \sum_{\alpha_1\dots\alpha_3} \delta_{\mathbf{k}_1+\mathbf{k}_2+\mathbf{k}_3,0}$$

$$(-F_{\alpha_1\dots\alpha_3}(0) + F_{\alpha_1\dots\alpha_3}(\mathbf{k}_1) + F_{\alpha_1\dots\alpha_3}(\mathbf{k}_2) + F_{\alpha_1\dots\alpha_3}(\mathbf{k}_3))$$

$$\left(\xi_{m_1\alpha_1}(\mathbf{k}_1) + \xi_{m_1\alpha_1}^{\dagger}(-\mathbf{k}_1)\right)\left(\xi_{m_2\alpha_2}(\mathbf{k}_2) + \xi_{m_2\alpha_2}^{\dagger}(-\mathbf{k}_2)\right)\left(\xi_{m_3\alpha_3}(\mathbf{k}_3) + \xi_{m_3\alpha_3}^{\dagger}(-\mathbf{k}_3)\right).$$

$$(\text{B.5})$$

B.4   Four-phonon interaction of H_4

For the fourth order part of the Hamiltonian reads:

$$H_4 = \frac{1}{4!} \sum_{\mathbf{l}_1\ldots\mathbf{l}_4} \sum_{\alpha_1\ldots\alpha_4} \Phi_{\alpha_1\ldots\alpha_4}\left(\mathbf{l}_1\ldots\mathbf{l}_4\right) u_{\alpha_1}(\mathbf{l}_1)\ldots u_{\alpha_4}(\mathbf{l}_4) \quad .$$

The function $\Phi_{\alpha_1\cdots\alpha_4}\left(\mathbf{l}_1\cdots\mathbf{l}_4\right)$ is only non zero, if the set $\{\mathbf{l}_1\mathbf{l}_2\mathbf{l}_3\mathbf{l}_4\}$ contains not more than two different lattice vectors $\mathbf{l}$'s. Now we have to examine three different cases:

- All $\mathbf{l}_i$ are the same $\mathbf{l}_{1,2,3,4} = \mathbf{l}$.

- We have two pairs of the same $\mathbf{l}_i$. For instance $\mathbf{l}_1 = \mathbf{l}_2 = \mathbf{l}$ and $\mathbf{l}_3 = \mathbf{l}_4 = \mathbf{l}' \neq \mathbf{l}$.

- Three $\mathbf{l}_i$ are the same, for instance, $\mathbf{l}_1 = \mathbf{l}_2 = \mathbf{l}_3 = \mathbf{l}$ and the fourth is different $\mathbf{l}_4 = \mathbf{l}' \neq \mathbf{l}$.

We consider the first case, where all $\mathbf{l}_i$ are the same and expand it in Fourier series:

$$\frac{1}{4!} \sum_{\mathbf{l}} \Phi_{\alpha_1\ldots\alpha_4}(\mathbf{llll}) u_{\alpha_1}(\mathbf{l})\ldots u_{\alpha_4}(\mathbf{l})$$

$$= -\frac{1}{4!N^4} \sum_{\mathbf{l}} \sum_{\mathbf{k}_1\ldots\mathbf{k}_4} \sum_{m_1\ldots m_4} \left(\xi_{m_1\alpha_1}(\mathbf{k}_1) + \xi^\dagger_{m_1\alpha_1}(-\mathbf{k}_1)\right)\ldots$$

$$\left(\xi_{m_4\alpha_4}(\mathbf{k}_4) + \xi^\dagger_{m_4\alpha_4}(-\mathbf{k}_4)\right) \mathrm{e}^{\mathrm{i}l(\mathbf{k}_1+\cdots+\mathbf{k}_4)} \sum_{\mathbf{l}'\neq\mathbf{l}} F_{\alpha_1\ldots\alpha_4}(\mathbf{l}-\mathbf{l}')$$

$$= -\frac{1}{4!} \frac{\omega_d^2 m}{a^2 N^4} \sum_{\mathbf{k}_1\ldots\mathbf{k}_4} \sum_{m_1\ldots m_4} \left(\xi_{m_1\alpha_1}(\mathbf{k}_1) + \xi^\dagger_{m_1\alpha_1}(-\mathbf{k}_1)\right)\ldots$$

$$\left(\xi_{m_4\alpha_4}(\mathbf{k}_4) + \xi^\dagger_{m_4\alpha_4}(-\mathbf{k}_4)\right) \delta_{\mathbf{k}_1+\cdots+\mathbf{k}_4} \tilde{F}_{\alpha_1\ldots\alpha_4}(0) \quad ,$$

where $F_{\alpha_1\cdots\alpha_4}(\mathbf{k})$ can be found in equation (B.9). For the second case, where we have two pairs of equal $\mathbf{l}_i$ we get:

$$\sum_{\mathbf{l},\mathbf{l}'\neq\mathbf{l}} \Phi_{\alpha_1\ldots\alpha_4}(\mathbf{l}\mathbf{l}\mathbf{l}'\mathbf{l}')u_{\alpha_1}(\mathbf{l})u_{\alpha_2}(\mathbf{l})u_{\alpha_3}(\mathbf{l}')u_{\alpha_4}(\mathbf{l}')$$

$$= -\frac{1}{N^4}\sum_{\mathbf{l}}\sum_{\mathbf{k}_1\ldots\mathbf{k}_4}\sum_{m_1\ldots m_4} \left(\xi_{m_1\alpha_1}(\mathbf{k}_1) + \xi^\dagger_{m_1\alpha_1}(-\mathbf{k}_1)\right)\left(\xi_{m_2\alpha_2}(\mathbf{k}_2) + \xi^\dagger_{m_2\alpha_2}(-\mathbf{k}_2)\right)$$

$$\left(\xi_{m_3\alpha_3}(\mathbf{k}_3) + \xi^\dagger_{m_3\alpha_3}(-\mathbf{k}_3)\right)\left(\xi_{m_4\alpha_4}(\mathbf{k}_4) + \xi^\dagger_{m_4\alpha_4}(-\mathbf{k}_4)\right)\mathrm{e}^{\mathrm{i}l(\mathbf{k}_1+\cdots+\mathbf{k}_4)}$$

$$\sum_{\mathbf{l}'\neq\mathbf{l}} \Phi_{\alpha_1\ldots\alpha_4}(\mathbf{l}-\mathbf{l}')\mathrm{e}^{\mathrm{i}(\mathbf{k}_3+\mathbf{k}_4)(\mathbf{l}-\mathbf{l}')}$$

$$= -\frac{\omega_d^2 m}{a^2 N^4}\sum_{\mathbf{k}_1\ldots\mathbf{k}_4}\sum_{m_1\ldots m_4} \left(\xi_{m_1\alpha_1}(\mathbf{k}_1) + \xi^\dagger_{m_1\alpha_1}(-\mathbf{k}_1)\right)\left(\xi_{m_2\alpha_2}(\mathbf{k}_2) + \xi^\dagger_{m_2\alpha_2}(-\mathbf{k}_2)\right)$$

$$\left(\xi_{m_3\alpha_3}(\mathbf{k}_3) + \xi^\dagger_{m_3\alpha_3}(-\mathbf{k}_3)\right)\left(\xi_{m_4\alpha_4}(\mathbf{k}_4) + \xi^\dagger_{m_4\alpha_4}(-\mathbf{k}_4)\right)\delta_{\mathbf{k}_1+\cdots+\mathbf{k}_4}\tilde{F}_{\alpha_1\ldots\alpha_4}(\mathbf{k}_3+\mathbf{k}_4).$$

The other two contributions for this case can be obtained in a similar way. And finely, for the third case, in where three $\mathbf{l}_i$ are equal to $\mathbf{l}$, the fourth is equal to $\mathbf{l}'\neq\mathbf{l}$ we have:

$$\sum_{\mathbf{l},\mathbf{l}'\neq\mathbf{l}} \Phi_{\alpha_1\ldots\alpha_4}(\mathbf{l}\mathbf{l}\mathbf{l}\mathbf{l}')u_{\alpha_1}(\mathbf{l})u_{\alpha_2}(\mathbf{l})u_{\alpha_3}(\mathbf{l})u_{\alpha_4}(\mathbf{l}')$$

$$= \frac{1}{N^4}\sum_{\mathbf{l}}\sum_{\mathbf{k}_1\ldots\mathbf{k}_4}\sum_{m_1\ldots m_4} \left(\xi_{m_1\alpha_1}(\mathbf{k}_1) + \xi^\dagger_{m_1\alpha_1}(-\mathbf{k}_1)\right)\left(\xi_{m_2\alpha_2}(\mathbf{k}_2) + \xi^\dagger_{m_2\alpha_2}(-\mathbf{k}_2)\right)$$

$$\left(\xi_{m_3\alpha_3}(\mathbf{k}_3) + \xi^\dagger_{m_3\alpha_3}(-\mathbf{k}_3)\right)\left(\xi_{m_4\alpha_4}(\mathbf{k}_4) + \xi^\dagger_{m_4\alpha_4}(-\mathbf{k}_4)\right)\mathrm{e}^{\mathrm{i}l(\mathbf{k}_1+\cdots+\mathbf{k}_4)}$$

$$\sum_{\mathbf{l}'\neq\mathbf{l}} \Phi_{\alpha_1\ldots\alpha_4}(\mathbf{l}-\mathbf{l}')\mathrm{e}^{\mathrm{i}\mathbf{k}_4(\mathbf{l}-\mathbf{l}')}$$

$$= \frac{\omega_d^2 m}{a^2}\sum_{\mathbf{k}_1\ldots\mathbf{k}_4}\sum_{m_1\ldots m_4} \left(\xi_{m_1\alpha_1}(\mathbf{k}_1) + \xi^\dagger_{m_1\alpha_1}(-\mathbf{k}_1)\right)\left(\xi_{m_2\alpha_2}(\mathbf{k}_2) + \xi^\dagger_{m_2\alpha_2}(-\mathbf{k}_2)\right)$$

$$\left(\xi_{m_3\alpha_3}(\mathbf{k}_3) + \xi^\dagger_{m_3\alpha_3}(-\mathbf{k}_3)\right)\left(\xi_{m_4\alpha_4}(\mathbf{k}_4) + \xi^\dagger_{m_4\alpha_4}(-\mathbf{k}_4)\right)\delta_{\mathbf{k}_1+\cdots+\mathbf{k}_4}\tilde{F}_{\alpha_1\ldots\alpha_4}(\mathbf{k}_4),$$

and, in the same way, we get the remaining three combinations for this case.

Finally, the fourth order term of the Hamiltonian reads:

$$
\begin{aligned}
H_4 = \frac{\omega_d^2 m}{a^2 4!} \sum_{\mathbf{k}_1 \ldots \mathbf{k}_4} \sum_{m_1 \ldots m_4} \sum_{\alpha_1 \ldots \alpha_3} \delta_{\mathbf{k}_1 + \mathbf{k}_2 + \mathbf{k}_3 + \mathbf{k}_4, 0} \\
\left(-\tilde{F}_{\alpha_1 \ldots \alpha_4}(0) + \tilde{F}_{\alpha_1 \ldots \alpha_4}(\mathbf{k}_1) + \tilde{F}_{\alpha_1 \ldots \alpha_4}(\mathbf{k}_2) + \tilde{F}_{\alpha_1 \ldots \alpha_4}(\mathbf{k}_3) + \tilde{F}_{\alpha_1 \ldots \alpha_4}(\mathbf{k}_4) \right. \\
\left. - \tilde{F}_{\alpha_1 \ldots \alpha_4}(\mathbf{k}_1 + \mathbf{k}_2) - \tilde{F}_{\alpha_1 \ldots \alpha_4}(\mathbf{k}_1 + \mathbf{k}_3) - \tilde{F}_{\alpha_1 \ldots \alpha_4}(\mathbf{k}_1 + \mathbf{k}_4) \right) \\
\left(\xi_{m_1 \alpha_1}(\mathbf{k}_1) + \xi_{m_1 \alpha_1}^\dagger(-\mathbf{k}_1) \right) \left(\xi_{m_2 \alpha_2}(\mathbf{k}_2) + \xi_{m_2 \alpha_2}^\dagger(-\mathbf{k}_2) \right) \\
\left(\xi_{m_3 \alpha_3}(\mathbf{k}_3) + \xi_{m_3 \alpha_3}^\dagger(-\mathbf{k}_3) \right) \left(\xi_{m_4 \alpha_4}(\mathbf{k}_4) + \xi_{m_4 \alpha_4}^\dagger(-\mathbf{k}_4) \right) \quad .
\end{aligned}
\tag{B.6}
$$

B.4.1   Fourier transform of the derivatives

We calculate the Fourier transforms of equations (B.1), (B.2) and (B.3) and obtain the expression for the dimensionless function $F_{\alpha\alpha'}(\mathbf{k})$ in equations (4.10), (B.5) and (B.6). For the second order we calculate:

$$
\tilde{\Phi}_{\alpha_1 \alpha_2}(\mathbf{k}) = \omega_d^2 m F_{\alpha_1 \alpha_2}(\mathbf{k}) = \sum_{\mathbf{l}} e^{i \mathbf{k} \mathbf{r}(\mathbf{l})} \Phi_{\alpha\alpha'}(\mathbf{l}) \quad ,
\tag{B.7}
$$

with $\omega_d^2 = d^2 n^{3/2}/(ma^2)$. Since the values for the addenda decay with $1/|\mathbf{r}(\mathbf{l})|^5$ we approximate the transform by taking only the nearest neighbors into account. This results in:

$$
\begin{aligned}
F_{xx}(\mathbf{k}) &= -\frac{3}{2}\left(\cos \mathbf{k} \mathbf{r}_1 + \cos \mathbf{k}(\mathbf{r}_1 - \mathbf{r}_2) \right) - 24 \cos \mathbf{k} \mathbf{r}_2 + 27 \\
F_{xy}(\mathbf{k}) &= -15 \frac{\sqrt{3}}{2}\left(\cos \mathbf{k} \mathbf{r}_1 - \cos \mathbf{k}(\mathbf{r}_1 - \mathbf{r}_2) \right) \\
F_{yx}(\mathbf{k}) &= F_{xy} \\
F_{yy}(\mathbf{k}) &= -\frac{33}{2}\left(\cos \mathbf{k} \mathbf{r}_1 + \cos \mathbf{k}(\mathbf{r}_1 - \mathbf{r}_2) \right) + 6 \cos \mathbf{k} \mathbf{r}_2 + 27 \quad .
\end{aligned}
$$

For the third order we calculate in the same way the Fourier transform:

$$
\tilde{\Phi}_{\alpha_1 \alpha_2 \alpha_3}(\mathbf{k}) = \frac{\omega_d^2 m}{a} F_{\alpha_1 \alpha_2 \alpha_3}(\mathbf{k}) = \sum_{\mathbf{l}} e^{i \mathbf{k} \mathbf{r}(\mathbf{l})} \Phi_{\alpha_1 \alpha_2 \alpha_3}(\mathbf{l}) \quad ,
\tag{B.8}
$$

and, with the same argument as for the second order we only consider the nearest neighbors in the sum and obtain:

$$F_{xxx}(\mathbf{k}) = \mathrm{i}\left\{\frac{75}{4}\left(\sin\mathbf{k}\left(\mathbf{r}_1 - \mathbf{r}_2\right) - \sin\mathbf{k}\mathbf{r}_1\right) + 120\sin\mathbf{k}\mathbf{r}_2\right\}$$

$$F_{xxy}(\mathbf{k}) = \mathrm{i}\frac{\sqrt{3}}{4}45\left(\sin\mathbf{k}\mathbf{r}_1 + \sin\mathbf{k}\left(\mathbf{r}_1 - \mathbf{r}_2\right)\right)$$

$$F_{xyy}(\mathbf{k}) = \mathrm{i}\left\{\frac{255}{4}\left(\sin\mathbf{k}\mathbf{r}_1 - \sin\mathbf{k}\left(\mathbf{r}_1 - \mathbf{r}_2\right)\right) - 30\sin\mathbf{k}\mathbf{r}_2\right\}$$

$$F_{yyy}(\mathbf{k}) = \mathrm{i}\frac{\sqrt{3}}{4}135\left(\sin\mathbf{k}\mathbf{r}_1 + \sin\mathbf{k}\left(\mathbf{r}_1 - \mathbf{r}_2\right)\right) \quad .$$

Finely, for the Fourier transform of the fourth order (equation (B.3)) reads:

$$\tilde{\Phi}_{\alpha_1\cdots\alpha_4}(\mathbf{k}) = \frac{\omega_d^2 m}{a^2}F_{\alpha_1\cdots\alpha_4}(\mathbf{k}) = \sum_{\mathbf{l}}\mathrm{e}^{\mathrm{i}\mathbf{k}\mathbf{r}(\mathbf{l})}\Phi_{\alpha_1\cdots\alpha_4}(\mathbf{l}) \quad , \tag{B.9}$$

which can be approximated by taking only into account the nearest neighbors:

$$\tilde{F}_{xxxx}(\mathbf{k}) = -\frac{855}{8}\left(\cos\mathbf{k}\mathbf{r}_1 + \cos\mathbf{k}\left(\mathbf{r}_1 - \mathbf{r}_2\right)\right) + 720\cos\mathbf{k}\mathbf{r}_2$$

$$\tilde{F}_{xxxy}(\mathbf{k}) = -\sqrt{3}\frac{315}{8}\left(\cos\mathbf{k}\mathbf{r}_1 - \cos\mathbf{k}\left(\mathbf{r}_1 - \mathbf{r}_2\right)\right)$$

$$\tilde{F}_{xxyy}(\mathbf{k}) = \frac{1395}{8}\left(\cos\mathbf{k}\mathbf{r}_1 + \cos\mathbf{k}\left(\mathbf{r}_1 - \mathbf{r}_2\right)\right) - 180\cos\mathbf{k}\mathbf{r}_2$$

$$\tilde{F}_{xyyy}(\mathbf{k}) = \sqrt{3}\frac{1575}{8}\left(\cos\mathbf{k}\mathbf{r}_1 - \cos\mathbf{k}\left(\mathbf{r}_1 - \mathbf{r}_2\right)\right)$$

$$\tilde{F}_{yyyy}(\mathbf{k}) = \frac{1665}{8}\left(\cos\mathbf{k}\mathbf{r}_1 + \cos\mathbf{k}\left(\mathbf{r}_1 - \mathbf{r}_2\right)\right) + 90\cos\mathbf{k}\mathbf{r}_2 \quad .$$

B.5   Second order expansion of the H_3 term

The explicit expression for the second order term for the three-phonon expansion (see section 4.8.2) reads:

$$
\begin{aligned}
&\mathord{\multimap}\!\!\mathord{\bigcirc}\!\!\mathord{\multimap}_{\alpha\alpha'}(\mathbf{l},\mathbf{l}';t,t') \\
&= -\mathrm{i}\frac{\omega_d^4 m^2}{a^2 3!^2 N^8}\frac{1}{2\hbar^2}\sum_{\mathbf{q}\mathbf{q}'}\sum_{mm'}\sum_{\alpha_1...\alpha_3}\sum_{\alpha_1'...\alpha_3'}\sum_{\mathbf{k}_1...\mathbf{k}_3}\sum_{\mathbf{k}_1'...\mathbf{k}_3'}\sum_{m_1...m_3 m_1'...m_3'}\mathrm{e}^{\mathrm{i}\mathbf{q}\mathbf{r}_l}\mathrm{e}^{\mathrm{i}\mathbf{q}'\mathbf{r}_l'}\int\!\mathrm{d}t_1\!\int\!\mathrm{d}t_2 \\
&\delta_{\mathbf{k}_1+\mathbf{k}_2+\mathbf{k}_3,0}\delta_{\mathbf{k}_1'+\mathbf{k}_2'+\mathbf{k}_3',0}\left(-F_{\alpha_1...\alpha_3}(0)+F_{\alpha_1...\alpha_3}(\mathbf{k}_1)+F_{\alpha_1...\alpha_3}(\mathbf{k}_2)+F_{\alpha_1...\alpha_3}(\mathbf{k}_3)\right) \\
&\left(-F_{\alpha_1'...\alpha_3'}(0)+F_{\alpha_1'...\alpha_3'}(\mathbf{k}_1')+F_{\alpha_1'...\alpha_3'}(\mathbf{k}_2')+F_{\alpha_1'...\alpha_3'}(\mathbf{k}_3')\right) \\
&\langle\mathcal{T}\left(\xi_{m\alpha}(\mathbf{q})+\xi_{m\alpha}^\dagger(-\mathbf{q})\right)\left(\xi_{m'\alpha'}(\mathbf{q}')+\xi_{m'\alpha'}^\dagger(-\mathbf{q}')\right)\left(\xi_{m_1\alpha_1}(\mathbf{k}_1)+\xi_{m_1\alpha_1}^\dagger(-\mathbf{k}_1)\right) \\
&\left(\xi_{m_2\alpha_2}(\mathbf{k}_2)+\xi_{m_2\alpha_2}^\dagger(-\mathbf{k}_2)\right)\left(\xi_{m_3\alpha_3}(\mathbf{k}_3)+\xi_{m_3\alpha_3}^\dagger(-\mathbf{k}_3)\right)\left(\xi_{m_1'\alpha_1'}(\mathbf{k}_1')+\xi_{m_1'\alpha_1'}^\dagger(-\mathbf{k}_1')\right) \\
&\left(\xi_{m_2'\alpha_2'}(\mathbf{k}_2')+\xi_{m_2'\alpha_2'}^\dagger(-\mathbf{k}_2')\right)\left(\xi_{m_3'\alpha_3'}(\mathbf{k}_3')+\xi_{m_3'\alpha_3'}^\dagger(-\mathbf{k}_3')\right)\rangle \quad.
\end{aligned}
$$

The sums are calculated by using the Wick theorem, taking into account only connected diagrams. In total, we have 36 non-vanishing contractions, which are the same , and the final result, expressed in terms of the Green's functions from equation (4.29), is:

$$
\begin{aligned}
&\mathord{\multimap}\!\!\mathord{\bigcirc}\!\!\mathord{\multimap}_{\alpha\alpha'}(\mathbf{l},\mathbf{l}';t,t') \\
&= \frac{(-\mathrm{i})^5}{N^2}\sum_{\mathbf{q}}\mathrm{e}^{\mathrm{i}\mathbf{q}(\mathbf{r}_l-\mathbf{r}_l')}\frac{\omega_d^4}{2a^6\omega_0^2}\sum_{\alpha_1...\alpha_3}\sum_{\alpha_1'...\alpha_3'}\sum_{\mathbf{k}}\int\mathrm{d}t_1\int\mathrm{d}t_2\int\frac{\mathrm{d}\Omega}{2\pi}\int\frac{\mathrm{d}\Omega'}{2\pi} \\
&\int\frac{\mathrm{d}\omega}{2\pi}\int\frac{\mathrm{d}\omega'}{2\pi}\mathrm{e}^{\mathrm{i}\Omega(t-t_1)}\mathrm{e}^{\mathrm{i}\Omega'(t'-t_2)}\mathrm{e}^{\mathrm{i}\omega(t_1-t_2)}\mathrm{e}^{\mathrm{i}\omega'(t_1-t_2)}\mathcal{F}_{\alpha_1\cdots\alpha_3}\mathcal{F}^*_{\alpha_1'\cdots\alpha_3'} \\
&\mathcal{D}^0_{\alpha\alpha_1}(\mathbf{q},\Omega)\mathcal{D}^0_{\alpha_2\alpha_2'}(\mathbf{k},\omega)\mathcal{D}^0_{\alpha_3\alpha_3'}(\mathbf{q}-\mathbf{k},\omega')\mathcal{D}^0_{\alpha'\alpha_1'}(\mathbf{q},\Omega') \quad, \qquad (\mathrm{B}.10)
\end{aligned}
$$

with

$$
\mathcal{F}_{\alpha_1\cdots\alpha_3} = -F_{\alpha_1...\alpha_3}(0)+F_{\alpha_1...\alpha_3}(\mathbf{q})+F_{\alpha_1...\alpha_3}(\mathbf{k})+F_{\alpha_1...\alpha_3}(\mathbf{q}-\mathbf{k}) \quad.
$$

After performing the Fourier transform in both, space and time variables, we obtain:

$$
\begin{aligned}
&\mathord{\multimap}\!\!\mathord{\bigcirc}\!\!\mathord{\multimap}_{\alpha\alpha'}(\mathbf{q};\Omega) = -\frac{\mathrm{i}}{N}\frac{\omega_d^4}{2a^6\omega_0^2}\sum_{\alpha_1...\alpha_3}\sum_{\alpha_1'...\alpha_3'}\sum_{\mathbf{k}}\int\frac{\mathrm{d}\omega}{2\pi}\mathcal{F}_{\alpha_1...\alpha_3}\mathcal{F}^*_{\alpha_1'...\alpha_3'} \\
&\mathcal{D}^0_{\alpha\alpha_1}(\mathbf{q},\Omega)\mathcal{D}^0_{\alpha_2\alpha_2'}(\mathbf{k},\omega)\mathcal{D}^0_{\alpha_3\alpha_3'}(\mathbf{q}-\mathbf{k},\Omega-\omega)\mathcal{D}^0_{\alpha'\alpha_1'}(\mathbf{q},-\Omega) \quad.
\end{aligned}
$$

The corresponding contribution to the self-energy is:

$$\Sigma^{(3)}_{\alpha_1\alpha'}(\mathbf{q},\Omega) = -\frac{\mathrm{i}}{N}\frac{\omega_d^4}{2\omega_0^2 a^6}\sum_{\alpha_2\alpha_3}\sum_{\alpha_2'\alpha_3'}\sum_{\mathbf{k}}\int\frac{\mathrm{d}\omega}{2\pi}\mathcal{D}^0_{\alpha_2\alpha_2'}(\mathbf{k},\omega)\mathcal{D}^0_{\alpha_3\alpha_3'}(\mathbf{q}-\mathbf{k},\Omega-\omega)$$
$$\mathcal{F}_{\alpha_1\ldots\alpha_3}\mathcal{F}^*_{\alpha_1'\ldots\alpha_3'}\quad.$$

With an explicit form of the zero order Green's function from equation (4.30), we can now perform the integration over ω. We have to consider three different cases:

$$\lim_{\delta\to 0}\int\frac{\mathrm{d}\omega}{2\pi}\frac{1}{(\omega+\omega_{m_1}(\mathbf{k})-\mathrm{i}\delta)(\omega-\omega_{m_1}(\mathbf{k})+\mathrm{i}\delta)}$$
$$\times\frac{1}{(\Omega-\omega+\omega_{m_2}(\mathbf{k})-\mathrm{i}\delta)(\Omega-\omega-\omega_{m_2}(\mathbf{k})+\mathrm{i}\delta)}$$
$$=-\frac{\mathrm{i}(\omega_{m_1}(\mathbf{k})+\omega_{m_2}(\mathbf{k}))}{2\omega_{m_1}(\mathbf{k})\omega_{m_2}(\mathbf{k})\left(\Omega^2-(\omega_{m_1}(\mathbf{k})\,i+\omega_{m_2}(\mathbf{k}))^2\right)}$$

$$\lim_{\delta\to 0}\int\frac{\mathrm{d}\omega}{2\pi}\frac{1}{(\omega+\omega_{m_1}(\mathbf{k})-\mathrm{i}\delta)(\omega-\omega_{m_1}(\mathbf{k})+\mathrm{i}\delta)}$$
$$\times\frac{\omega}{(\Omega-\omega+\omega_{m_2}(\mathbf{k})-\mathrm{i}\delta)(\Omega-\omega-\omega_{m_2}(\mathbf{k})+\mathrm{i}\delta)}$$
$$=-\frac{\mathrm{i}\Omega}{2\omega_{m_2}\left(\Omega^2-(\omega_{m_1}(\mathbf{k})+\omega_{m_2}(\mathbf{k}))^2\right)}$$

$$\lim_{\delta\to 0}\int\frac{\mathrm{d}\omega}{2\pi}\frac{\omega}{(\omega+\omega_{m_1}-\mathrm{i}\delta)(\omega-\omega_{m_1}i(\mathbf{k})+\mathrm{i}\delta)}$$
$$\times\frac{\omega}{(\Omega-\omega+\omega_{m_2}(\mathbf{k})-\mathrm{i}\delta)(\Omega-\omega-\omega_{m_2}(\mathbf{k})+\mathrm{i}\delta)}$$
$$=-\frac{\mathrm{i}\left(\Omega^2-\omega_{m_2}(\mathbf{k})^2-\omega_{m_1}(\mathbf{k})\omega_{m_2}(\mathbf{k})\right)}{2\omega_{m_2}(\mathbf{k})\left(\Omega^2-(\omega_{m_1}(\mathbf{k})+\omega_{m_2}(\mathbf{k}))^2\right)}$$

After combining all contributions, the considered contribution to the self-energy takes the form:

$$
\begin{aligned}
\Sigma^{(3)}_{\alpha\alpha'}(\mathbf{q},\Omega) \quad = \quad & -\frac{\omega_d^4}{4a^2 N}\sum_{\mathbf{k}}\sum_{m_1 m_2=\pm}\frac{\omega_{m_1}(\mathbf{k})\omega_{m_2}(\mathbf{q}-\mathbf{k})}{\left(\omega_{m_1}^4(\mathbf{k})-\omega_T^2(\mathbf{k})\omega_L^2(\mathbf{k})\right)}
\end{aligned}
$$

$$
\frac{1}{\left(\omega_{m_2}^4(\mathbf{q}-\mathbf{k})-\omega_T^2(\mathbf{q}-\mathbf{k})\omega_L^2(\mathbf{q}-\mathbf{k})\right)}\frac{1}{\left(\Omega^2-(\omega_{m_1}(\mathbf{k})+\omega_{m_2}(\mathbf{q}-\mathbf{k}))^2\right)}
$$

$$
\{(\omega_{m_1}(\mathbf{k})+\omega_{m_2}(\mathbf{q}-\mathbf{k}))
$$

$$
\left[\mathcal{F}_{\alpha xx}\mathcal{F}^*_{\alpha' xx}\left(e_T^2\omega_L^2+e_L^2\omega_T^2-\omega_{m_1}^2\right)|_{\mathbf{k}}\left(e_T^2\omega_L^2+e_L^2\omega_T^2-\omega_{m_2}^2\right)|_{\mathbf{q}-\mathbf{k}}\right.
$$

$$
+\mathcal{F}_{\alpha yy}\mathcal{F}^*_{\alpha' yy}\left(e_L^2\omega_L^2+e_T^2\omega_T^2-\omega_{m_1}^2\right)|_{\mathbf{k}}\left(e_L^2\omega_L^2+e_T^2\omega_T^2-\omega_{m_2}^2\right)|_{\mathbf{q}-\mathbf{k}}
$$

$$
+\mathcal{F}_{\alpha xy}\mathcal{F}^*_{\alpha' xy}\left(e_T^2\omega_L^2+e_L^2\omega_T^2-\omega_{m_1}^2\right)|_{\mathbf{k}}\left(e_L^2\omega_L^2+e_T^2\omega_T^2-\omega_{m_2}^2\right)|_{\mathbf{q}-\mathbf{k}}
$$

$$
+\mathcal{F}_{\alpha yx}\mathcal{F}^*_{\alpha' yx}\left(e_L^2\omega_L^2+e_T^2\omega_T^2-\omega_{m_1}^2\right)|_{\mathbf{k}}\left(e_T^2\omega_L^2+e_L^2\omega_T^2-\omega_{m_2}^2\right)|_{\mathbf{q}-\mathbf{k}}
$$

$$
+\left(e_T^2\omega_L^2+e_L^2\omega_T^2-\omega_{m_1}^2\right)|_{\mathbf{k}}\left(e_T e_L(\omega_L^2-\omega_T^2)\right)|_{\mathbf{q}-\mathbf{k}}\left(\mathcal{F}_{\alpha xy}\mathcal{F}^*_{\alpha' xx}+\mathcal{F}_{\alpha xx}\mathcal{F}^*_{\alpha' xy}\right)
$$

$$
+\left(e_L^2\omega_L^2+e_T^2\omega_T^2-\omega_{m_1}^2\right)|_{\mathbf{k}}\left(e_T e_L(\omega_L^2-\omega_T^2)\right)|_{\mathbf{q}-\mathbf{k}}\left(\mathcal{F}_{\alpha yx}\mathcal{F}^*_{\alpha' yy}+\mathcal{F}_{\alpha yy}\mathcal{F}^*_{\alpha' yx}\right)
$$

$$
+\left(e_T e_L(\omega_L^2-\omega_T^2)\right)|_{\mathbf{k}}\left(e_T^2\omega_L^2+e_L^2\omega_T^2-\omega_{m_2}^2\right)|_{\mathbf{q}-\mathbf{k}}\left(\mathcal{F}_{\alpha yx}\mathcal{F}^*_{\alpha' xx}+\mathcal{F}_{\alpha xx}\mathcal{F}^*_{\alpha' yx}\right)
$$

$$
+\left(e_T e_L(\omega_L^2-\omega_T^2)\right)|_{\mathbf{k}}\left(e_L^2\omega_L^2+e_T^2\omega_T^2-\omega_{m_2}^2\right)|_{\mathbf{q}-\mathbf{k}}\left(\mathcal{F}_{\alpha xy}\mathcal{F}^*_{\alpha' yy}+\mathcal{F}_{\alpha yy}\mathcal{F}^*_{\alpha' xy}\right)
$$

$$
+\left(e_T e_L(\omega_L^2-\omega_T^2)\right)|_{\mathbf{k}}\left(e_T e_L(\omega_L^2-\omega_T^2)\right)|_{\mathbf{q}-\mathbf{k}}
$$

$$
\left(\mathcal{F}_{\alpha yy}\mathcal{F}^*_{\alpha' xx}+\mathcal{F}_{\alpha xx}\mathcal{F}^*_{\alpha' yy}+\mathcal{F}_{\alpha yx}\mathcal{F}^*_{\alpha' xy}+\mathcal{F}_{\alpha xy}\mathcal{F}^*_{\alpha' yx}\right)
$$

$$
\left.-\omega_c^2\omega_{m_1}(\mathbf{k})\omega_{m_2}(\mathbf{q}-\mathbf{k})\left(\mathcal{F}_{\alpha yx}\mathcal{F}^*_{\alpha' xy}+\mathcal{F}_{\alpha xy}\mathcal{F}^*_{\alpha' yx}-\mathcal{F}_{\alpha yy}\mathcal{F}^*_{\alpha' xx}-\mathcal{F}_{\alpha xx}\mathcal{F}^*_{\alpha' yy}\right)\right]
$$

$$
+\mathrm{i}\omega_c\omega_{m_1}(\mathbf{k})\Omega
$$

$$
\left(\left(e_T^2\omega_L^2+e_L^2\omega_T^2-\omega_{m_1}^2\right)|_{\mathbf{k}}\left(\mathcal{F}_{\alpha xx}\mathcal{F}^*_{\alpha' xy}-\mathcal{F}_{\alpha xy}\mathcal{F}^*_{\alpha' xx}\right)\right.
$$

$$
+\left(e_L^2\omega_L^2+e_T^2\omega_T^2-\omega_{m_1}^2\right)|_{\mathbf{k}}\left(\mathcal{F}_{\alpha yx}\mathcal{F}^*_{\alpha' yy}-\mathcal{F}_{\alpha yy}\mathcal{F}^*_{\alpha' yx}\right)
$$

$$
+\left(e_T^2\omega_L^2+e_L^2\omega_T^2-\omega_{m_2}^2\right)|_{\mathbf{q}-\mathbf{k}}\left(\mathcal{F}_{\alpha xx}\mathcal{F}^*_{\alpha' yx}-\mathcal{F}_{\alpha yx}\mathcal{F}^*_{\alpha' xx}\right)
$$

$$
+\left(e_L^2\omega_L^2+e_T^2\omega_T^2-\omega_{m_2}^2\right)|_{\mathbf{q}-\mathbf{k}}\left(\mathcal{F}_{\alpha xy}\mathcal{F}^*_{\alpha' yy}-\mathcal{F}_{\alpha yy}\mathcal{F}^*_{\alpha' xy}\right)
$$

$$
+\left(e_T e_L(\omega_L^2-\omega_T^2)\right)|_{\mathbf{k}}\left(\mathcal{F}_{\alpha xx}\mathcal{F}^*_{\alpha' yy}-\mathcal{F}_{\alpha yy}\mathcal{F}^*_{\alpha' xx}+\mathcal{F}_{\alpha yx}\mathcal{F}^*_{\alpha' xy}-\mathcal{F}_{\alpha xy}\mathcal{F}^*_{\alpha' yx}\right)
$$

$$
\left.+\left(e_T e_L(\omega_L^2-\omega_T^2)\right)|_{\mathbf{q}-\mathbf{k}}\left(\mathcal{F}_{\alpha xx}\mathcal{F}^*_{\alpha' yy}-\mathcal{F}_{\alpha yy}\mathcal{F}^*_{\alpha' xx}+\mathcal{F}_{\alpha xy}\mathcal{F}^*_{\alpha' yx}-\mathcal{F}_{\alpha yx}\mathcal{F}^*_{\alpha' xy}\right)\right)\}.
$$

B.6 First order expansion of the H_4 term

The first order perturbation theory leads to:

$$
\begin{aligned}
&\bigcirc_{\alpha\alpha'}(l,l';t,t') \\
&= \frac{\omega_d^2 m}{4!a^2 N^6 \hbar} \sum_{\mathbf{q}\mathbf{q}'} \sum_{mm'} \sum_{\alpha_1...\alpha_4} \sum_{\mathbf{k}_1...\mathbf{k}_4} \sum_{m_1...m_4} \mathrm{e}^{\mathrm{i}\mathbf{q}\mathbf{r}_l} \mathrm{e}^{\mathrm{i}\mathbf{q}'\mathbf{r}'_l} \int \mathrm{dt}_1 \delta_{\mathbf{k}_1+\mathbf{k}_2+\mathbf{k}_3+\mathbf{k}_4,0} \\
&(F_{\beta_1...\beta_4}(0) - F_{\beta_1...\beta_4}(\mathbf{k}_1) - F_{\beta_1...\beta_4}(\mathbf{k}_2) - F_{\beta_1...\beta_4}(\mathbf{k}_3) \\
&- F_{\beta_1...\beta_4}(\mathbf{k}_4) + F_{\beta_1...\beta_4}(\mathbf{k}_1+\mathbf{k}_2) + F_{\beta_1...\beta_4}(\mathbf{k}_1+\mathbf{k}_3) + F_{\beta_1...\beta_4}(\mathbf{k}_1+\mathbf{k}_4)) \\
&\langle T \left(\xi_{m\alpha}(\mathbf{q}) + \xi^\dagger_{m\alpha}(-\mathbf{q}) \right) \left(\xi_{m'\alpha'}(\mathbf{q}') + \xi^\dagger_{m'\alpha'}(-\mathbf{q}') \right) \left(\xi_{m_1\alpha_1}(\mathbf{k}_1) + \xi^\dagger_{m_1\alpha_1}(-\mathbf{k}_1) \right) \\
&\left(\xi_{m_2\alpha_2}(\mathbf{k}_2) + \xi^\dagger_{m_2\alpha_2}(-\mathbf{k}_2) \right) \left(\xi_{m_3\alpha_3}(\mathbf{k}_3) + \xi^\dagger_{m_3\alpha_3}(-\mathbf{k}_3) \right) \left(\xi_{m_4\alpha_4}(\mathbf{k}_4) + \xi^\dagger_{m_4\alpha_4}(-\mathbf{k}_4) \right) \rangle
\end{aligned}
$$

Using Wicks theorem, we obtain 12 non-vanishing contractions. The number of all combinations for the contractions is 12. Taking the zero order Green's function in equation (4.29) into account, we obtain:

$$
\begin{aligned}
&\bigcirc_{\alpha\alpha'}(l,l';t,t') \\
&= (-\mathrm{i})^3 \frac{\omega_d^2}{2\omega_0 a^4 N^2} \sum_{\mathbf{q}} \mathrm{e}^{\mathrm{i}\mathbf{q}(\mathbf{r}_l - \mathbf{r}'_l)} \sum_{\alpha_1...\alpha_4} \sum_{\mathbf{k}} \int \mathrm{dt}_1 \int \frac{\mathrm{d}\Omega}{2\pi} \int \frac{\mathrm{d}\Omega'}{2\pi} \int \frac{\mathrm{d}\omega}{2\pi} \\
&\mathrm{e}^{\mathrm{i}\Omega(t-t_1)} \mathrm{e}^{\mathrm{i}\Omega'(t_1-t')} \mathrm{e}^{\mathrm{i}\omega 0} \mathcal{F}_{\alpha_1\cdots\alpha_4} \mathcal{D}^0_{\alpha\alpha_1}(\mathbf{q},\Omega) \mathcal{D}^0_{\alpha_2\alpha_3}(\mathbf{k},\omega) \mathcal{D}^0_{\alpha'\alpha_4}(\mathbf{q},\Omega') \quad,
\end{aligned}
$$

with

$$
\begin{aligned}
\mathcal{F}_{\alpha_1\cdots\alpha_4} =\ & 2F_{\alpha_1...\alpha_4}(0) - 2F_{\alpha_1...\alpha_4}(\mathbf{q}) - 2F_{\alpha_1...\alpha_4}(\mathbf{k}) \\
& + F_{\alpha_1...\alpha_4}(\mathbf{q}-\mathbf{k}) + F_{\alpha_1...\alpha_4}(\mathbf{q}+\mathbf{k}) \quad.
\end{aligned}
$$

Here we use $\mathcal{F}_{\alpha_1\cdots\alpha_4}(\mathbf{k}) = \mathcal{F}_{\alpha_1\cdots\alpha_4}(-\mathbf{k})$.
The Fourier transform with respect to space and time variables leads us to:

$$
\begin{aligned}
\bigcirc_{\alpha\alpha'}(\mathbf{q};\Omega) =\ & \mathrm{i}\frac{\omega_d^2}{2\omega_0 a^4 N} \sum_{\alpha_1...\alpha_4} \sum_{\mathbf{k}} \int \frac{\mathrm{d}\omega}{2\pi} \mathcal{F}_{\alpha_1\cdots\alpha_4} \mathcal{D}^0_{\alpha\alpha_1}(\mathbf{q},\Omega) \\
& \mathcal{D}^0_{\alpha_2\alpha_3}(\mathbf{k},\omega) \mathcal{D}^0_{\alpha'\alpha'_4}(\mathbf{q},\Omega) \quad.
\end{aligned}
$$

We calculate the negative corresponding self-energy contribution:

$$
-\Sigma^{(4)}_{\alpha\alpha'}(\mathbf{q},\Omega) = \mathrm{i}\frac{\omega_d^2}{2\omega_0 a^4 N} \sum_{\alpha_2\alpha_3} \sum_{\mathbf{k}} \int \frac{\mathrm{d}\omega}{2\pi} \mathcal{D}^0_{\alpha_2\alpha_3}(\mathbf{k},\omega) \mathcal{F}_{\alpha\alpha_2\alpha_3\alpha'} \quad.
$$

Using the explicit expression in equation (4.30) we integrate over ω. The possible integrations are:

$$
\lim_{\delta \to 0} \int \frac{d\omega}{2\pi} \frac{1}{(\omega - \omega_m + i\delta)(\omega + \omega_m - i\delta)}
$$
$$
= -\frac{i}{2\omega_m}
$$
$$
\lim_{\delta \to 0} \int \frac{d\omega}{2\pi} \frac{\omega}{(\omega - \omega_m + i\delta)(\omega + \omega_m - i\delta)}
$$
$$
= 0
$$

Finely we get:

$$
\Sigma_{\alpha\alpha'}^{(4)} = -\frac{\omega_d^2}{4a^2 N} \sum_k \sum_m \frac{\omega_m}{\omega_m^4 - \omega_T^2 \omega_L^2} \left(\mathcal{F}_{\alpha x x \alpha'} \left(\omega_T^2 e_L^2 + \omega_L^2 e_T^2 - \omega_m^2 \right) \right.
$$
$$
\left. + \mathcal{F}_{\alpha y y \alpha'} \left(\omega_T^2 e_T^2 + \omega_L^2 e_L^2 - \omega_m^2 \right) + \left(\mathcal{F}_{\alpha x y \alpha'} + \mathcal{F}_{\alpha y x \alpha'} \right) e_T e_L \left(\omega_L^2 - \omega_T^2 \right) \right) \quad .
$$

B.7   Computation of γ

The modified melting parameter [148, 149, 150] is defined as $\gamma = \langle (\mathbf{u}(\mathbf{l}_1) - \mathbf{u}(0))^2 \rangle / a^2$. Using the Green's functions in equation (4.29), we can express the γ in the following form:

$$
\gamma = -i\frac{2}{a^2} \left(\mathcal{D}_{xx}(\mathbf{r} = 0, t = 0) + \mathcal{D}_{yy}(\mathbf{r} = 0, t = 0) \right.
$$
$$
\left. - \mathcal{D}_{xx}(\mathbf{r} = \mathbf{r}_1, t = 0) - \mathcal{D}_{yy}(\mathbf{r} = \mathbf{r}_1, t = 0) \right)
$$
$$
= -i\frac{2}{a^2} \int_{-\infty}^{\infty} \frac{d\omega}{2\pi} \sum_{\mathbf{k}} \left(1 - \cos \mathbf{k} \mathbf{r}_1 \right) \left(\mathcal{D}_{xx}(\mathbf{k}, \omega) + \mathcal{D}_{yy}(\mathbf{k}, \omega) \right) \quad ,
$$

where $\mathcal{D}(\mathbf{k}, \omega) = \mathcal{D}(-\mathbf{k}, \omega)$ is used. This holds, because all $\omega_{-,+,T,L}(\mathbf{k})$ are even in $\mathbf{k}$. The expression for the Green's function is:

$$
\mathcal{D}_{\alpha\alpha}(\mathbf{k}, \omega) = \omega_0 a^2 \left[\sum_{m=\pm} A_0 \hat{\mathcal{M}}_{0,\alpha\alpha} \frac{\omega_{0,m}^2(\mathbf{k}) \left(\omega_{0,L}^2(\mathbf{k}) - \omega_{0,m}^2(\mathbf{k}) \right)}{\left(\omega_{0,m}^4(\mathbf{k}) - \omega_{0,T}^2(\mathbf{k}) \omega_{0,L}^2(\mathbf{k}) \right) \left(\omega^2 - \omega_{0,m}^2(\mathbf{k}) \right)} \right.
$$
$$
\left. + A_1 \hat{\mathcal{M}}_{1,\alpha\alpha} \frac{\omega_{1,m}^2(\mathbf{k}) \left(\omega_{1,T}^2(\mathbf{k}) - \omega_{1,m}^2(\mathbf{k}) \right)}{\left(\omega_{1,m}^4(\mathbf{k}) - \omega_{1,T}^2(\mathbf{k}) \omega_{1,L}^2(\mathbf{k}) \right) \left(\omega^2 - \omega_{1,m}^2(\mathbf{k}) \right)} \right] \quad ,
$$

and together with:

$$\omega_{m=\pm}^2(\mathbf{k}) = \frac{1}{2}\left(\omega_T^2(\mathbf{k}) + \omega_L^2(\mathbf{k}) + \omega_c^2\right)$$
$$\pm\sqrt{\frac{1}{4}\left(\omega_T^2(\mathbf{k}) + \omega_L^2(\mathbf{k}) + \omega_c^2\right)^2 - \omega_T^2(\mathbf{k})\omega_L^2(\mathbf{k})} \quad,$$

where $\omega_0 = 2\hbar/(a^2 m)$, the exact formula for γ reads:

$$\begin{aligned}
\gamma &= \frac{\omega_0}{N}\sum_{\mathbf{k}}\left(\cos\mathbf{k}\mathbf{r}_1 - 1\right)\\
&\quad\left[A_0\frac{\omega_{0,+}(\mathbf{k})\left(\omega_{0,L}^2(\mathbf{k}) - \omega_{0,-}^2(\mathbf{k})\right) - \omega_{0,-}(\mathbf{k})\left(\omega_{0,L}^2(\mathbf{k}) - \omega_{0,+}^2(\mathbf{k})\right)}{\omega_{0,+}(\mathbf{k})\omega_{0,-}(\mathbf{k})\left(\omega_{0,-}^2(\mathbf{k}) - \omega_{0,+}^2(\mathbf{k})\right)}\right.\\
&\quad\left.+ A_1\frac{\omega_{1,+}(\mathbf{k})\left(\omega_{1,T}^2(\mathbf{k}) - \omega_{1,-}^2(\mathbf{k})\right) - \omega_{1,-}(\mathbf{k})\left(\omega_{1,T}^2(\mathbf{k}) - \omega_{1,+}^2(\mathbf{k})\right)}{\omega_{1,+}(\mathbf{k})\omega_{1,-}(\mathbf{k})\left(\omega_{1,-}^2(\mathbf{k}) - \omega_{1,+}^2(\mathbf{k})\right)}\right]\\
&= \frac{\omega_0}{N}\sum_{\mathbf{k}}\left(1 - \cos\mathbf{k}\mathbf{r}_1\right)\left[A_0\frac{\omega_{0,T}(\mathbf{k}) + \omega_{0,L}(\mathbf{k})}{\omega_{0,T}(\mathbf{k})\left(\omega_{0,-}(\mathbf{k}) + \omega_{0,+}(\mathbf{k})\right)}\right.\\
&\quad\left.+ A_1\frac{\omega_{1,T}(\mathbf{k}) + \omega_{1,L}(\mathbf{k})}{\omega_{1,L}(\mathbf{k})\left(\omega_{1,-}(\mathbf{k}) + \omega_{1,+}(\mathbf{k})\right)}\right],
\end{aligned}$$

(B.11)

where we use the relation $\omega_-^2(\mathbf{k})\omega_+^2(\mathbf{k}) = \omega_T^2(\mathbf{k})\omega_L^2(\mathbf{k})$.

Bibliography

[1] http://www.caam.rice.edu/software/ARPACK/.

[2] J. R. Abo-Shaeer, C. Raman, J. M. Vogels, and W. Ketterle, *Observation of Vortex Lattices in Bose-Einstein Condensates,* Science **292** (2001) 476.

[3] A. A. Abrikosov, L. P. Gor'kov, and I. Y. Dzyanloshinski, *Quantum Field Theoretical Methods in Statistical Physics,* Pergamon Press, Oxford, 1965.

[4] I. Affleck, T. Kennedy, E. H. Lieb, and H. Tasaki, *Valence Bond Ground-States in Isotropic Quantum Antiferromagnets,* Comm. Math. Phys. **115** (1988) 477.

[5] V. Ahufingers, L. Sanchez-Palencis, A. Kantian, A. Sanpera, and M. Lewenstein, *Disordered ultracold atomic gases in optical lattices: A case study of Fermi-Bose mixtures,* cond-mat/0508042.

[6] A. Albus, S. A. Gardiner, F. Illuminati, and M. Wilkens, *Quantum field theory of dilute homogeneous Bose-Fermi mixtures at zero temperature: General formalism and beyond mean-field corrections,* Phys. Rev. A **65** (2002) 053607.

[7] A. Albus, F. Illuminati, and J. Eisert, *Ground-state properties of trapped Bose-Fermi mixtures: Role of exchange correlation,* Phys. Rev. A **67** (2003) 063606.

[8] A. Albus, F. Illuminati, and J. Eisert, *Mixtures of bosonic and fermionic atoms in optical lattices,* Phys. Rev. A **68** (2003) 023606.

[9] E. Altman, E. Demler, and M. D. Lukin, *Probing many-body states of ultracold atoms via noise correlations,* Phys. Rev. A **70** (2004) 013603.

[10] M. H. Anderson, J. R. Ensher, M. R. Matthews, C. E. Wieman, and E. A. Cornell, *Observation of Bose-Einstein condensation in a dilute atomic vapor,* Science **269** (1995) 198.

[11] P. W. Anderson, *Absence of Diffusion in Certain Random Lattices,* Phys. Rev. **109** (1958) 1492.

[12] P. W. Anderson, *Resonating Valence Bonds - New Kind of Insulator,* Mater. Res. Bull. **8** (1973) 153.

[13] N. W. Ashcroft and D. N. Mermin, *Solid State Physics,* Holt , Rinhaut and Winston, Phyladelphia, 1976.

[14] A. Auerbach, *Interacting Electrons and Quantum Magnetism,* Springer, New York, 1994.

[15] M. Baranov, K. Osterloh, and M. Lewenstein, *Fractional quantum hall states in ultracold rapidly rotating dipolar fermi gases,* Phys. Rev. Lett. **94** (2005) 070404.

[16] M. Baranov, L. Dobrek, K. Goral, L. Santos, and M. Lewenstein, *Ultracold dipolar gases - a challenge for experiments and theory,* Physica Scripta T **102** (2002) 74.

[17] M. Bartenstein, A. Altmeyer, S. Riedl, R. Geursen, S. Jochim, C. Chin, J. H. Denschlag, R. Grimm, A. Simoni, E. Tiesinga, C. J. Williams, and P. S. Julienne, *Precise Determination of ^6Li Cold Collision Parameters by Radio-Frequency Spectroscopy on Weakly Bound Molecules,* Phys. Rev. Lett. **94** (2005) 103201.

[18] M. Bartenstein, A. Altmeyer, S. Riedl, S. Jochim, R. Geursen, C. Chin, J. H. Denschlag, and R. Grimm, *Exploring the BEC-BCS Crossover with an Ultracold Gas of ^6Li Atoms,* cond-mat/0412712.

[19] G. G. Batrouni, V. Rousseau, R. T. Scalettar, M. Rigol, A. Muramatsu, P. J. H. Denteneer, and M. Troyer, *Mott Domains of Bosons Confined on Optical Lattices,* Phys. Rev. Lett. **89** (2002) 117203.

[20] B. Bernu, P. Lecheminant, C. Lhuillier, and L. Pierre, *Exact spectra, spin susceptibilities, and order parameter of the quantum Heisenberg antiferromagnet on the triangular lattice,* Phys. Rev. B **50** (1994) 10048.

[21] B. Bernu, C. Lhuillier, and L. Pierre, *Signature of Néel order in exact spectra of quantum antiferromagnets on finite lattices,* Phys. Rev. Lett. **69** (1992) 2590.

[22] H. Bethe, *Zur Theorie der Metalle. Eigenwerte und Eigenfunktionen der linearen Atomkette.,* Z. Phys. **71** (1931) 205.

[23] H. L. Bethlem, G. Berden, F. M. H. Crompvoets, R. T. Jongma, A. van Roij, and G. Meijer, *Electrostatic trapping of ammonia molecules,* Nature **406** (2000) 491.

[24] D. D. Betts, J. Schulenburg, G. E. Stewart, J. Richter, and J. S. Flynn, *Exact diagonalization of the $S = 1/2$ Heisenberg antiferromagnet on*

finite bcc lattices to estimate properties on the infinite lattice, J. Phys. A: Math. Gen. **31** (1998) 7685.

[25] K. Binder and D. W. Heermann, *Monte Carlo Simulation in Statistical Physics,* Springer Series in Solid-State Science, 1988.

[26] J.-P. Blaizot and G. Ripka, *Quantum Theory of Finite Systems,* MIT Press, Cambridge, 1986.

[27] I. Bloch. privat communication.

[28] E. L. Bolda and D. F. Walls, *Detection of Vorticity in Bose-Einstein Condensed Gases by Matter-Wave Interference,* Phys. Rev. Lett. **81** (1998) 5477.

[29] L. Bonsall, *Some static and dynamical properties of a two-dimensional Wigner crystal,* Phys. Rev. B **15** (1977) 1959.

[30] S. N. Bose, *Plancks Gesetz und Lichtquantenhypothese,* Z. Phys. **26** (1924) 178.

[31] H. Böttger, *Principles of the Theory of Lattice Dynamics,* Physik-Verl., Weinheim, 1983.

[32] C. C. Bradley, C. A. Sackett, J. J. Tollett, and R. G. Hulet, *Evidence of Bose-Einstein Condensation in an Atomic Gas with Attractive Interactions,* Phys. Rev. Lett. **75** (1995) 1687.

[33] V. Bretin, S. Stock, Y. Seurin, and J. Dalibard, *Fast Rotation of a Bose-Einstein Condensate,* Phys. Rev. Lett. **92** (2004) 050403.

[34] R. H. Brown and R. Q. Twiss, *Correlation between photons in two coherent beams of light,* Natur **117** (1956) 27.

[35] H. P. Büchler and G. Blatter, *Supersolid versus Phase Separation in Atomic Bose-Fermi Mixtures,* Phys. Rev. Lett. **91** (2003) 130404.

[36] P. Buonsante, V. Penna, and A. Vezzani, *Analytical mean-field approach to the phase diagram of ultracold bosons in optical superlattices,* Phys. Rev. A **70** (2004) 061603.

[37] P. Buonsante, V. Penna, and A. Vezzani, *Analytical mean-field approach to the phase diagram of ultracold bosons in optical superlattices,* Laser Physics **15(2)** (2005) 361.

[38] P. Buonsante and A. Vezzani, *Cell strong-coupling perturbative approach to the phase diagram of ultracold bosons in optical superlattices,* Phys. Rev. A **72** (2005) 013614.

[39] S. Burger, K. Bongs, S. Dettmer, W. Ertmer, K. Sengstock, A. Sanpera, G. V. Shlyapnikov, and M. Lewenstein, *Dark Solitons in Bose-Einstein Condensates,* Phys. Rev. Lett. **83** (1999) 5198.

[40] S. Burger, S. L. Cataliotti, C. Fort, P. Maddaloni, F. Minardi, and M. Inguscio, *Evidence of quasi 2D Bose-Einstein condensation in an optical lattice.,* Europhys. Lett. **57** (2002) 1.

[41] D. C. Cabra, H.-U. Everts, A. Honecker, P. Pujol, and F. Stauffer. privat communication.

[42] P. Capuzzi and E. S. Hernández, *Zero-sound density oscillations in Fermi-Bose mixtures,* Phys. Rev. A **64** (2001) 043607.

[43] P. Carruthers and M. M. Nieto, *Phase and Angle Variables in Quantum Mechanics,* Rev. Mod. Phys. **40** (1986) 411.

[44] M. A. Cazalilla and A. F. Ho, *Instabilities in Binary Mixtures of One-Dimensional Quantum Degenerate Gases,* Phys. Rev. Lett. **91** (2003) 150403.

[45] F. Chevy, K. W. Madison, V. Bretin, and J. Dalibard, *Interferometric detection of a single vortex in a dilute Bose-Einstein condensate,* Phys. Rev. A **64** (2001) 031601(R).

[46] C. Chin, M. Bartenstein, A. Altmeyer, S. Riedl, S. Jochim, J. H. Denschlag, , and R. Grimm, *Observation of the pairing gap in a strongly interacting Fermi gas,* Science **305** (2004) 1128.

[47] S. Chu, L. Hollberg, J. E. Bjorkholm, A. Cable, and A. Ashkin, *Three-dimensional viscous confinement and cooling of atoms by resonance radiation pressure,* Phys. Rev. Lett. **55** (1985) 48.

[48] J. I. Cirac and P. Zoller, *New frontiers in quantum information with atoms and ions,* Physics Today **57** (2004) 38.

[49] S. R. Clark and D. Jaksch, *Dynamics of the superfluid to Mott-insulator transition in one dimension,* Phys. Rev. A **70** (2004) 043612.

[50] E. A. Cornell. privat communications.

[51] S. L. Cornish, N. R. Claussen, J. L. Roberts, E. A. Cornell, and C. E. Wieman, *Stable ^{85}Rb Bose-Einstein Condensates with Widely Tunable Interactions,* Phys. Rev. Lett. **85** (2000) 1795.

[52] M. Cramer, J. Eisert, and F. Illuminati, *Inhomogeneous atomic Bose-Fermi mixtures in cubic lattices,* Phys. Rev. Lett. **93** (2004) 190405.

[53] M. Cramer, J. Eisert, M. B. Plenio, and J. Dreißig, *Entanglement-area law for general bosonic harmonic lattice systems,* Phys. Rev. A **73** (2006) 012309.

[54] G. F. Dale, T. C. Killian, W. Willmann, L. Landhuis, S. C. Moss, D. Kleppner, and T. J. Greytak, *Bose-Einstein Condensation of Atomic Hydrogen,* Phys. Rev. Lett. **81** (1998) 3811.

[55] A. J. Daley, P. O. Fedichev, and P. Zoller, *Single-atom cooling by superfluid immersion: A nondestructive method for qubits,* Phys. Rev. A **69** (2004) 022306.

[56] A. J. Daley, C. Kollath, U. Schollwöck, and G. Vidal, *Time-dependent density-matrix renormalization-group using adaptive effective Hilbert spaces,* Journal of Statistical Mechanics: Theory and Experiment.(2004) Art. No. P04005 APR.

[57] J. Dalibard and C. Cohen-Tannoudji, *Laser cooling below the Doppler limit by polarization gradients: simple theoretical models,* J.O.S.A. B **6** (1989) 2023.

[58] B. Damski. privat communication; The nummerics is done by B. Damski.

[59] B. Damski, H.-U. Everts, A. Honecker, H. Fehrmann, L. Santos, and M. Lewenstein, *Atomic Fermi Gas in the Trimerized Kagomé Lattice at 2/3 Filling,* Phys. Rev. Lett. **95** (2005) 060403.

[60] B. Damski, L. Santos, E. Tiemann, M. Lewenstein, S. Kotochigova, P. Julienne, and P. Zoller, *Creation of a dipolar superfluid in optical lattices,* Phys. Rev. Lett. **90** (2003) 110401.

[61] B. Damski, J. Zakrzewski, L. Santos, P. Zoller, and M. Lewenstein, *Atomic Bose and Anderson Glasses in Optical Lattices,* Phys. Rev. Lett. **91** (2003) 080403.

[62] K. K. Das, *Bose-Fermi Mixtures in One Dimension,* Phys. Rev. Lett. **90** (2003) 170403.

[63] K. B. Davis, M.-O. Mewes, M. R. Andrews, N. J. van Druten, D. S. Durfee, D. M. Kurn, and W. Ketterle, *Bose-Einstein Condensation in a Gas of Sodium Atoms,* Phys. Rev. Lett. **75** (1995) 3969.

[64] K. B. Davis, M.-O. Mewes, M. A. Joffe, M. R. Andrews, and W. Ketterle, *Evaporative Cooling of Sodium Atoms,* Phys. Rev. Lett. **74** (1995) 5202.

[65] P. G. de Gennes, *Superconductivity of Metals and Alloys,* W. A. Benjamin, 1966.

[66] R. B. Diener, G. A. Georgakis, J. Zhong, M. Raizen, and Q. Niu, *Transition between extended and localized states in a one-dimensional incommensurate optical lattice,* Phys. Rev. A **64** (2001) 033416.

[67] E. A. Donley, N. R. Claussen, S. T. Thompson, and C. E. Wieman, *Atom-molecule coherence in a Bose-Einstein condensate,* Nature **417** (2002) 529.

[68] U. Dorner, P. Fedichev, D. Jaksch, M. Lewenstein, and P. Zoller, *Entangling strings of neutral atom in 1D atomic pipeline structures,* Phys. Rev. Lett. **91** (2003) 073601.

[69] P. G. Drazin and R. S. Johnson, *Solitons: an introduction,* Cambridge University Press, 1989.

[70] L.-M. Duan, E. Demler, and M. D. Lukin, *Controlling Spin Exchange Interactions of Ultracold Atoms in Optical Lattices,* Phys. Rev. Lett. **91** (2003) 090402.

[71] W. Dür, L. Hartmann, M. Hein, M. Lewenstein, and H.-J. Briegel, *Entanglement in Spin Chains and Lattices with Long-Range Ising-Type Interactions,* Phys. Rev. Lett. **94** (2005) 097203.

[72] W. Dür, G. Vidal, and J. I. Cirac, *Three qubits can be entangled in two inequivalent ways,* Phys. Rev. A **62** (2000) 062314.

[73] A. Einstein, *Quantentheorie des einatomigen idealen Gases,* Sitzungsbericht Kgl. Preuss. Akad. Wiss. 1924(1924) 261. ibid 1925, 3 (1925).

[74] D. Eliezer and G. W. Semenoff, *Intersection Forms and the Geometry of Lattice Chern-Simons Theory,* Phys. Lett. B **286** (1992) 118.

[75] F. H. L. Essler, H. Frahm, F. Göhmann, A. Klümper, and V. E. Korepin, *The One-Dimensional Hubbard Model,* Cambridge University Press, 2005.

[76] H. U. Everts. privat communication.

[77] P. O. Fedichev, Y. Kagan, G. V. Shlyapnikov, and J. T. M. Walraven, *Influence of Nearly Resonant Light on the Scattering Length in Low-Temperature Atomic Gases,* Phys. Rev. Lett. **77** (1996) 2913.

[78] H. Fehrmann, M. A. Baranov, B. Damski, M. Lewenstein, and L. Santos, *Mean-field theory of Bose-Fermi mixtures in optical lattices,* Opt. Comm. **243** (2004) 23.

[79] R. P. Feynman, *Quantum-Mechanical Computers,* Foundations of Physics **16** (1986) 507.

[80] M. P. A. Fisher, P. B. Weichman, G. Grinstein, and D. S. Fisher, *Boson localization and the superfluid-insulator transition,* Phys. Rev. B **40** (1989) 546.

[81] B. P. Flannery, W. H. Press, S. A. Teukolsky, and W. T. Vetterling, *Numerical Recipes, The Art of Scientific Computing,* Cambridge University Press, 1987.

[82] V. Fock, *Näherungsmethode zur Lösung des quantenmechanischen Mehrkörperproblems,* Zeits. f. Physik **61** (1930) 126.

[83] M. M. Fogler, A. A. Koulakov, and B. I. Shklovskii, *Ground state of a two-dimensional electron liquid in a weak magnetic field,* Phys. Rev. B **54** (1996) 1853.

[84] S. Fölling, F. Gerbier, A. Widera, O. Mandel, T. Gericke, and I. Bloch, *Spatial quantum noise interferometry in expanding ultracold atom clouds,* Nature **434** (2005) 481.

[85] E. Fradkin, *Jordan-Wigner transformation for quantum-spin systems in two dimensions and fractional statistics,* Phys. Rev. Lett. **63** (1989) 322.

[86] J. K. Freericks and H. Monien, *Strong-coupling expansions for the pure and disordered Bose-Hubbard model,* Phys. Rev. B **53** (1996) 2691.

[87] H. Fukuyama, *Two dimensional wigner crystallization caused by magnetic field,* Solid State Com. **19** (1976) 551.

[88] H. Fukuyama and Y. Nagaoka, *Anderson Localization,* Springer Series in Solid State Sciences, 1982.

[89] J. J. Garca-Ripoll and J. I. Cirac, *Quantum computation with cold bosonic atoms in an optical lattice,* Phil. Trans. R. Soc. Lond. A **361** (2003) 1537.

[90] J. J. Garca-Ripoll, M. A. Martin-Delgado, and J. I. Cirac, *Implementation of spin Hamiltonians in optical lattices,* Phys. Rev. Lett. **93** (2004) 250405.

[91] U. Gavish and Y. Castin, *Matter-Wave Localization in Disordered Cold Atom Lattices,* Phys. Rev. Lett. **95** (2005) 020401.

[92] A. Georges, G. Kotliar, and W. Krauth, *Dynamical mean-field theory of strongly correlated fermion systems and the limit of infinite dimensions,* Rev. Mod. Phys. **68** (1996) 13.

[93] T. Gianmarchi, *Quantum Physics in One Dimension,* Oxford University Press, Oxford, 2004.

[94] S. M. Girvin, *Anomalous quantum Hall effect and two-dimensional classical plasmas: Analytic approximations for correlation functions and ground-state energies,* Phys. Rev. B **30** (1984) 558.

[95] M. O. Goerbig, P. Lederer, and C. M. Smith, *Competition between quantum-liquid and electron-solid phases in intermediate Landau levels,* Phys. Rev. B **69** (2004) 115327.

[96] A. O. Gogolin, A. A. Nersesyan, and A. M. Tsvelik, *Bosonization and Strongly Correlated Systems,* Cambridge University Press, Cambridge, 1998.

[97] K. Góral, L. Santos, and M. Lewenstein, *Quantum Phases of Dipolar Bosons in Optical Lattices,* Phys. Rev. Lett. **88** (2002) 170406. For a general review see [16].

[98] A. Görlitz, J. M. Vogels, A. E. Leanhardt, C. Raman, T. L. Gustavson, J. R. Abo-Shaeer, A. P. Chikkatur, S. Gupta, S. Inouye, T. Rosenband, and W. Ketterle, *Realization of Bose-Einstein Condensates in Lower Dimension,* Phys. Rev. Lett. **87** (2001) 130402.

[99] M. Greiner, I. Bloch, O. Mandel, T. W. Hänsch, and T. Esslinger, *Exploring Phase Coherence in a 2D Lattice of Bose-Einstein Condensates,* Phys. Rev. Lett. **87** (2001) 160405.

[100] M. Greiner, O. Mandel, T. Esslinger, T. W. Hänsch, and I. Bloch, *Quantum phase transition from a superfluid to a Mott insulator in a gas of ultracold atoms,* Nature **415** (2002) 39.

[101] M. Greiner, O. Mandel, T. W. Hänsch, and I. Bloch, *Collapse and revival of the matter wave field of a Bose-Einstein condensate,* Nature **419** (2002) 51.

[102] M. Greiner, C. A. Regal, and D. S. Jin, *Emergence of a molecular Bose-Einstein condensate from a Fermi gas,* Nature **426** (2003) 537.

[103] M. Greiner, C. A. Regal, and D. S. Jin, *Probing the Excitation Spectrum of a Fermi Gas in the BCS-BEC Crossover Regime,* Phys. Rev. Lett. **94** (2005) 070403.

[104] A. Griesmaier, J. Werner, S. Hensler, J. Stuhler, and T. Pfau, *Bose-Einstein condensation of Chromium,* Phys. Rev. Lett. **94** (2005) 160401.

[105] G. Grynberg, B. Lounis, P. Verkerk, J.-Y. Courtois, and C. Salomon, *Quantized motion of cold cesium atoms in two- and three-dimensional optical potentials,* Phys. Rev. Lett. **70** (1993) 2249.

[106] L. Guidoni and P. Verkerk, *Direct observation of atomic localization in optical superlattices,* Phys. Rev. A **57** (1998) R1501.

[107] K. Günter, T. Stöferle, H. Moritz, M. Köhl, and T. Esslinger, *Bose-Fermi Mixtures in a Three-dimensional Optical Lattice,* cond-mat/0604139.

[108] Z. Hadzibabic, S. Gupta, C. A. Stan, C. H. Schunck, M. W. Zwierlein, K. Dieckmann, and W. Ketterle, *Fiftyfold Improvement in the Number of Quantum Degenerate Fermionic Atoms,* Phys. Rev. Lett. **91** (2003) 160401.

[109] Z. Hadzibabic, C. A. Stan, K. Dieckmann, S. Gupta, M. W. Zwierlein, A. Görlitz, and W. Ketterle, *Two-Species Mixture of Quantum Degenerate Bose and Fermi Gases,* Phys. Rev. Lett. **88** (2002) 160401.

[110] W. Hänsel, J. Reichel, P. Hommelhoff, and T. W. Hänsch, *Bose-Einstein condensation on a microelectronic chip,* Nature **413** (2001) 498.

[111] D. R. Hartree, *The wave mechanics of an atom with a non-coulomb central field.,* Proc. Camb. Phil. Soc. **24** (1928) 89.

[112] D. Hellweg, L. Cacciapuoti, M. Kottke, T. Schulte, K. Sengstock, W. Ertmer, and J. Arlt, *Measurement of Spatial Correlation Function of Phase Fluctuating Bose-Einstein Condensates,* Phys. Rev. Lett. **91** (2003) 010406.

[113] H. F. Hess, *Evaporative cooling of magnetically trapped and compressed spin-polarized hydrogen,* Phys. Rev. B **34** (1986) 3476.

[114] K. Hida, *Ground state and elementary excitations of the S=1 kagome Heisenberg antiferromagnet,* J. Phys. Soc. of Japan **69** (2000) 4003.

[115] W. Hofstetter, J. I. Cirac, P. Zoller, E. Demler, and M. D. Lukin, *High-temperature superfluidity of fermionic atoms in optical lattices,* Phys. Rev. Lett. **89** (2002) 220407.

[116] L. Huerta and J. Zanelli, *Bose-Fermi transformation in three-dimensional space,* Phys. Rev. Lett. **71** (1993) 3622.

[117] A. Hutton and S. Bose, *Mediated entanglement and correlations in a star network of interacting spin,* Phys. Rev. A **69** (2004) 042312.

[118] M. V. Isakov, S. Wessel, R. G. Melko, K. Sengupta, and Y. B. Kim, *Valence Bond Solids and Unconventional Quantum Criticality in Hard-Core Bosons in the Kagomé Lattice,* cond-mat/0602430.

[119] D. Jaksch, H.-J. Briegel, J. I. Cirac, C. W. Gardiner, and P. Zoller, *Entanglement of atoms via cold controlled collisions,* Phys. Rev. Lett. **82** (1999) 1975.

[120] D. Jaksch, C. Bruder, J. I. Cirac, C. W. Gardiner, and P. Zoller, *Cold Bosonic Atoms in Optical Lattices,* Phys. Rev. Lett. **81** (1998) 3108.

[121] D. Jaksch and P. Zoller, *Creation of effective magnetic fields in optical lattices: the Hofstadter butterfly for cold neutral atoms,* New J. Phys. **5** (2003) 56.

[122] D. Jaksch and P. Zoller, *The cold atom Hubbard toolbox,* Annals of Physics **315** (2005) 52.

[123] W. Jastrzebski, P. Kortyka, P. Kowalczyk, O. Docenko, M. Tamanis, R. Ferber, A. Pashov, H. Knöckel, and E. Tiemann, *Accurate characterisation of the $C(3)^1\Sigma^+$ state of the NaRb molecule,* EPJD, published Online: 19 July 2005 http://dx.doi.org/10.1140/epjd/e2005-00186-5.

[124] H. W. Jiang, R. L. Willett, H. L. Stormer, D. C. Tsui, L. N. Pfeiffer, and K. W. West, *Quantum liquid versus electron solid around $\nu = 1/5$ Landau-level filling,* Phys. Rev. Lett. **65** (1990) 633.

[125] S. Jochim, M. Bartenstein, A. Altmeyer, G. Hendl, S. Riedl, C. Chin, J. H. Denschlag, and R. Grimm, *Bose-Einstein condensation of molecules,* Science **302** (2003) 2101.

[126] T. Jolicœur and J. C. L. Guillou, *Spin-wave results for the triangular Heisenberg antiferromagnet,* Phys. Rev. B **40** (1989) 2727.

[127] P. H. Jones, M. Goonasekera, and F. Renzoni, *Rectifying Fluctuations in an Optical Lattice,* Phys. Rev. Lett. **93** (2004) 073904.

[128] J. Joo, Y. J. Park, S. Oh, and J. Kim, *Quantum teleportation via a W state,* New J. Phys. **5** (2003) 136.

[129] M. Y. Kagan, I. V. Brodsky, D. V. Efremov, and A. V. Klaptsov, *Composite fermions, trios, and quartets in a Fermi-Bose mixture,* Phys. Rev. A **70** (2004) 023607.

[130] L. Khaykovich, F. Schreck, G. Ferrari, T. Bourdel, J. Cubizolles, L. D. Carr, Y. Castin, and C. Salomon, *Formation of a matter-wave bright soliton,* Science **296** (2002) 1290.

[131] J. Kinnunen, M. Rodriguez, and P. Törmä, *Pairing gap and in-gap excitations in trapped fermionic superfluids,* Science **305** (2004) 1131.

[132] T. Kinoshita, T. Wenger, and D. S. Weiss, *Observation of a one-dimensional Tonks-Girardeau gas,* Science **305** (2004) 1125.

[133] W. Kohn, *Analytic Properties of Bloch Waves and Wannier Functions,* Phys. Rev. **115** (1959) 809.

[134] C. Kollath, U. Schollwöck, and W. Zwerger, *Spin-charge separation in cold Fermi gases: A real time analysis,* Phys. Rev. Lett **95** (2005) 176401.

[135] A. B. Kuklov and B. V. Svistunov, *Counterflow Superfluidity of Two-Species Ultracold Atoms in a Commensurate Optical Lattice,* Phys. Rev. Lett. **90** (2003) 100401.

[136] P. K. Lam and S. M. Grivin, *Liquid-solid transition and the fractional quantum-Hall effect,* Phys. Rev. B **30** (1984) 473.

[137] J. I. Latorre, E. Rico, and G. Vidal, *Ground state entanglement in quantum spin chains,* QIC **4** (2004) 48.

[138] R. B. Laughlin, *Anomalous Quantum Hall Effect: An Incompressible Quantum Fluid with Fractionally Charged Excitations,* Phys. Rev. Lett. **50** (1983) 1395.

[139] P. Lecheminant, B. Bernu, C. Lhuillier, L. Pierre, and P. Sindzingre, *Order versus disorder in the quantum Heisenberg antiferromagnet on the kagomé lattice using exact spectra analysis,* Phys. Rev. B **56** (1997) 2521.

[140] P. A. Lee, *Gauge field, Aharonov-Bohm flux, and high-T[c] supercon-ductivity,* Phys. Rev. Lett. **63** (1989) 680.

[141] P. W. Leung and V. Elser, *Numerical studies of a 36-site kagomé an-tiferromagnet,* Phys. Rev. B **47** (1993) 5459.

[142] M. Lewenstein, L. Santos, M. A. Baranov, and H. Fehrmann, *Atomic Bose-Fermi Mixtures in an Optical Lattice,* Phys. Rev. Lett. **92** (2004) 050401.

[143] R. M. Lewis, Y. Chen, L. W. Engel, D. C. Tsui, P. D. Ye, L. N. Pfeiffer, and K. W. West, *Evidence of a First-Order Phase Transition Between Wigner-Crystal and Bubble Phases of 2D Electrons in Higher Landau Levels,* Phys. Rev. Lett. **93** (2004) 176808.

[144] C. Lhuillier, *Frustrated Quantum Magnets,* cond-mat/0502464.

[145] F. A. Lindemann, *Über die Berechnung molekularer Eigenfrequenzen.,* Phys. Z. **11** (1910) 609.

[146] X.-J. Liu and H. Hu, *Collisionless and hydrodynamic excitations of trapped boson-fermion mixture,* Phys. Rev. A **67** (2003) 023613.

[147] F. London, *On the Bose-Einstein Condensation,* Phys. Rev. **54** (1938) 947.

[148] Y. E. Lozovik and V. M. Farztdinov, *Oscillation spectra and phase diagram of two-dimensional electron crystal: "New" (3+4)-self-consistent approximation,* Solid Sate Com. **54** (1985) 725.

[149] Y. E. Lozovik, V. M. Farztdinov, and B. Abdullaev, *2D electron crystal in quantised magnetic fields, melting induced by zero-point oscillations,* J. Phys. C: Solid State Phys. **18** (1985) L807.

[150] Y. E. Lozovik, D. R. Musin, and V. I. Yudson, *Range of existence of a two-dimensional electron crystal in a strong magnetic field,* Sov. Phys. Solid State **21** (1979) 1132.

[151] J. E. Lye, L. Fallani, M. Modugno, D. Wiersma, C. Fort, and M. Inguscio, *Bose-Einstein condensate in a random potential,* Phys. Rev. Lett. **95** (2005) 070401.

[152] K. Machida, T. Mizushima, and M. Ichioka, *Collective oscillations of vortices in Bose-Einstein condensates under rotation,* Laser Physics **15** (2005) 660.

[153] K. W. Madison, F. Chevy, W. Wohlleben, and J. Dalibard, *Vortex Formation in a Stirred Bose-Einstein Condensate,* Phys. Rev. Lett. **84** (2000) 806.

[154] M. Mambrini and F. Mila, *RVB description of the low-energy singlets of the spin 1/2 kagome antiferromagnet,* Eur. Phys. J. B **17** (2000) 651.

[155] O. Mandel, M. Greiner, A. Widera, T. Rom, T. W. Hänsch, and I. Bloch, *Controlled collisions for multi-particle entanglement of optically trapped atoms,* Nature **425** (2003) 6961.

[156] A. D. Martino, M. Thorwart, R. Egger, and R. Graham, *Exact results for one-dimensional disordered bosons with strong repulsion,* Phys. Rev. Lett. **94** (2005) 060402.

[157] N. Marzari and D. Vanderbilt, *Maximally localized generalized Wannier functions for composite energy bands,* Phys. Rev. B **56** (1997) 12847.

[158] N. Masuhara, J. M. Doyle, J. C. Sandberg, D. Kleppner, and T. J. Greytak, *Evaporative Cooling of Spin-Polarized Atomic Hydrogen,* Phys. Rev. Lett. **61** (1988) 935.

[159] L. Mathey and D.-W. Wang, *Phase diagrams of one-dimensional Bose-Fermi mixtures of ultra-cold atoms,* cond-mat/0602437.

[160] M. R. Matthews, B. P. Anderson, P. C. Haljan, D. S. Hall, C. E. Wieman, and E. A. Cornell, *Vortices in a Bose-Einstein Condensate,* Phys. Rev. Lett. **83** (1999) 2498.

[161] M. R. Matthews, B. P. Anderson, P. C. Haljan, D. S. Hall, C. E. Wieman, and E. A. Cornell, *Experimental studies of equilibrium vortex properties in a Bose-condensed gas,* Phys. Rev. A **70** (2004) 063607.

[162] M.-O. Mewes, M. R. Andrews, D. M. Kurn, D. S. Durfee, C. G. Townsend, and W. Ketterle, *Output Coupler for Bose-Einstein Condensed Atoms,* Phys. Rev. Lett. **78** (1997) 582.

[163] T. Meyer, U. V. Poulsen, K. Eckert, M. Lewenstein, and D. Bruß, *Finite size effects in entangled rings of qubits,* Int. J. Quant. Inf. **2** (2004) 149.

[164] F. Mila, *Low-Energy Sector of the S = 1/2 Kagome Antiferromagnet,* Phys. Rev. Lett. **81** (1998) 2356.

[165] F. Mintert and C. Wunderlich, *Ion-trap quantum logic using long-wavelength radiation,* Phys. Rev. Lett. **87** (2001) 257904.

[166] G. Misguich and C. Lhuillier, *Frustrated spin systems,* World-Scientific, Singapore, 2005.

[167] G. Modugno, F. Ferlaino, R. Heidemann, G. Roati, and M. Inguscio, *Production of a Fermi gas of atoms in an optical lattice,* Phys. Rev. A **68** (2003) 011601.

[168] G. Modugno, G. Ferrari, G. Roati, R. J. Brecha, A. Simoni, and M. Inguscio, *Bose-Einstein Condensation of Potassium Atoms by Sympathetic Cooling,* Science **294** (2001) 1320.

[169] H. Moritz, T. Stöferle, M. Köhl, and T. Esslinger, *Exciting Collective Oscillations in a Trapped 1D Gas,* Phys. Rev. Lett. **91** (2003) 250402.

[170] C. J. Myatt, E. A. Burt, R. W. Ghrist, E. A. Cornell, and C. E. Wieman, *Production of Two Overlapping Bose-Einstein Condensates by Sympathetic Cooling,* Phys. Rev. Lett. **78** (1997) 586.

[171] P. Nikolic and T. Senthil, *Physics of low-energy singlet states of the Kagome lattice quantum Heisenberg antiferromagnet,* Phys. Rev. B **68** (2003) 214415.

[172] K. M. O'Connor and W. K. Wootters, *Entangled rings,* Phys. Rev. A **63** (2001) 052302.

[173] P. Öheberg, G. Jueliūnas, J. Ruseckas, and M. Fleischhauer, *Filled Landau levels in neutral quantum gases,* Phys. Rev. A **72** (2005) 053632.

[174] M. Olshanii, *Atomic Scattering in the Presence of an External Confinement and a Gas of Impenetrable Bosons,* Phys. Rev. Lett. **81** (1998) 938.

[175] R. Onofrio, D. S. Durfee, C. Raman, M. Köhl, C. E. Kuklewicz, and W. Ketterle, *Surface Excitations of a Bose-Einstein Condensate,* Phys. Rev. Lett. **84** (2000) 810.

[176] T. Osborne and M. A. Nielsen, *Entanglement in a simple quantum phase transition,* Phys. Rev. A **66** (2002) 032110.

[177] S. Ospelkaus, C. Ospelkaus, O. Wille, M. Succo, P. Ernst, K. Sengstock, and K. Bongs, *Localization of bosonic atoms by fermionic impurities in a 3d optical lattice,* cond-mat/0604179.

[178] A. Osterloh, L. Amico, G. Falci, and R. Fazio, *Scaling of entanglement close to a quantum phase transition,* Nature **416** (2002) 608.

[179] K. Osterloh. privat communication.

[180] K. Osterloh, M. Baig, L. Santos, P. Zoller, and M. Lewenstein, *Cold Atoms in Non-Abelian Gauge Potentials: From the Hofstadter "Moth" to Lattice Gauge Theory,* Phys. Rev. Lett. **95** (2005) 010403.

[181] B. Paredes, A. Widera, V. Murg, O. Mandel, S. Folling, I. Cirac, G. V. Shlyapnikov, T. W. Hänsch, and I. Bloch, *Tonks-Girardeau gas of ultracold atoms in an optical lattice,* Nature **429** (2004) 277.

[182] P. Pedri, L. Pitaevskii, and S. Stringari, *Expansion of a Coherent Array of Bose-Einstein Condensates,* Phys. Rev. Lett. **87** (2001) 220401.

[183] O. Penrose and L. Onsager, *Bose-Einstein Condensation and Liquid Helium,* Phys. Rev. **104** (1956) 576.

[184] D. S. Petrov, C. Salomon, and G. V. Shlyapnikov, *Weakly Bound Dimers of Fermionic Atoms,* Phys. Rev. Lett. **93** (2004) 090404.

[185] D. S. Petrov, G. V. Shlyapnikov, and J. T. M. Walraven, *Phase-Fluctuating 3D Bose-Einstein Condensates in Elongated Traps,* Phys. Rev. Lett. **87** (2001) 050404.

[186] K. I. Petsas, A. B. Coates, and G. Grynberg, *Crystallography of optical lattices,* Phys. Rev. A **50** (1994) 5173.

[187] D. Porras and J. I. Cirac, *Effective quantum spin systems with trapped ions,* Phys. Rev. Lett. **92** (2004) 207901.

[188] R. E. Prange and S. M. Girvin, *The Quantum Hall Effect,* Springer Varlag, New York, 1987.

[189] H. Pu, W. Zhang, M. Wilkens, and P. Meystre, *Phonon Spectrum and Dynamical Stability of a Dilute Quantum Degenerate Bose-Fermi Mixture,* Phys. Rev. Lett. **88** (2002) 070408.

[190] P. Rabl, A. J. Daley, P. O. Fedichev, J. I. Cirac, and P. Zoller, *Defect-Suppressed Atomic Crystals in an Optical Lattice,* Phys. Rev. Lett. **91** (2003) 110403.

[191] S. Rapsch, U. Schollwöck, and W. Zwerger, *Density matrix renormalization group for disordered bosons in one dimension,* Europhysics Letters **46** (1999) 559.

[192] A. Recati, P. O. Fedichev, W. Zwerger, and P. Zoller, *Spin-Charge Separation in Ultracold Quantum Gases,* Phys. Rev. Lett. **90** (2003) 020401.

[193] G. Ritt, C. Geckeler, T. Salger, G. Cennini, and M. Weitz, *Fourier Synthesis of Conservative Atom Potentials,* cond-mat/0512018.

[194] J. Ruseckas, G. Juzeliunas, P. Öhberg, and M. Fleischhauer, *Non-Abelian Gauge Potentials for Ultracold Atoms with Degenerate Dark States,* Phys. Rev. Lett. **95** (2005) 010404.

[195] S. Sachdev, *Quantum Phase Transitions,* Cambridge University Press, Cambridge, 1999.

[196] A. Sanpera, A. Kantian, L. Sanchez-Palencia, J. Zakrzewski, and M. Lewenstein, *Atomic Fermi-Bose Mixtures in Inhomogeneous and Random Lattices: From Fermi Glass to Quantum Spin Glass and Quantum Percolation,* Phys. Rev. Lett. **93** (2004) 040401.

[197] F. P. D. Santos, J. Léonard, J. Wang, C. J. Barrelet, F. Perales, E. Rasel, C. S. Unnikrishnan, M. Leduc, and C. Cohen-Tannoudji, *Bose-Einstein Condensation of Metastable Helium,* Phys. Rev. Lett. **86** (2001) 3459.

[198] L. Santos, M. A. Baranov, J. I. Cirac, H.-U. Everts, H. Fehrmann, and M. Lewenstein, *Atomic Quantum Gases in Kagomé Lattices,* Phys. Rev. Lett. **93** (2004) 030601.

[199] S. D. Sarma and A. Pinczuk, *Perspectives in Quantum Hall Effects,* Wiley, 1997.

[200] F. Schreck, L. Khaykovich, K. L. Corwin, G. Ferrari, T. Bourdel, J. Cubizolles, and C. Salomon, *Quasipure Bose-Einstein Condensate Immersed in a Fermi Sea,* Phys. Rev. Lett. **87** (2001) 080403.

[201] T. Schulte, S. Drenkelforth, J. Kruse, W. Ertmer, J. Arlt, K. Sacha, J. Zakrzewski, and M. Lewenstein, *Routes towards Anderson-Like localization of Bose-Einstein condensates in disordered optical lattices,* Phys. Rev. Lett **95** (2005) 170411.

[202] T. Schulte, L. Santos, A. Sanpera, and M. Lewenstein, *Vortex-vortex interactions in toroidally trapped Bose-Einstein condensates,* Phys. Rev. A **66** (2002) 033602.

[203] V. Schweikhard, I. Coddington, P. Engels, V. P. Mogendorff, and E. A. Cornell, *Rapidly Rotating Bose-Einstein Condensates in and near the Lowest Landau Level,* Phys. Rev. Lett. **92** (2004) 040404.

[204] K. Sengupta, N. Dupuis, and P. Majumdar, *Bose-Fermi mixtures in an optical lattice,* cond-mat/0603162.

[205] J. P. Shaffer, W. Chalupczak, and N. P. Biglow, *Photoassociative Ionization of Hetronuclear Molecules in a Novel Two-Species Magneto-optical Trap,* Phys. Rev. Lett. **82** (1998) 1124.

[206] R. Shankar, *Renormalization-Group Approach to Interacting Fermions,* Rev. Mod. Phys. **66** (1994) 129.

[207] K. E. Strecker, G. B. Partridge, A. G. Truscott, and R. G. Hulet, *Formation and propagation of matter-wave soliton trains,* Nature **417** (2002) 150.

[208] J. Stuhler, A. Griesmaier, T. Koch, M. Fattori, S. Giovanazzi, P. Pedri, L. Santos, and T. Pfau, *Observation of Dipole-Dipole Interaction in a Degenerate Quantum Gas,* Phys. Rev. Lett. **95** (2005) 150406.

[209] V. Subrahmanyam, *Block spins and chirality in the frustrated Heisenberg model on kagomé and triangular lattices,* Phys. Rev. B **52** (1995) 1133.

[210] Y. Takasu, K. Maki, K. Komori, T. Takano, K. Honda, M. Kumakura, T. Yabuzaki, and Y. Takahashi, *Spin-Singlet Bose-Einstein Condensation of Two-Electron Atoms,* Phys. Rev. Lett. **91** (2003) 040404.

[211] M. Theis, G. Thalhammer, K. Winkler, M. Hellwig, G. Ruff, R. Grimm, and J. H. Denschlag, *Tuning the Scattering Length with an Optically Induced Feshbach Resonance,* Phys. Rev. Lett. **93** (2004) 123001.

[212] E. Tiesinga, B. J. Verhaar, and H. T. C. Stoof, *Threshold and resonance phenomena in ultracold ground-state collisions,* Phys. Rev. A **47** (1993) 4114.

[213] E. Timmermans, P. Tommasini, M. Hussein, and A. Kerman, *Feshbach resonances in atomic Bose-Einstein condensates,* Phys. Rep. **315** (1999) 199.

[214] D. C. Tsui, H. L. Stormer, and A. C. Gossard, *Two-Dimensional Magnetotransport in the Extreme Quantum Limit,* Phys. Rev. Lett. **48** (1982) 1559.

[215] A. M. Tsvelik, *Quantum field theory in condensed matter physics,* Cambridge University Press, 1995.

[216] S. Y. T. van de Meerakker, R. T. Jongma, H. L. Bethlem, and G. Meijer, *Accumulating NH radicals in a magnetic trap,* Phys. Rev. A **64** (2001) 041401.

[217] S. Y. T. van de Meerakker, B. G. Sartakov, A. P. Mosk, R. T. Jongma, and G. Meijer, *Optical pumping of metastable NH radicals into the paramagnetic ground state,* Phys. Rev. A **68** (2003) 032508.

[218] D. van Oosten, P. van der Straten, and H. T. C. Stoof, *Quantum phases in an optical lattice,* Phys. Rev. A **63** (2001) 053601.

[219] F. Verstraete and J. I. Cirac, *Renormalization algorithms for Quantum-Many Body Systems in two and higher dimensions,* cond-mat/0407066.

[220] F. Verstraete and J. I. Cirac, *Valence-bond states for quantum computation,* Phys. Rev. A **70** (2004) 060302.

[221] F. Verstraete, M. A. Martin-Delgado, and J. I. Cirac, *Diverging Entanglement Length in Gapped Quantum Spin Systems,* Phys. Rev. Lett. **92** (2004) 087201.

[222] F. Verstraete, M. Popp, and J. I. Cirac, *Entanglement versus Correlations in Spin Systems,* Phys. Rev. Lett. **92** (2004) 027901.

[223] F. Verstraete, D. Porras, and J. I. Cirac, *Density Matrix Renormalization Group and Periodic Boundary Conditions: A Quantum Information Perspective,* Phys. Rev. Lett. **93** (2004) 227205.

[224] G. Vidal, *Efficient Classical Simulation of Slightly Entangled Quantum Computations,* Phys. Rev. Lett. **91** (2003) 147902.

[225] G. Vidal, *Efficient Simulation of One-Dimensional Quantum Many-Body Systems,* Phys. Rev. Lett. **93** (2004) 040502.

[226] G. Vidal, J. I. Latorre, E. Rico, and A. Kitaev, *Entanglement in Quantum Critical Phenomena,* Phys. Rev. Lett. **90** (2003) 227902.

[227] L. Viverit and S. Giorgini, *Ground-state properties of a dilute Bose-Fermi mixture,* Phys. Rev. A **66** (2002) 063604.

[228] C. Waldtmann, H. U. Everts, B. Bernu, C. Lhuillier, P. Sindzingre, P. Lecheminant, and L. Pierre, *First excitations of the spin 1/2 Heisenberg antiferromagnet on the kagome lattice,* Eur. Phys. J. B **2** (1998) 501.

[229] G. H. Wannier, *The Structure of Electronic Excitation Levels in Insulating Crystals,* Phys. Rev. **52** (1937) 191.

[230] T. Weber, J. Herbig, M. Mark, H.-C. Nägerl, and R. Grimm, *Bose-Einstein condensation of cesium,* Science **299** (2003) 232.

[231] M. Weitz, G. Cennini, G. Ritt, and C. Geckeler, *Optical multiphoton lattices,* Phys. Rev. A **70** (2004) 043414.

[232] X.-G. Wen, *Effective Lagrangian for holes in the spin-liquid state,* Phys. Rev. B **39** (1989) 7223.

[233] S. Wessel, F. Alet, M. Troyer, and G. G. Batrouni, *Quantum Monte Carlo simulations of confined bosonic atoms in optical lattices,* Phys. Rev. A **70** (2004) 053615.

[234] S. Wessel and M. Troyer, *Supersolid hard-core bosons on the triangluar Lattice,* Phys. Rev. Lett. **95** (2005) 127205.

[235] S. R. White, *Density matrix formulation for quantum renormalization groups,* Phys. Rev. Lett. **69** (1992) 2863.

[236] P. B. Wiegmann, *Superconductivity in strongly correlated electronic systems and confinement versus deconfinement phenomenon,* Phys. Rev. Lett. **60** (1988) 821.

[237] E. Wigner, *On the Interaction of Electrons in Metals,* Phys. Rev. **46** (1934) 1002.

[238] W. K. Wootters, *Entangled Chains,* Contemp. Math. **305** (2002) 299.

[239] H. Yi and H. A. Fertig, *Laughlin-Jastrow-correlated Wigner crystal in a strong magnetic field,* Phys. Rev. B **58** (1998) 4019.

[240] J. Zhang, E. G. M. V. Kempen, T. Bourdel, L. Khaykovich, J. Cubizolles, F. Chevy, M. Teichmann, L. Tarruell, S. J. J. M. F. Kokkelmans, and C. Salomon, *Expansion of a lithium gas in the BEC-BCS crossover,* cond-mat/0410167.

[241] M. W. Zwierlein, C. H. Schunck, C. A. Stan, S. M. F. Raupach, and W. Ketterle, *Formation Time of a Fermion Pair Condensate,* cond-mat/0412675.

[242] M. W. Zwierlein, C. A. Stan, C. H. Schunck, S. M. F. Raupach, S. Gupta, Z. Hadzibabic, and W. Ketterle, *Observation of Bose-Einstein Condensation of Molecules,* Phys. Rev. Lett. **91** (2003) 250401.

[243] M. W. Zwierlein, C. A. Stan, C. H. Schunck, S. M. F. Raupach, A. J. Kerman, and W. Ketterle, *Condensation of Pairs of Fermionic Atoms near a Feshbach Resonance,* Phys. Rev. Lett. **92** (2004) 120403.

Index

Curriculum Vitae

personal data

surname	Fehrmann
first name	Henning
birthday	07.10.1975
birthplace	Havelberg

School Education

10/1982–09/1989	Oberschule in Parchim and Paulinenaue
10/1989–07/1995	Gymnasium in Nauen and Hannover
school leaving	Abitur

Study

10/1996–09/2002	diploma in physics at the University of Hannover

Studies In The UK

10/1999–09/2000	physics at the University of Lancaster

List of publications

B. Damski, H. Fehrmann, H.U. Everts, M.A. Baranov, L. Santos, and M. Lewenstein, *Quantum gases in trimerized kagomé lattices*, Phys. Rev. A **72**, (2005) 053612.

B. Damski, H.U. Everts, A. Honecker, H. Fehrmann, L. Santos, and M. Lewenstein, *Atomic fermi gas in the trimerized kagomé lattice at 2/3 filling*, Phys. Rev. Lett. **95** (2005), 060403.

H. Fehrmann, M.A. Baranov, B. Damski, M. Lewenstein, and L. Santos, *Mean-field theory of Bose-Fermi mixtures in optical lattices*, Optics Comm. **243** (2004), 23.

L. Santos, M.A. Baranov, J.I. Cirac, H.U. Everts, H. Fehrmann, and M. Lewenstein, *Atomic quantum gases in Kagomé lattices*, Phys. Rev. Lett. **93** (2004), 030601.

M. Lewenstein, L. Santos, M.A. Baranov, and H. Fehrmann, *Atomic Bose-Fermi mixtures in an optical lattice* Phys. Rev. Lett. **92** (2004), 050401.

H. Fehrmann, M. Baranov, M. Lewenstein, and L. Santos, *Quantum phases of Bose-Fermi mixtures in optical lattices* Optics Express **12** (2004), 55.

A. Kambili, H. Fehrmann, C.J. Lambert, and J.H. Jefferson, *A Hartree-Fock study of charge redistribution in a two-dimensional mesoscopic structure* Journal of Phys.-Cond. Matt. **13** (2001), L495.

ACKNOWLEDGEMENT